

Electronic Thesis and Dissertation Repository

4-22-2021 2:00 PM

Time-dependent fragility assessment of aged concrete gravity dam subjected to seismic load-with application to a dam in Korea

Jungmyung Kim, *The University of Western Ontario*

Supervisor: Han-Ping Hong, *The University of Western Ontario*

A thesis submitted in partial fulfillment of the requirements for the Doctor of Philosophy degree in Civil and Environmental Engineering

© Jungmyung Kim 2021

Follow this and additional works at: <https://ir.lib.uwo.ca/etd>

Recommended Citation

Kim, Jungmyung, "Time-dependent fragility assessment of aged concrete gravity dam subjected to seismic load-with application to a dam in Korea" (2021). *Electronic Thesis and Dissertation Repository*. 7761.

<https://ir.lib.uwo.ca/etd/7761>

This Dissertation/Thesis is brought to you for free and open access by Scholarship@Western. It has been accepted for inclusion in Electronic Thesis and Dissertation Repository by an authorized administrator of Scholarship@Western. For more information, please contact wlsadmin@uwo.ca.

Abstract

Dams play an essential role in society. Many concrete gravity dams in Korea and the world have been in service for some time and may already exceed their design working life. These dams are subjected to natural loads such as seismic loads. These old dams may need to be requalified by carrying out safety and reliability assessments. The reliability assessment is complicated by the fact that the strength and stiffness of the concrete are uncertain and time-varying. The uncertainty in both the material properties as well as in the loads needs to be considered in evaluating the reliability of existing dams using simple or sophisticated techniques reliability analysis techniques.

An overall framework to assess the fragility and safety of concrete gravity dam subjected to the seismic load is presented in the present thesis. The framework emphasizes the practical issues on the time-dependent seismic fragility curves assessment of gravity dam. The components of this framework consist of the nonlinear inelastic finite element modeling and dynamic analysis, the modeling of time-dependent concrete strength due to aging and degradation, the probabilistic analysis procedure leading to the fragility curves by considering failure criteria (i.e., limits state functions), and simple reliability analysis by considering seismic hazard.

The valuable and very limited number of samples from an actual dam is used to develop and validate the adopted time-dependent model of concrete strength. Nonlinear inelastic finite element models of an existing concrete gravity dam - Chungju Dam in Korea are developed and used to show the applicability of the proposed framework to assess the time-dependent seismic fragility curves and reliability. Two finite element software (one proprietary and the other commercially available software) are used to validate the developed finite element models. A sensitivity analysis of the dynamic characteristics of the dam to the material variability is presented by using the developed finite element models.

For the development of seismic fragility curves, several limit state functions based on cracking and displacements are considered, nonlinear inelastic time history analysis is performed, and the Latin hypercube sampling technique is employed for the probabilistic analysis. The

results show the importance of considering the time-dependent concrete strength degradation in evaluating the time-dependent seismic fragility curves and reliability.

Keywords

Fragility analysis, Concrete gravity dam, Degradation model, Latin Hypercube sampling, Concrete Damaged Plasticity model.

Summary for Lay Audience

Dams are essential facilities. Many concrete gravity dams have been in service for some time and may already exceed their design working life. Existing old dams may need accurate assessments of performance and safety. However, the assessment of the dam is performed according to very simplified procedures and ignored the nonlinear inelastic behavior under earthquakes and the uncertainty in material properties over time.

This study focuses on the development of the overall framework to evaluate the seismic fragility curve and reliability of concrete gravity dams. The framework highlights the need to consider the material properties over time to assess the seismic fragility curve and reliability of the dam. The main tasks of this framework consist of the nonlinear inelastic finite element modeling and dynamic analysis, the modeling of time-dependent concrete strength due to aging and degradation, the probabilistic analysis procedure, and simple reliability analysis by considering seismic hazard.

A valuable and very limited number of samples collected from actual dams are used to develop and validate the time-dependent concrete strength model adopted. Nonlinear Inelastic Finite Element Model of Existing Concrete Gravity Dam - Domestic Chungju Dam is developed and used to show the applicability of the proposed framework to evaluate seismic vulnerability curves and reliability over time.

For the development of seismic fragility curves, several limit state functions based on cracking and displacements are considered, nonlinear inelastic time history analysis is performed, and the Latin hypercube sampling technique is employed for the probabilistic analysis. The results show the importance of considering the time-dependent concrete strength degradation in evaluating the time-dependent seismic fragility curves and reliability.

Table of Contents

Abstract	ii
Table of Contents	v
List of Tables	vi
List of Figures	ix
List of Appendix	xii
Chapter 1	1
1 Introduction	1
1.1 Introduction	1
1.2 Research Objective	3
1.3 Outline of Thesis	4
Chapter 2	6
2 Overview of Performance Evaluation of Aging Concrete Gravity Dams and Concrete Damage Evaluation	6
2.1 Introduction	6
2.2 Some Design Consideration	7
2.3 Generation Consideration for Modeling and Analysis of Concrete Gravity Dam	10
2.4 Statistics of Aged of Dams in Korea	11
2.5 Performance of Existing Dams	12
2.6 Safety Factor for Different Failure Modes	16
2.7 Overview of Seismic Response Analysis Based on Finite Element Method	19
2.8 Concrete Plastic Damage Model and Model Implementation	23
2.8.1 Concrete Plastic Damage Model	23
2.8.2 Damage Functions for Concrete in compression and tension	29
2.9 Summary	35

Chapter 3.....	36
3 Degradation Modeling of Concrete in Concrete Gravity Dam and Its Application.....	36
3.1 Introduction.....	36
3.2 Modeling Time-Varying Concrete Strength.....	39
3.2.1 Modeling Degradation Using Gamma Process.....	39
3.2.2 Modeling Degradation of Concrete based experimental.....	41
3.2.3 Model for Aged Concrete Strength.....	44
3.2.4 Proposed Model for Time-Varying Compressive Strength.....	46
3.3 Application to Time-Varying Concrete Strength Model to Chungju dam.....	48
3.4 Summary.....	53
Chapter 4.....	55
4 Finite Element Modeling of a Concrete Gravity Dam : a Case Study.....	55
4.1 Introduction.....	55
4.2 Developed the Finite Element Model of a Dam.....	56
4.3 Validation of the developed FE Model.....	58
4.3.1 Forces acting on a Concrete Gravity Dam and Static Analysis.....	58
4.3.2 Modal Analysis results.....	62
4.4 Time-history response of Dam subjected to ground motions : Parametric Investigation.....	65
4.5 Summary and conclusion.....	70
Chapter 5.....	71
5 Probabilistic analysis and development of fragility curve of a Concrete Gravity dam.....	71
5.1 Introduction.....	71
5.2 Probabilistic models.....	74
5.2.1 Probabilistic models for material properties.....	74
5.2.2 Simulation of the random variables for the concrete dam.....	77

5.2.3 Seismic Loading Consideradtion	79
5.3 Consideration of Limit State Functions	84
5.4 Developed Fragility curves	87
5.4.1 Tensile Cracking at the toe or upstream face of the dam	88
5.4.2 Tensile Cracking at the Neck of the dam	92
5.4.3 Excessive Deformation of the Dam	94
5.5 Use of the fragility curves for reliability analysis.....	97
5.6 Summary	98
Chapter 6.....	99
6 Conclusions and Future Research	99
6.1 Summary and Conclusion.....	99
6.2 Future research.....	100
References	102
Appendices.....	109

List of Tables

Table 2.1: Dams in Korea	12
Table 2.2: Historic failure of concrete and masonry gravity dams	14
Table 2.3: Parameters of CPDM	28
Table 3.1: Major aging scenarios for concrete dams	37
Table 3.2: Experimental Data of Concrete Compressive Strength for Chungju Dam	50
Table 3.3: Shape and scale parameters of degradation for Chungju Dam	52
Table 4.1: Material properties of Chungju dam	56
Table 4.2: Modal frequencies of Chungju dam from different models	65
Table 4.3: Cases for Parametric Analysis	66
Table 4.4: Modal frequencies for the considered cases shown in Table 4.3	66
Table 4.5: Result of dynamic Analysis	69
Table 5.1: Statistics for the considered random variables	74
Table 5.2: Case study for the considered random variables	78
Table 5.3: Spectrum parameters	80
Table 5.4: Seismic risk factor	80
Table 5.5: Selected ground motions	82
Table 5.6: Fitted model parameters by considering limit state function g_3	91
Table 5.7: Fitted model parameters by considering limit state function g_4	94
Table 5.8a: Fitted model parameters by considering limit state function $g_7(a)$	96

Table 5.8b: Fitted model parameters by considering limit state function $g_7(\mathbf{b})$	96
Table 5.9: Estimated failure probability at a given year by considering different limit state functions.....	98

List of Figures

Figure 1.1: Diagram showing the framework for assessing the time-dependent seismic fragility curves and reliability	3
Figure 2.1: Loads in current design practices according to Korean Design Standard	8
Figure 2.2: Number of dams by construction years	12
Figure 2.3: Major aging sceneries	15
Figure 2.4: General deterioration process of the concrete dam	15
Figure 2.5: External causes of a deterioration process	16
Figure 2.6: Failure modes of concrete dams	16
Figure 2.7: Boundary condition of dams	21
Figure 2.8: Representation of CPDM	24
Figure 2.9: Uniaxial loading-unloading law	26
Figure 2.10: Yield surface in the deviatoric plan for several values of K_c	28
Figure 2.11: Assumed uniaxial model of concrete behavior	29
Figure 3.1: Deterioration process with time	37
Figure 3.2: Continuous Gamma degradation process	41
Figure 3.3: Change of concrete strength over time	45
Figure 3.4: Procedure to model the concrete strength with time t	48
Figure 3.5: Procedure to find model parameters	49
Figure 3.6: Comparison of the models and observed time-varying concrete strength	53
Figure 4.1: Location of Chungju Dam and a photo of the dam	55

Figure 4.2: Dimensions of Chungju Dam (Block #10).....	56
Figure 4.3: The Model of dam-reservoir-foundation system in ABAQUS	57
Figure 4.4: Forces acting on a gravity dam.....	58
Figure 4.5: Distribution of uplift pressure on a gravity dam	60
Figure 4.6: Distribution of uplift pressure on the Chungju dam.....	60
Figure 4.7: Stress contour of Analysis results for K-water and ABAQUS model	63
Figure 4.8: Horizontal and Vertical Displacement of ABAQUS model	63
Figure 4.9: Mode shapes of Chungju Dam	64
Figure 4.10: Horizontal ground motion record from San Fernando earthquake.....	68
Figure 4.11: Time histories the displacement at the top of the dam, the stress at the upper stream and downstream of the toe	69
Figure 5.1: Procedures of seismic fragility analysis of concrete dam	73
Figure 5.2: Design response spectrum characterization	80
Figure 5.3: Target Spectrum of Chungju dam	81
Figure 5.4: Response spectra of horizontal component of selected ground motions.....	83
Figure 5.5: Response spectra of vertical component of selected ground motions.....	84
Figure 5.6: Limit State Function of Chungju Dam.....	87
Figure 5.7: Cracking profiles of limit state g_3	90
Figure 5.8: Graph of failure probability for tensile cracking at toe or upstream face	91
Figure 5.9: Cracking profiles of limit state g_4	93
Figure 5.10: Graph of failure probability for the neck of the dam	94

Figure 5.11: Graph of failure probability for Excessive Deformation $g_7 - a$ 95

Figure 5.12: Graph of failure probability for Excessive Deformation $g_7 - b$ 96

List of Appendix

Appendix A: Values of the limit state functions obtained from the finite element modeling and simulation analysis.....	108
---	------------

Chapter 1

1.1 Introduction

Dams have been used for a long time and are essential infrastructure for our society. Dams play an important role in many countries, including Korea. They represent considerable value in terms of fixed capital assets and investment for future generations. Dams provide services such as water supply, irrigation, flood control, and hydropower energy, contributing significantly to the development of Korea since 1910.

Similar to any other infrastructure, dams, including concrete gravity dams, are aging. The internal and external environmental conditions of the dams are changing and affect their structural properties. Moreover, dams are subjected to environmental and seismic loads. The design of new and the analysis of existing dams in Korea and other countries are usually based on static analysis methods, although sophisticated nonlinear inelastic finite element modeling and time history analysis are available. The use of the static method is for convenience and simplicity.

More than 17,000 dams have been built worldwide, many of which have been in service for over 50 years and may already close to or have exceeded their design service life. As a dam is aging, there is an incentive to manage this valuable asset economically or to extend the dam's design service life by taking the safety constraints into account. The aging affects the structural properties of the dam and the ability of the dam to withstand various loadings caused by operations, environmental changes, and earthquakes.

The need to consider the seismic hazard for dams in Korea becomes more pressing because of the occurrence of the 2018 Pohang earthquake with an earthquake magnitude of 4.6 for a region in Korea that was not prone to significant seismic hazard. The urgency of considering the seismic hazard for evaluating existing dams is stressed in Bernier et al. (2016) and Hariri-Ardebili (2018), indicating that many existing dams were built using outdated analysis methods and limited understanding of seismicity. In fact, dams in Korea are designed and assessed based on the traditional safety factor methodology. There are several drawbacks associated with the use of the safety factor approach for design; mainly,

its use does not lead to reliability consistent design. In other words, two designs with the same safety factor do not imply that they meet the same tolerable failure probability. This is because the degree of uncertainty involved in the structural properties and loads is different for dams located at different geographical locations (Lupoi and Callali 2012; Bernier et al. 2016; Hariri-Ardebili 2018).

The commonly used methods for structural reliability analysis include the first-order second-moment reliability method, the first-order reliability method, and simulation techniques (Madsen et al. 2006). The first-order second moment and the first-order reliability method are very efficient. However, they require the evaluation of gradients or partial derivatives of the structural responses with respect to the values of the random variables. Analytical expressions for such derivatives are rarely available, and their numerical approximation may not be stable or existent, especially for responses obtained by considering nonlinear inelastic behavior. The simple simulation technique is robust and time-consuming. It seems that the use of the Latin hypercube sampling technique (McKay et al. 1976; Iman and Conover 1982) is popular for assessing dam safety (Ghanaat et al. 2012). Often, less than about 15 replicated (or simulated) samples of a dam are considered (Hariri-Ardebili and Saouma 2016). The safety analysis of concrete gravity dams in seismic regions is essential due to the high potential of fatalities and economic losses if they fail. The evaluation is to investigate whether the probability of the capacity of the dam to withstand extreme environmental and seismic loading is below a tolerable failure probability.

Besides selecting a technique to evaluate the reliability, a fundamental issue for the reliability evaluation is to provide probabilistic characterizations of the material strength of the dam by considering the aging and degradation and of loads, including the seismic loads. The time-dependent strength degradation by considering the gain due to aging and the strength loss due to degradation is a well-known but complicated phenomenon. It involves chemical and physical processes. The leaching of water saturates the numerous pores of the concrete and induces stresses in the concrete. The shrinkage of concrete due to the moisture effect may induce micro-cracks; the strength of the material will be mostly different from that at the time of construction. The time-dependent concrete strength must

be considered in assessing the safety of the dam. Yet, to the author's knowledge, the stochastic modeling and use of such a time-dependent strength to assess the safety of gravity concrete dam have not been explored or reported in the literature. Partly, this is due to actual samples of time-dependent strength of an actual dam is rarely available.

1.2 Research Objective

The main objective of the present thesis is to provide an overall framework to assess the fragility and safety of concrete gravity dam subjected to seismic load. The framework emphasizes the practical issues on the time-dependent seismic fragility curves assessment of gravity dam. The components of this framework consist of the nonlinear inelastic finite element modeling and dynamic analysis, the modeling of time-dependent concrete strength due to aging and degradation, the probabilistic analysis procedure leading to the fragility curves by considering failure criteria (i.e., limits state functions), and simple reliability analysis by considering seismic hazard. A diagram showing the framework for the time-dependent fragility curves and reliability is presented in Figure 1.1.

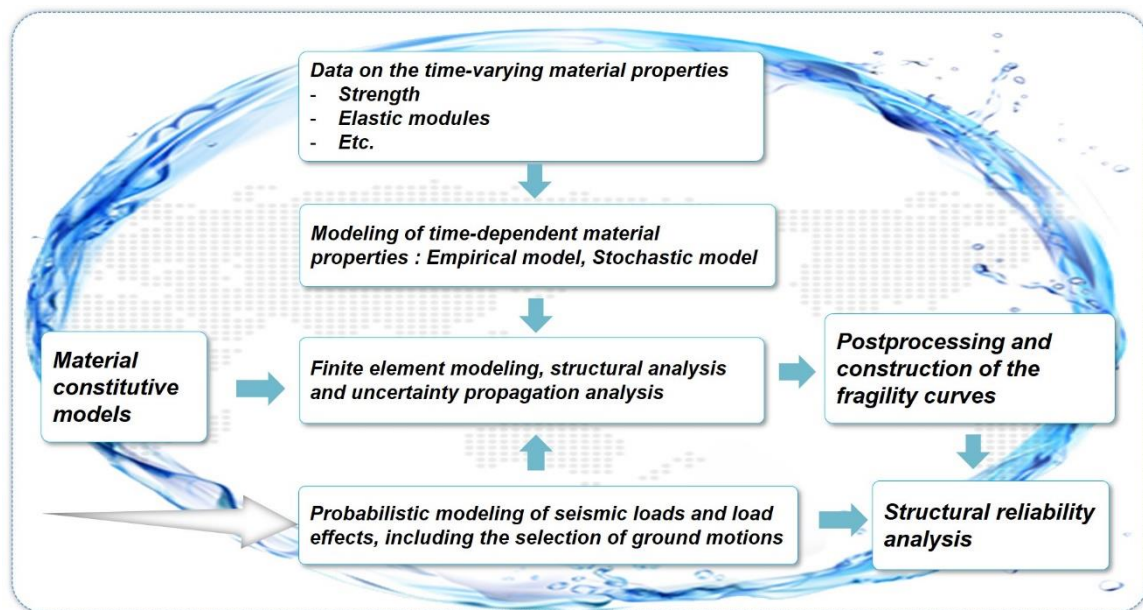


Figure 1.1 Diagram showing the framework for assessing the time-dependent seismic fragility curves and reliability.

The framework is explained through a “case study” by using an actual concrete gravity dam - Chungju Dam in Korea, which was designed in 1980. Two finite element modeling

software, one proprietary and the other commercially available, are used to modeling the dam. To model time-dependent concrete strength, a small number of samples for the considered dam is employed. The limit state functions applicable to concrete gravity dam are reviewed, and those associated with cracking and deformation are considered. The assessment of the seismic fragility curve, which is defined as the conditional probability of failure or exceedance of a specific limit state at a given seismic intensity measure (i.e., seismic spectral acceleration), is based on the Latin hypercube sampling technique. Since the strength is time-dependent, the fragility curve developed in the present study is time-dependent. The reliability analysis is carried out using the simple simulation technique.

The research questions to be considered in the present thesis are: a) What are the major causes and effects of the degradation of concrete dams? b) What are the changes to the performance or dynamic characteristics of concrete gravity concrete dams due to degradation? c) Could a stochastic model or empirical model used to represent the time-dependent concrete strength adequately? d) Are the characteristics of the time-dependent seismic fragility curves? and e) Does the time-dependent seismic reliability of gravity dam varies drastically?

1.3 Outline of Thesis

The thesis consists of six chapters. In Chapter 2, we carry on a literature review on a performance evaluation of aging concrete gravity dams and concrete damage evaluation. We provide a simple review of the current design standards and requirements used for designing dams. Also, the structural behavior of dams subjected to hydrologic and seismic hazard, as well as statistics of aging dam failure, are presented. The review emphasizes the limit states considered in the design and construction of the concrete gravity dams; it serves as the basis for the modeling of time-dependent concrete strength, nonlinear inelastic finite element modeling, and seismic fragility curve assessment.

Chapter 3 is focused on the modeling of the degradation of in-service concrete in concrete gravity dam. A literature review of degradation models reveals two significant trends: an experimental-data driven model and a stochastic process-based model. The former is based on the explanation of physical degradation, and the latter is based on statistical

quantities (Frangopol et al., 2004). Both of these models are considered and applied to the actual time-dependent samples of concrete strength from Chungju Dam. The models considered are an empirical model, which requires curve fitting using observations and a stochastic process (i.e., gamma process) based model.

In Chapter 4, the general consideration of the finite element modeling of the concrete gravity dam is reviewed. Models of Chungju Dam are developed and implemented in proprietary software and in the commercial software - ABAQUS. The modeling considers sophisticated nonlinear material behavior and material yielding criterion. A comparison of the results obtained by using the implemented finite element models in both packages is presented. Also, a sensitivity analysis of the dynamic characteristics of the dam to the material variability is presented.

Chapter 5 is focused on integrating time-dependent concrete strength modeling and the finite element model to assess the seismic fragility curves of the concrete gravity dam. For the assessment, the use of Latin hypercube sampling with very limited samples is considered, as this approach is practical and accepted in the literature. Moreover, the use of a small sample size does not limit the applicability of the established overall framework. The sample size can be increased drastically if sufficient resource is available. The established fragility curves by considering several limit state functions are used for the seismic reliability analysis using the simple simulation technique. The considered limit state functions are focused on the stress-related limit states since they are more relevant and capture the nonlinear behaviour of the responses.

Finally, the conclusions and recommendations derived from the present thesis are given in Chapter 6. In addition, a few future research topics are suggested.

Chapter 2

2 Overview of Performance Evaluation of Aging Concrete Gravity Dams and Concrete Damage Evaluation

2.1 Introduction

A dam is designed to impound and store water behind it safely throughout its lifetime. A concrete gravity dam is a massive structure with a substantially triangular profile that consists of rigid monoliths situated side by side. Its axis runs straight from one end to the other (as opposed to an arch dam, which has a curved axis). The structural stability of a concrete gravity dam is derived entirely from its weight. Unlike other types of concrete dams (e.g., buttress, arch, cupola dams), it has a relatively large base area, reducing the stresses on the foundation. Construction is carried out by pouring concrete in a series of lifts high, depending on dam size and construction method, creating construction joints within each monolith. An indispensable feature of concrete gravity dams is the spillway used to safely discharge water during floods and when the reservoir is full. Auxiliary features of concrete gravity dams that are necessary for the safe and serviceable operation and adequate maintenance include penstocks and associated valves and gates, private galleries and shafts, cofferdams for diversion during construction, cutoffs, drainpipes, and grout curtains to reduce seepage under and around the dam.

The resistance of a concrete dam is due to its geometry and self-weight and shear, the compressive and tensile strength of concrete, foundation, and, where relevant, reinforcement. The most important forces are hydrostatic force, ice load, and uplift pressure, which will be discussed in more detail in subsequent sections. Forces from sediment and earthquakes are important in design concrete gravity dams. Earth pressure and traffic load can be of importance, and loads of temperature, shrinkage, and creep are often substantial, but they are beyond the scope of this thesis. The capacity of the dams to sustain the natural loads is time-varying due to aging, where aging refers to a class of deterioration associated with time-related changes in the properties of the materials.

There are several simple and sophisticated analysis methods of concrete gravity dam subjected to seismic excitation and degradation models of concrete. During the last few

decades, significant research activity has been devoted to the static and dynamic analysis of concrete gravity dams and material strength degradation modeling. The problem becomes even more complex when considering uncertainty in the stochastic seismic excitation and the time-varying stochastic degradations.

The main objectives of this chapter are to carry out a literature review of the performance evaluation of new and aging concrete gravity dams and of a concrete damage model that can be used to evaluate the damage of concrete gravity dams subjected to external loading. The review includes the simple design procedure of concrete gravity dams subjected to seismic excitations; it provides the essential theoretical background to analyze concrete gravity dams by using the finite element model. The review also covers the potential failure causes and failure modes focused on typical concrete dams commonly used in Korea. The review serves to identify some of the weaknesses of the analysis methods and procedures so to provide some of the basis for the proposed research objectives. The detail of the mathematical formulation of a concrete plasticity damage model found in the literature is described as it is used in the present study, although an additional modification to the model by including the aging effect is to be incorporated.

2.2 Some Design Considerations

A designed and constructed dam has to maintain its structural integrity in sustaining loads that arise during construction, regular operation, and extreme environmental events. More specifically, concrete gravity dams are designed to remain operational under normal conditions, to sustain minimal damage under rare operative conditions, and to prevent total loss of reservoir under extreme events. The initial load affecting concrete gravity dams is due to the differential hydrostatic head that occurs during hydrologic events up to and including the Probable Maximum Flood (PMF). Associated with the hydrostatic head are substantial uplift forces arising from pore water pressures that develop within the dam and the foundation. These uplift forces must be included in the overall equilibrium analysis of the monolith. The neglect of these forces results in the compressive stresses in the foundation being underestimated (De Boer and Ehlers, 1990; Yeh and Baier, 1992).

Other loads of lesser magnitude or importance are considered secondary loads, which may or may not be considered in the design: the sediment load (earth pressure due to silt deposits in the reservoir), dynamic wave pressure at the surface of the reservoir, ice load (due to formation of thick ice sheets on the reservoir), and thermal loads (due to temperature gradients caused by cement hydration and ambient and water temperature variations). In seismic hazard-prone areas, dynamic loads due to earthquake ground motions up to an intensity associated with the maximum credible earthquake (MCE) must be considered.

Current procedures for the design of concrete gravity dams are based on static, deterministic analyses. These involve rigid-body analysis of static equilibrium for monolith stability and foundation stresses. If required, seismic loads are approximated by pseudo-static forces obtained using a seismic coefficient analysis, i.e., the inertia and hydrodynamic forces are calculated in terms of the maxima acceleration selected for design and considered as equivalent to additional static loads. For gravity dams, the self-weight of the dam is sufficient to withstand the hydrostatic forces and transmit them to the ground. A typical array and distribution of loads used in current design practices are shown in Figure 2.1.

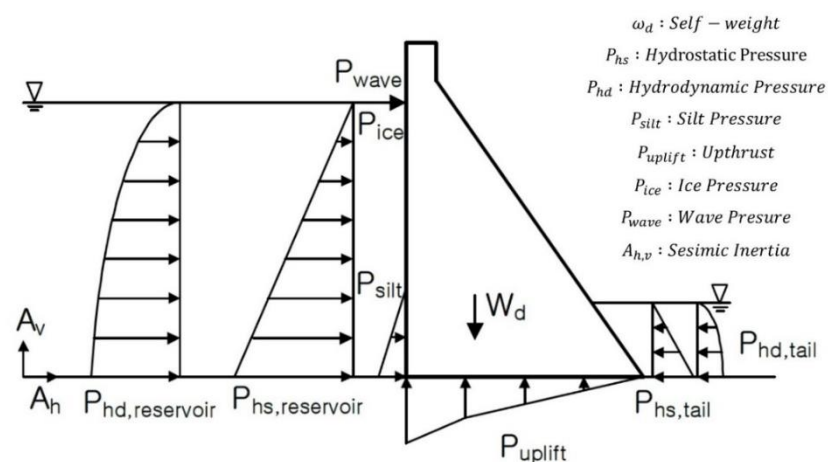


Figure 2.1. Loads in current design practices according to Korean Design Standard.

The governing criteria in the design of concrete gravity dams are that the dam must be safe from overturning, sliding, and bearing failure in the dam or foundation. Factors of safety are utilized in design to provide a margin of safety. These factors vary depending on the importance of the structure and on the hazard, lower factors of safety being assigned to

structures considered less critical, and check against events with a lower perceived probability of occurrence. The safety check against bearing failure requires that the computed stresses be limited to less than the allowable stress in compression for concrete or allowable bearing pressure for foundation materials. It is also a general practice that the location of the resultant force at any horizontal section in the dam must be kept within the kern (middle third of the dam) to ensure no tensile stresses are produced under any pool elevation.

The sliding stability of the dam is checked by using a factor of safety that compares the shear resistance with the total horizontal load. For overturning stability, the restoring and overturning moments about the toe of the monolith are compared. These factors of safety may vary for each criterion and are sometimes very conservative. The simplifications inherent in these design procedures are considerable. For one thing, the distribution of stresses on any horizontal plane is not necessarily linear. For another, the analysis does not take into account the constitutive properties of the concrete, properties of the foundation, and the dam-foundation interaction. The potential of a crack or a significant opening developing at the dam-foundation interface under extreme lateral force is not considered. The treatment of seismic loading is very simplistic.

The dynamic behavior of the dam and the energy content of the earthquake ground motions are not fully incorporated into the analysis. The complex dam-foundation-reservoir interaction is neglected in both the hydrologic and seismic cases. In recent years, there has been a move towards the use of advanced analytical and numerical methods (such as finite element (FE) analysis) to gain a more comprehensive picture of dam behavior. The use of FE analysis is often focused on the crack propagation at the heel of the dam (e.g., Dewey et al., 1994), dynamic response and behavior of a dam-foundation system (e.g., Chavez and Fenves, 1995), and the treatment of uplift forces (e.g., Yeh and Baier, 1992). Increased computational capabilities, advances in numerical analysis theories, and availability of FE software have encouraged the use of FE analysis. Dams are designed and assessed based on an adopted factor of safety, S_f , in Korea to cope with uncertainty in material strength and loads. The design requires that the ratio of the resisting forces, R , to the loading forces, S , to be equal to or greater than S_f (i.e., $S_f \leq R/S$).

Usually, a value of S_f much greater than unity is used to provide confidence in the design dam. For example, the minimum acceptable factor of safety against sliding failure of a dam under normal loading conditions is considered to be equal to 4 (Korean dam design standard, 2011). One of the advantages of using the safety factor methodology is that its application is simple. It has been traditionally used for stability analyses. The selection of target S_f could be based on experience and historical dam performance data, including subjective judgment.

There are several drawbacks associated with the use of the factor of safety methodology. For example, the use of the same S_f value for two designs may not result in consistent tolerable failure probability because the value of S_f alone could not cope with the magnitude of the uncertainty (Madsen et al., 2006). This problem is partially overcome by using the limit state design format with calibrated partial safety factor or load and resistance factors. Although this approach has been implemented in many structural design codes in many countries, its use in the design of dams is relatively limited.

2.3 Generation Consideration for Modeling and Analysis of Concrete Gravity Dam

For concrete dams, it is often assumed that the dam is infinitely long so to simplify the 3-dimensional (3D) problem to a two-dimensional (2D) problem (i.e., in a plane perpendicular to the dam). This simplification could be appropriate if the length of the dam is considerably greater than its height. This assumption, however, is not appropriate for dams with a relatively small length to height ratio. In such a case, a 3D analysis may be necessary and could be a computationally intensive task for a design office. Fahjan et al. (2003) proposed a 3D model taking into account the canyon profile. The computational effort required for their 3D model analysis was so high that it might only be beneficial if the canyon is very narrow. In general, the 3D analysis allows the rigorous determination of displacements and stresses within the dam.

In general, the stability of the dam does not depend on the strain along the axis parallel to the longitudinal axis for the gravity dam, as the geometry and loading do not vary significantly along the longitudinal axis of the dam. The 2-D plane strain approximation

could be considered appropriate for gravity dams (MOCT, 2019). This is especially the case if only static loads are considered.

Gravity concrete dams in the seismic prone region could experience severe earthquake loading during the design working life. Cracking of concrete and damages to the dams may occur and need to be assessed. The assessment should be carried out by considering the nonlinear inelastic material characteristics. For example, the nonlinear response of a small-scale model of the Koyna dam was investigated by Mridha and Maity (2014) using ABAQUS. The crack propagation due to tensile damages was computed, and the results were compared with the experimental results. The nonlinear dynamic analysis may be adopted if cracks due to severe seismic excitation are likely to occur in the dam body. The choice of nonlinear analysis procedure for a particular dam will mainly depend on the geometry, material, and dynamic characteristics of the dam-reservoir-foundation system.

2.4 Statistics of Age of Dams in Korea

Dams could be divided into three groups - earth or rockfill dams, masonry dams, and concrete dams – according to the construction material. Dams in Korea are mostly fill-dam types. The number of a concrete gravity dam is very small; it is 2% of all the dams. Therefore, most existing research works on the dam safety management of Korean dams are concentrated on the fill-dam. The studies on the safety of a concrete gravity dam are limited. However, it should be noted that rock and earth-fill dams are usually associated with concrete intake and discharge facilities, which means that almost all Korean dam facilities contain concrete components. The behavior of these components is similar to that of concrete gravity. Therefore, advantages could be taken from the research findings for concrete components.

There is no new major dam construction in Korea in the past decade. The focus of the dam industry has mainly been on maintaining the aging dam portfolio or retrofitting the dams for an adopted safety requirement.

Many of the dams in Korea are old (see Table 2.1 and Figure 2.2). Most of the concrete gravity dams in Korea were built in the primary water system, and many early large dams

in Korea were concrete dams. Although concrete is inherently durable, some concrete dams may need to be retrofitted because of deficiencies in their design and construction or as a result of the aging and environmental attack (Corns et al., 1988). Moreover, the failure of concrete dams located in the main water system can lead to substantial economic, environmental, and human losses. There are many important and valuable large concrete dams in Korea (or elsewhere) that have been in service for nearly or more than 50 years. The need to deal with the aging of the concrete dams is increasing as many of them enter old age. Therefore, more research on concrete gravity dams with aging effects is more necessary than before.

Table 2.1. Dams in Korea.

Managing Institution / Time of Construction		Before 1945	46~59	46~59	46~59	46~59	After 1990	Total
Total (unit Site)	Sites	9,558	2,042	3,618	1,547	550	366	17,681
	Ratio	56.5%	9.9%	21.5%	8.4%	2.5%	1.2%	100%

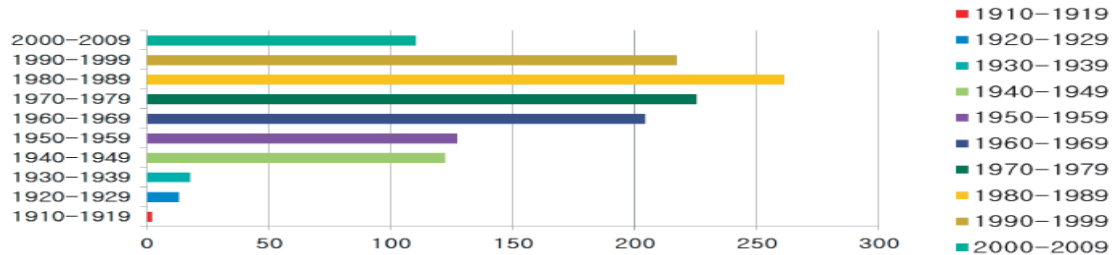


Figure 2.2. A number of dams by construction years.

2.5 Performance of Existing Dams

The behavior of concrete gravity dams subjected to loading is complex because of the interaction of different materials and dam-reservoir-foundation interaction. The behavior depends on the magnitude of the loads. At low loading levels, the dam-foundation system remains permanently elastic, displacements are small, drains are fully active, and full control of the reservoir is maintained. In the elastic range, there are no permanent deformations. Following the onset of nonlinear inelastic behavior, material cracking occurs, deformations may become permanent, drainage characteristics of the dam, and

operation of gates begin to be affected. At this stage, the use of 2D rigid-body analysis may not be appropriate, and 3D modeling and analysis should be considered. Also, excessive deformations may cause visually objectionable cracking and functional disruption. Finally, at ultimate conditions before impending failure, the drains become ineffective due to large deformations, and the structure becomes unstable due to sliding, flotation, or loss of bearing capacity.

The primary source of information on dam failures incidents (failures and accidents) is the International Commission on Large Dams (ICOLD), which maintains the World Register of Dams (ICOLD, 1998), where more than 34,000 dams from over 80 countries are registered. ICOLD has published reports on dam failure and incidents around the world (ICOLD, 1983). Similar reports have been published for incidents in the U.S. (USCOLD, 1976, 1988). Studies based on these data (Wahlstrom, 1975; Johnson, 1976; Blind, 1983; Duffaut, 1986; Douglas et al., 1999) indicate that the primary sources of dam failure have been: overtopping, foundation failure, slides of banks or dam slopes, design and construction errors, cracks in the dam, earthquakes, and acts of war.

The statistics showed that 35% of failures were direct results of floods exceeding the spillway capacity, 25% resulted from foundation problems (such as seepage, piping, excess pore pressures, low cutoff, fault movement, settlement, and rock slides), and the remaining 40% resulted from other causes (improper design and construction, material failure, misuse and acts of war) (Johnson 1976). Concrete gravity dams, however, are less vulnerable to overtopping as compared to embankment dams. The majority of failures or damages in concrete gravity dams have been associated with flaws in the foundation. Unlike the dam, which is above ground and easy to inspect, flaws in the foundation may not be detected until significant damage has been incurred. ICOLD has identified the major aging scenarios. The case histories on the aging of concrete dams are considered to amount to 482. Most failure cases (about 77%) have occurred in the dam body. In the deterioration of the dam body, the reactions between materials and the environment are the primary scenarios; the degradation due to chemical reactions of material with the environment, the loss of strength under permanent and repeated actions, the reduced resistance to freezing and thawing.

Studies of records of dam failures and incidents generally suggest that the annual probability of failure is on the order of 10^{-4} to 10^{-3} . In this case, failure is defined as (a) major structural failure involving the complete abandonment of the dam or (b) severe damage to the dam, which can be successfully repaired and used. For example, it was reported (Cheng, 1993) that the annual probability of failure of gravity dams is 1.1×10^{-3} , while for concrete gravity dams that were commissioned from 1930-1992 and have been in service for at least five years, it is 1.4×10^{-5} (Douglas et al., 1999). It was also shown that this probability varies with age, time of service, and height of the dam. For example, for gravity dams completed in 1941~1950, the annual probability of failure after five years of service was 1.6×10^{-4} , while for dams of height greater than 165 ft (50 m), the probability of failure was given as 4.0×10^{-4} (Cheng, 1993). It is worth noting that human error in the design, construction, or operation of dams, quality assurance, inspection, maintenance schedules, and early warning systems has often played a role in dam incidents and failures.

Douglas et al. (1999) summarized the historical failures of concrete and masonry gravity dams. All failure modes are included, and the results are shown in Table 2.2. The dams built before 1930 has a much higher failure frequency than those built after 1930. The concrete dams fail due to one or combinations of the several causes (FEMA 2006): overtopping caused by floods that exceed the discharge capacity, deliberate acts of sabotage, structural failure of materials used in dam construction, movement or failure of the foundation supporting the dam, settlement and cracking of concrete dams, and inadequate maintenance and upkeep.

Table 2.2. Historical failure of concrete and masonry gravity dams.

Year Commissioned	Annual frequency of failure of Concrete gravity Dams ($\times 10^{-5}$)		
	Overall	First 5 years	After five years
1700 ~ 1929	15	100	9
1930 ~ 1992	3.5	14	1.4

These causes have had an effect on the stability of the concrete gravity dams. The effect of aging on different components of the dam is shown in Figure 2.3, according to ICOLD.

There is a total of 482 cases, each is attributed to a significant aging scenario, and some processes are coupled. These cases do not necessarily represent the aging of concrete dams. Nevertheless, the sample contains sufficient data to be suitable for selecting the major aging scenarios of concrete dams.

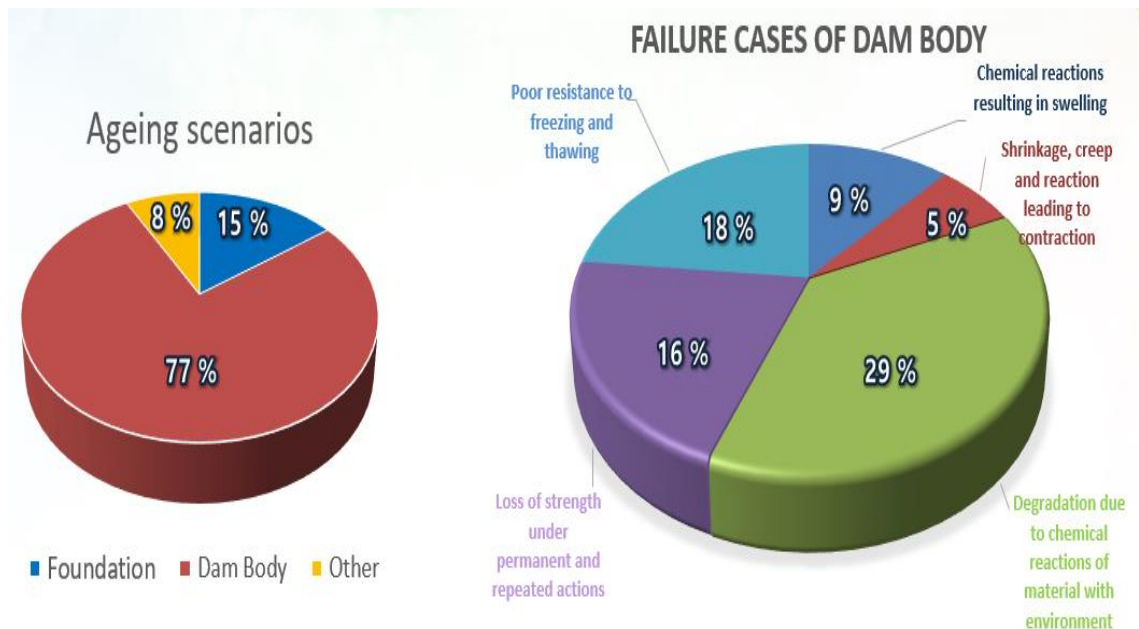


Figure 2.3. Major aging sceneries.

The possible physical and chemical processes causing strength degradation are illustrated in Figures 2.4 and 2.5. As the cracking is widened, the permeability of the material and the volume of water flowing into the concrete increase.

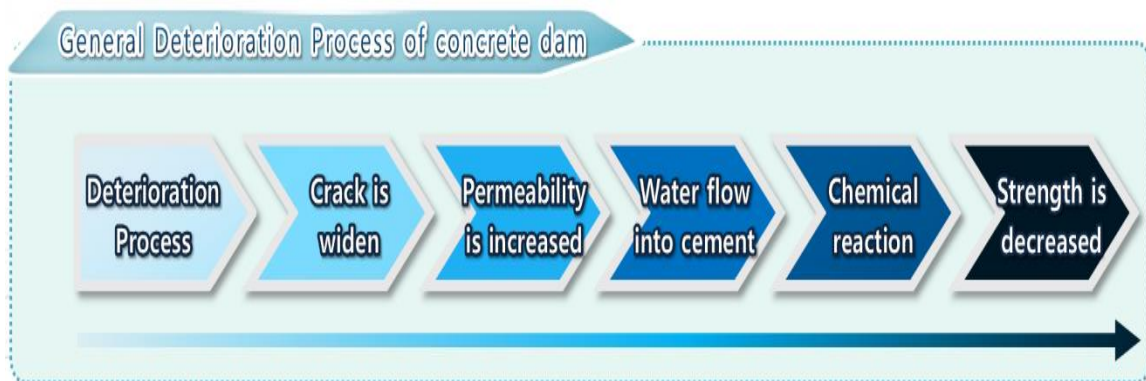


Figure 2.4. General deterioration process of the concrete dam.

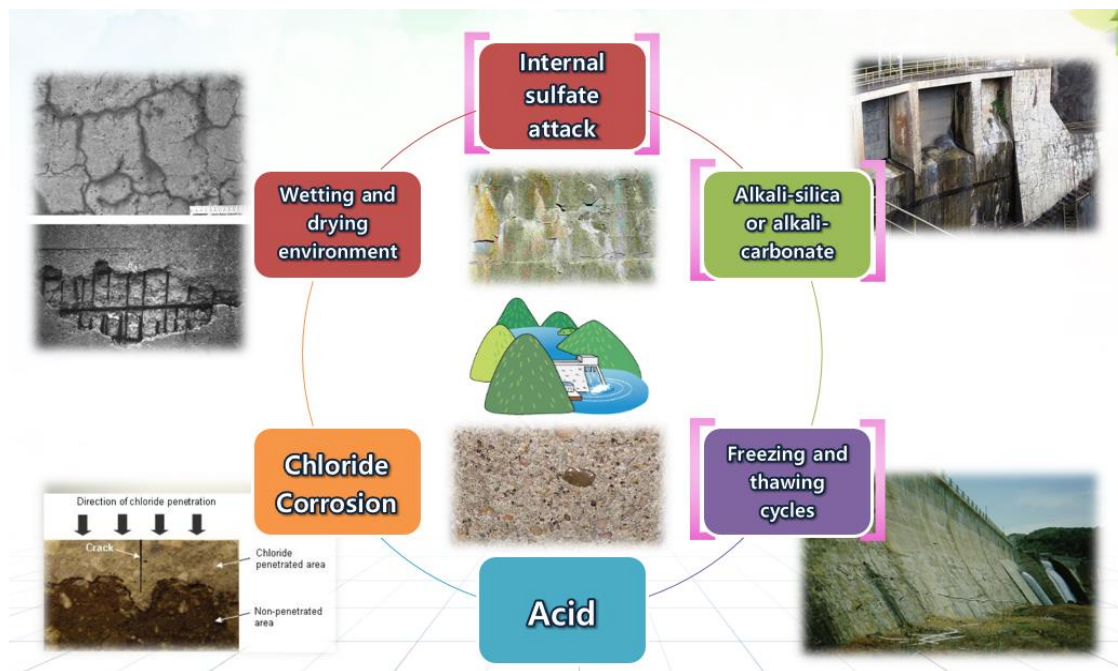


Figure 2.5. External causes of a deterioration process.

2.6 Safety Factor for Different Failure Modes

Failure of a dam can be categorized into three different failure modes: sliding stability, overturning stability, and overstressing (Korea Ministry of Land, 2011), as illustrated in Figure 2.6. The horizontal forces which act against the gravity dam cause overturning moments. However, practically, failure due to overturning does not occur, and a dam will fail by compression (i.e., overstressing) before overturning.

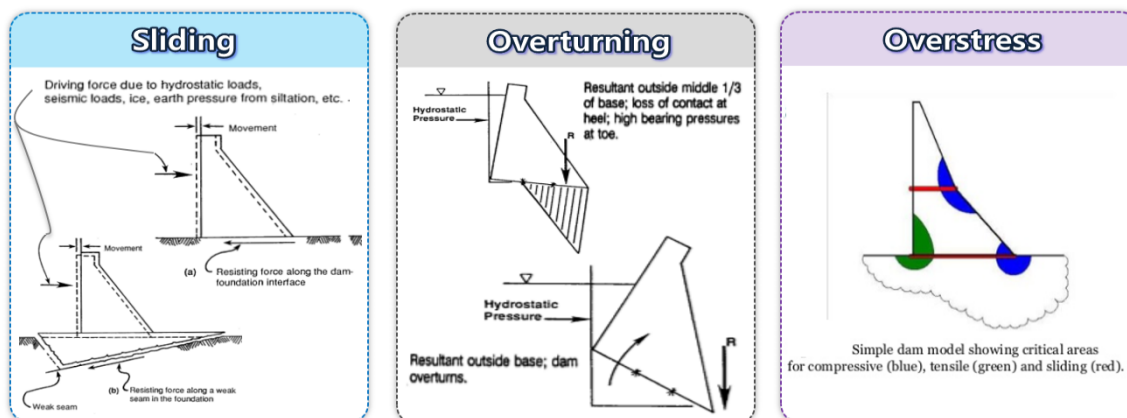


Figure 2.6. Failure modes of concrete dams.

The most used and accepted methods to evaluate safety factor by considering sliding failure mode is based on the Mohr-Coulomb equation, where the maximum allowable tangential stress for each point on the sliding plane is described as (Westberg, 2010):

$$\tau \leq c + \sigma_n \cdot \tan \phi \quad (2.1)$$

where c is the cohesion, σ_n is the effective normal stress to the sliding plane, and ϕ is the friction angle. By considering the contact area, Eq. (2.1) becomes:

$$T \leq \frac{c \cdot A + N \cdot \tan \phi}{S_f} \quad (2.2)$$

where T is the total force parallel to the sliding plane, N is the resultant of the vertical forces over the plane, ϕ is the friction angle, c is the cohesion, A is the total contact area, and S_f is the safety factor applied. As mentioned in Gustafsson et al. (2008) and Westberg (2010), the criterion is shown in Eq. (2.2) considers that, at failure, the ultimate capacity is reached at each point on the sliding surface. This is adequate for ductile materials. However, the sliding planes can often be considered semi-brittle.

In this thesis, sliding along the concrete components and sliding in the rock mass are not considered. For sliding along the concrete-rock interface, according to Gustafsson et al. (2008), the failure of a concrete-rock interface where cohesion exists is a brittle failure and will occur at no or minimal relative displacement to the failure plane. Until failure occurs, the shear resistance can be described by the Mohr-Coulomb criteria mentioned above. If the contact between concrete and rock is intact, the shear resistance, T_R , can be described as (Westberg and Johansson, 2016; Westberg, 2010):

$$T_R = c \cdot A + N' \cdot \tan \phi_i \quad (2.3)$$

where A is the base area, N' is the sufficient reasonable force to the sliding plane ($N' = N - U$, where U is the uplift pressure) and ϕ_i is the internal friction angle in the concrete-rock interface. However, the sliding surface may not be intact; it may be so that the bond within the concrete-rock interface may not exist, or a failure surface may be present. In this case, the shear resistance is given by a total friction angle, which is the sum of a base

friction angle ϕ_b . Furthermore, a dilation angle i which are estimated by the asperities which exist on the foundation surface. These asperities are commonly introduced during the construction of the dams (Westberg, 2010).

The following equation could be used to describe the shear resistance when the bonded contact does not exist or has previously failed,

$$T_R = N' \cdot \tan(\phi_b + i) \quad (2.4)$$

Gustafsson et al. (2008) recommended that only the intact concrete-rock bond may contribute to the shear resistance. If a failure occurs or if significant uncertainties exist concerning the quality of the concrete-rock bond, the shear resistance due to the contribution of the concrete strength should be neglected.

Overstressing will occur if the stresses induced in the dam body or foundation exceed the material capacity. For buttress dams, the front plate (head) will function as a cantilever beam, and one possible failure mode is the overstressing of the cantilever beam. Stresses for the dam body are often calculated based on beam model analysis using Navier's equation:

$$\sigma = \frac{V}{A} \pm \frac{M_c \cdot y_{tp}}{I} \quad (2.5)$$

where V is the vertical force, A the base area, M_c the moment around an axis through the center of gravity of the base area, y_{tp} the distance from the center of gravity to the point of interest and I the moment of inertia. As pointed out by Reinius (1962), the essential requirement for Navier's equation, that plane cross-sections remain plane, is not satisfied, and more significant stress concentrations will, therefore, occur at the heel and toe of the dam. Stresses from finite element analysis will represent the behavior of the response of the dam more accurately.

It is usually assumed (in the cracked base analysis) that if tensile stresses calculated by rigid body analysis occur at the dam heel, a crack will form, and water will percolate the crack, causing full uplift pressure along the whole crack length. The concrete to rock interface has tensile strength that, for all practical purposes, is assumed to be zero (ICOLD

1993). This is because joints or fractures may be located directly below the concrete/rock interface, and the rock mass will then not be able to develop any tensile capacity (FERC, 2002).

Overtipping may occur if the stabilizing forces, mainly from the self-weight, are less than the overturning forces. The criterion, where used, is usually given as:

$$\frac{M_R}{M_S} > S_f \quad (2.6)$$

where S_f is the safety factor defined earlier, M_R is the resisting moment, and M_S is the overturning moment. The overturning moments are calculated with respect to the toe or another point of the dam-foundation interface.

According to Korean Design Standard (2016) and several other design guidelines for dams, the resultant force usually falls within the mid-third of the base area. This comes from the “cracked base criteria” mentioned above: if the resultant force falls outside the mid-third of the base area, tensile forces will occur at the upstream heel of the dam, resulting in the full uplift pressure appearing in the cracks. This means that the criterion of resultant force within the mid-third of the base area is similar to overstressing, not an ultimate limit state.

2.7 Overview of Seismic Response Analysis Based on Finite Element Method

The response of a gravity dam could be solved based on the experimental or numerical method. Experiments are expensive, time-consuming, and usually do not allow much flexibility in parameter variation. Numerical methods have become popular with the development of computing capabilities and widely available software. Modeling of foundation-structure interaction processes is based on a variety of numerical methods (finite difference, finite element, finite volume, spectral, etc.), among which Finite Difference Method (FDM) and Finite Element Method (FEM) are the most popular methods. FEM is preferred by many since it can be used to represent the material

interfaces well. FEM discretizes the domain of the problem into disjoint (non-overlapping) elements and provides the solution at the nodes defining the elements.

There are several governing equations that need to be considered for the dam-reservoir system. The governing equation of wave propagation through the fluid is given by (Chopra and Chakrabarti, 1981):

$$\nabla p^2 = \frac{1}{c^2} \frac{\partial^2 p}{\partial t^2} = \frac{\rho}{\kappa} \frac{\partial^2 p}{\partial t^2}, \quad (2.7)$$

where $c = (\kappa/\rho)^{1/2}$, in which p is the pressure function, c is the acoustic wave speed, ρ is the fluid density, and κ is the fluid compressibility. If the fluid would be incompressible, Eq. (2.7) reduces to $\nabla p^2 = 0$. Solutions to this simplified governing equation could be obtained for some special cases. Since the simplifying assumption may not be appropriate but may not be appropriate in some circumstances, Eq. (2.7) is preferred for the dam-reservoir interaction problem.

The boundary conditions need to be considered to solve Eq. (2.7). In the reservoir upstream boundary (Γ_R) volumetric hydrodynamic pressure waves are created in the reservoir and propagate toward the upstream with the vibration of the dam. If the length of the reservoir is assumed to be infinity, then these waves would vanish. It should be noted that the length of the reservoir is often assumed as a finite length, L , in numerical modeling. Hence, an artificial boundary is applied to simulate the effect of an infinite reservoir in Figure 2.7. This boundary is modeled based on the Sommerfeld boundary as,

$$\frac{\partial p}{\partial n}(x, y, z) = -\frac{1}{c} \left(\frac{\partial p}{\partial t} \right) (x, y, z) , \quad (2.8)$$

For the rigid bottom of the reservoir (Γ_B), by assuming that the pressure gradient can be neglected due to the horizontal movement of the earth, this boundary condition simplifies to,

$$\frac{\partial p}{\partial n}(x, y, z) = 0 \quad (2.9)$$

For the free surface of the reservoir (Γ_F), by neglecting the effects of surface waves, the boundary condition can be stated as:

$$p(x, y, z) = 0 \quad (2.10)$$

For the fluid-structure interface (Γ_I) between the reservoir and the dam body, an interaction occurs, which is the result of an inertia force caused by the movement of the dam wall. The applied pressure on the reservoir face caused by the inertial force is given by,

$$\frac{\partial p}{\partial n}(x, y, z) = -\rho \cdot \ddot{u}_n(x, y, z) \quad (2.11)$$

in which ρ is the density of fluid and \ddot{u}_n is the acceleration vector in the direction normal to the common boundary of the fluid and structure.

For the foundation region boundary conditions, the nodes on edges A and B at the end of the foundation region (see Figure 2.7) are assumed to be constrained in the vertical direction, while it is free in the horizontal direction. The nodes at the horizontal line at the base (edge C) of the foundation region are assumed to be constrained in both directions, vertical and horizontal. The nodes at the interface between the dam body and foundation are coupled in vertical and horizontal directions. The same coupling is applied at the interface between the reservoir and the foundation.

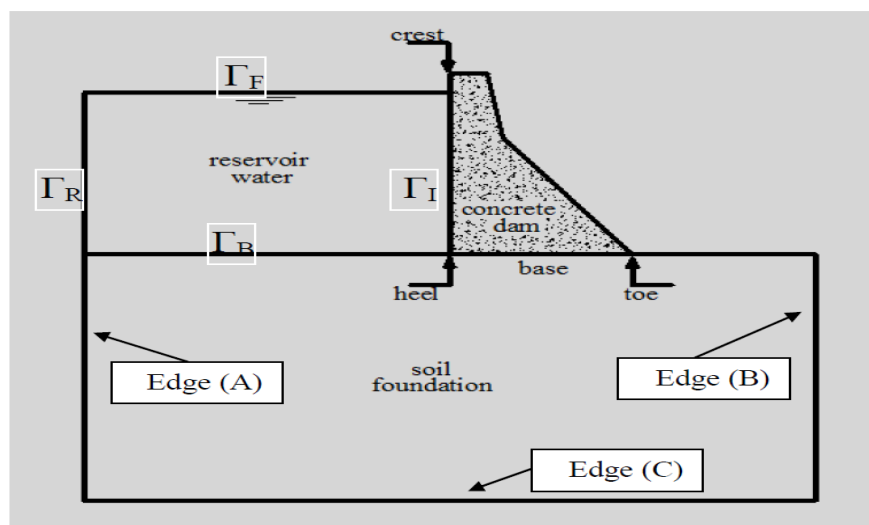


Figure 2.7. Boundary condition of dams.

In using the FEM, displacement vector for the discretized system for the dam can be written as (Zienkiewicz et al., 1981),

$$u = N_u \bar{u} \quad (2.12)$$

and for the fluid is given by,

$$p = N_p \bar{p} \quad (2.13)$$

where u and p are the nodal parameters of each field, and N_u and N_p are shape functions.

The governing equation in the discretized form of the concrete dam and the rock foundation can be written as,

$$[M]\ddot{u} + [C]\dot{u} + [K]\bar{u} - [Q]\bar{p} + [M]\ddot{u}_g = 0 \quad (2.14)$$

and, the coupling term $[Q]$ in Eq. (2.14) arises due to the acceleration and pressure at the dam-reservoir interface and can be expressed as

$$[Q]\bar{p} = \int_{\Gamma_1} N_u^T n p d\Gamma = \left(\int_{\Gamma_1} N_u^T n N_p d\Gamma \right) \bar{p} \quad (2.15)$$

where $[M]$, $[C]$ and $[K]$ are mass, damping, and stiffness matrices of the structure, respectively. \bar{u} , \dot{u} and \ddot{u} are displacement, velocity, and acceleration vectors, \ddot{u}_g is the external acceleration, respectively. In the above n is the direction vector of the normal to the interface.

For the fluid, Eq. (2.7) can be written in the following discretized form,

$$[S]\ddot{u} + [C]\dot{p} + [H]\bar{p} - [Q]^T \ddot{p} + q = 0 \quad (2.16)$$

where $[S]$, $[C]$, $[H]$ and q are pseudo fluid mass matrix, pseudo fluid damping matrix, pseudo fluid stiffness matrix, and prescribed flux vector respectively, Q is a transformation matrix that transforms the acceleration of structure to fluid pressure and also transforms the hydrodynamic pressure into applied loads on the structure to simulate fluid-structure interaction. $[S]$, $[C]$; and $[H]$ are given by,

$$[S] = - \int_{\Omega} N_p^T \frac{1}{c^2} N_p d\Omega + \int_{\Gamma_3} N_p^T \frac{1}{g} N_p d\Omega \quad (2.17)$$

$$[C] = \int_{\Gamma_4} N_p^T \frac{1}{c^2} N_p d\Omega \quad (2.18)$$

and,

$$[H] = \int_{\Omega} \nabla N^T \nabla N d\Omega \quad (2.19)$$

Based on the above, the coupled equation of the dam – reservoir - foundation system subjected to earthquake ground motion can be presented as (Zeidan, 2014):

$$\begin{bmatrix} M & 0 \\ Q^T & S \end{bmatrix} \begin{Bmatrix} \ddot{u} \\ \ddot{p} \end{Bmatrix} + \begin{bmatrix} C & 0 \\ 0 & \tilde{C} \end{bmatrix} \begin{Bmatrix} \dot{u} \\ \dot{p} \end{Bmatrix} + \begin{bmatrix} K & -Q \\ 0 & H \end{bmatrix} \begin{Bmatrix} u \\ p \end{Bmatrix} = \begin{bmatrix} M \cdot I \cdot \ddot{u}_g(t) \\ -\rho Q^T \cdot I \cdot \ddot{u}_g(t) \end{bmatrix} \quad (2.20)$$

2.8 Concrete Plastic Damage Model and Model Implementation

2.8.1 Concrete Plastic Damage Model

Quasi-brittle materials, such as concrete, exhibit nonlinear stress-strain response mainly because of micro-cracking, which could result in failure. In tension, failure is localized in a narrow band; in compression, failure usually begins in the outside and is more complex, involving volumetric expansion, strain localization, crushing, etc. In mixed stress states, failure usually depends on the ratio between the principal stresses. In tension, the behavior is closer to damage than to plasticity; conversely, in compression, the participation of plasticity is higher (Alfarah et al., 2017). The concrete plastic damage model presented in this section is essentially from Alfarah et al. (2017).

A nonlinear concrete response can be represented using plasticity or damage theory. However, none of these formulations alone is able to describe this phenomenon adequately. Plastic models might represent the observed deformation realistically in highly confined concrete but do not capture the stiffness degradation observed in experiments. Damage-based models are based on a gradual reduction of the elastic stiffness. In addition, fracture propagation can be represented by embedded crack models. It has been widely accepted

that the coupling between the damage and plasticity models is essential to capture the nonlinear behavior of concrete (Nguyen and Korsunsky, 2008). The coupled damage and plasticity models for concrete differ mainly in the coupling method and the damage evolution law.

By considering that concrete can be described with a multiaxial model that considers a parallel combination of scalar (isotropic) damaged elasticity and non-associated multi-hardening plasticity, a concrete plastic damage model (CPDM) was developed by Lubliner et al. (1989). This model is adopted to evaluate the nonlinear seismic behavior of the concrete gravity dam in the present study.

Figure 2.8 illustrates the uniaxial stress-strain relation for the plasticity, damage, and damage-plasticity models. Loading branches are represented with solid thick lines and unloading/reloading branches are plotted with dashed thin lines. E_0 is the initial (undamaged) elastic stiffness (deformation modulus), and ε^{el} and ε^{pl} are the elastic (recoverable) and plastic (irrecoverable) strain, respectively. Figure 2.8b shows that damage generates stiffness degradation since the slope of the unloading/reloading branch is $(1 - d)E_0$ where d is a damage variable ranging between 0 (no damage) and 1 (destruction).

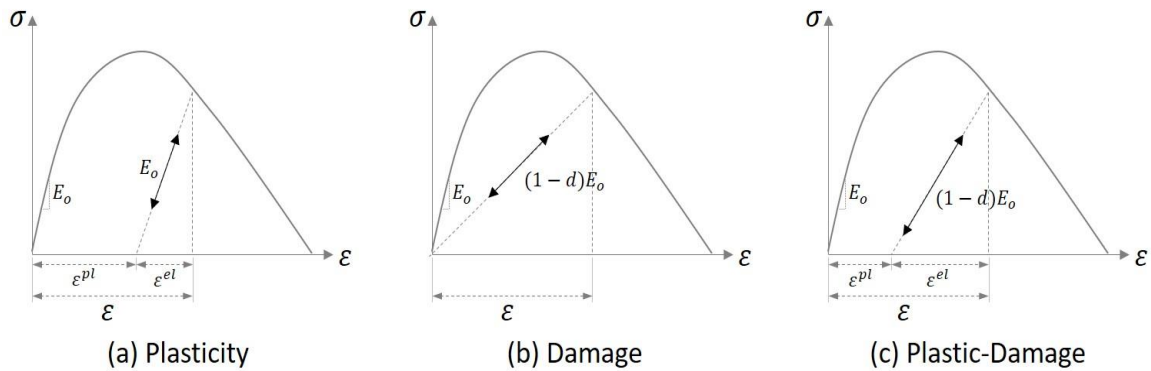


Figure 2.8. Representation of CPDM (after Alfarah et al. (2017)).

For uniaxial compression and tension, the stress-strain relation under uniaxial loading in the damage-plasticity behavior shown in Figure 2.8c can be written as:

$$\sigma_c = (1 - d_c)E_0(\varepsilon_c - \varepsilon_c^{pl}) \quad (2.21)$$

and,

$$\sigma_t = (1 - d_t)E_0(\varepsilon_t - \varepsilon_t^{pl}) \quad (2.22)$$

where the subscripts c and t refer to compression and tension, respectively. For uniaxial cyclic loading-unloading conditions, the damage plasticity model assumes that the degradation in the elastic stiffness is given by,

$$E = (1 - d)E_0 \quad (2.23)$$

where E is the reduced tangent stiffness, and d is a scalar degradation variable that is a function of stress state and compression and tension damage variables (d_c and d_t , respectively). d is given by,

$$1 - d = (1 - S_t d_c)(1 - S_c d_t) \quad (2.24)$$

In Eq. (2.24), S_c and S_t are dimensionless coefficients accounting for stress state and stiffness recovery effects, being given by,

$$S_c = 1 - h_c(1 - r^*(\sigma_{11})) \quad (2.25)$$

and,

$$S_t = 1 - h_t r^*(\sigma_{11}) \quad (2.26)$$

where σ_{11} is the first principal uniaxial stress (positive for tension), r^* is a stress state parameter being $r^*(\sigma_{11}) = 1$ for tension and $r^*(\sigma_{11}) = 0$ for compression, and h_c and h_t are weighting factors ranging between 0 and 1. h_c accounts for re-closing of cracks after tension-compression reversal; h_t represents a recovery of crushed concrete after compression-tension reversal. In this work, $h_c = 0.9$ and $h_t = 0$ is assumed; this means that 90% of the cracks close upon tension-compression reversal, and the crushed concrete does not experience any recovery. An illustration of the uniaxial stress-strain

loading-unloading behavior is presented in Figure 2.9, where the numbers given in the plot described the loading-unloading sequence.

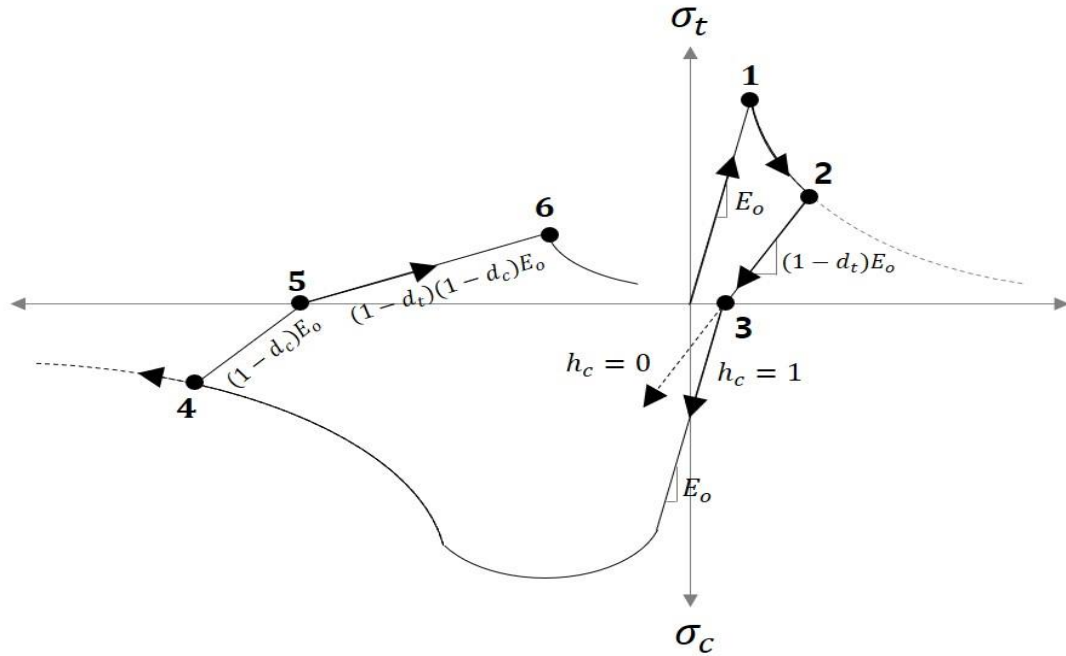


**Figure 2.9. Uniaxial loading-unloading law
(redrawn after Alfarah et al., 2017).**

For multiaxial condition, the stress-strain relationship is given by:

$$\sigma = (1 - d)D_0^{el} : (\varepsilon - \varepsilon^{pl}) \quad (2.27)$$

where D_0^{el} is the initial elastic stiffness tensor, and σ and ε are the stress and strain tensors, respectively. Scalar damage variable d retains the same meaning as for the uniaxial case, except that the scalar factor r^* for the uniaxial case is replaced by its corresponding multiaxial notation (i.e., the stress in $r^*(\sigma_{11})$ is replaced by its corresponding stress in multiaxial stresses).

The yield condition for the plasticity model is based on the loading function F given by Lubliner et al. (1989),

$$F = \frac{1}{1-\alpha} [q - 3\alpha\rho + \beta\langle\sigma_{max}\rangle - \gamma - \langle\sigma_{max}\rangle] - \bar{\sigma}_c = 0 \quad (2.28)$$

and,

$$\alpha = \frac{(f_{b0}/f_{c0})-1}{2(f_{b0}/f_{c0})-1}; \quad \beta = \frac{\bar{\sigma}_c}{\bar{\sigma}_t}(1 - \alpha) - (1 + \alpha); \quad \gamma = \frac{3(1-K_c)}{2K_c-1} \quad (2.29)$$

where $\langle \cdot \rangle$ is the Macaulay bracket (a notation used to describe the ramp function), p is the hydrostatic pressure stress, q is the Von Mises-equivalent effective stress (effective stress accounts for stress divided by $1 - d$), and f_{b0} and f_{c0} are the biaxial and uniaxial compressive yield strengths, respectively; since $f_{b0} \geq f_{c0}$, α ranges between 0 ($f_{b0} = f_{c0}$) and 0.5 ($f_{b0} \geq f_{c0}$). In Eqs. (2.28) and (2.29), σ_{max} is the maximum principal effective stress, and $\bar{\sigma}_c$ and $\bar{\sigma}_t$ are the effective compressive and tensile cohesion stress, respectively; $\bar{\sigma}_c$ and $\bar{\sigma}_t$ are defined as $\bar{\sigma}_c = \sigma_c/(1 - d_c)$ and $\bar{\sigma}_t = \sigma_t/(1 - d_t)$, and K_c is the ratio of other stress invariants on tensile and compressive meridians.

The plasticity model assumes non-associated potential plastic flow. The flow potential G is the Drucker-Prager hyperbolic function given by:

$$G = \sqrt{(\epsilon\sigma_{t0} \tan \psi)^2 + q^2} - p \tan \psi \quad (2.30)$$

where σ_{t0} is the uniaxial tensile stress at failure, ϵ is the eccentricity of the potential plastic surface, and ψ is the dilatancy angle measured in $p - q$ (deviatory) plan at high confining pressure.

As discussed previously, K_c is the ratio between the magnitudes of deviatoric stress in uniaxial tension and compression; K_c ranges between 0.5 (Rankine yield surface) and 1 (Von Mises). In this study, K_c is obtained from the Mohr-Coulomb yield surface function in cylindrical coordinates:

$$H(\rho, \xi, \theta, \phi, c) = \sqrt{2}\xi \sin \phi + \sqrt{3}\rho \cos \theta - \rho \sin \theta \sin \phi - \sqrt{6} c \cos \phi = 0 \quad (2.31)$$

where ρ is the octahedral radius, ξ is the distance from the origin of stress space to the stress plan, θ is the Lode similarity angle, ϕ is the friction angle, and c is the cohesion. In Eq. (2.31), $\rho = \sqrt{2J_2}$, $\xi = I_1/\sqrt{3}$, and $\sin \theta = 3\sqrt{3}J_3/2J_2^{3/2}$; I_1 is the first invariant of stress tensor and J_2 and J_3 are the second and third invariants of the deviatoric stress tensor, respectively.

For $\xi = 0$ and $\theta = \pm \pi/6$ (negative and positive for tension and compression meridian plans), the magnitudes of deviatory stress in uniaxial compression and tension at yield (ρ_{c0} and ρ_{t0}) and K_c are,

$$\rho_{c0} = \frac{2c\sqrt{6} \cos \phi}{3 - \sin \phi}, \rho_{t0} = \frac{2c\sqrt{6} \cos \phi}{3 + \sin \phi}, K_c = \frac{\rho_{t0}}{\rho_{c0}} = \frac{3 - \sin \phi}{3 + \sin \phi} \quad (2.32)$$

By assuming that $\phi = 32^\circ$ in Eq. (2.32) (Oller, 2014), an illustration of the yield surface in the deviatory plan for several values of K_c ranging from 0.5 to 1 is presented in Figure 2.10, where C.M. and T.M. denote the compression and tension meridian plans, respectively.

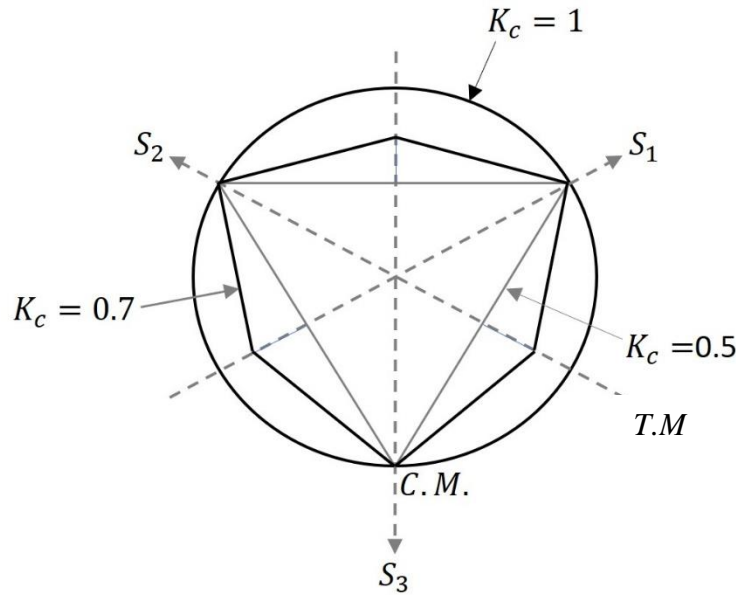


Figure 2.10. Yield surface in the deviatory plan for several values of K_c . (redrawn after Alfarah et al., 2017).

Eqs. (2.30), (2.28) and (2.29) show that concrete behavior depends on four constitutive parameters $K_c, \psi, f_{t0}/f_{c0}, \epsilon$; it can be assumed that $\psi = 13^\circ$ (Vermeer et al., 1984). The parameters of CPDM adopted in this thesis work are summarized in Table 2.3.

Table 2.3. Parameters of CPDM.

K_c	$\psi(^{\circ})$	f_{t0}/f_{c0}	ϵ
0.7	13	1.16	0.1

2.8.2 Damage Functions for Concrete in compression and tension

Consider the uniaxial model of concrete behavior illustrated in Figure 2.11, where ε_c^{ch} and ε_{c0}^{el} are the crushing and undamaged elastic components of strain, respectively; ε_c^{pl} and ε_c^{el} are the plastic and damaged elastic components, respectively. ε_c^{ck} and ε_{t0}^{el} are the cracking and elastic undamaged strain components, respectively; ε_t^{pl} and ε_t^{el} are the plastic and damaged elastic components, respectively.

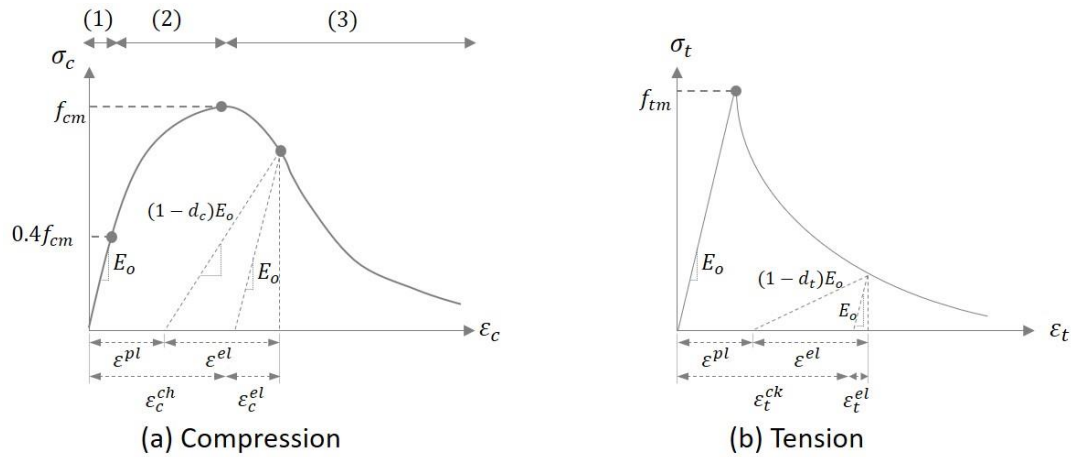


Figure 2.11. Assumed uniaxial model of concrete behavior (after Alfarah et al., 2017).

The approach for calculating the damage variables starts from the definition of the portion of the normalized energy dissipated by compression (i.e., damage function due to compression) d_c , and the portion of normalized energy dissipated tension (i.e., damage function due to tension) d_t (Alfarah et al., 2017):

$$d_c = \frac{1}{g_c} \int_0^{\varepsilon_c^{ch}} \sigma_c d\varepsilon_c^{ch}, d_t = \frac{1}{g_t} \int_0^{\varepsilon_t^{ck}} \sigma_t d\varepsilon_t^{ck} \quad (2.33)$$

where and the normalization coefficients g_c and g_t represent the energies per unit volume dissipated by damage along the entire deterioration process are given by,

$$g_c = \int_0^{\infty} \sigma_c d\varepsilon_c^{ch}, g_t = \int_0^{\infty} \sigma_t d\varepsilon_t^{ck} \quad (2.34)$$

Note that in Figure 2.11,

As can be observed from the definition, d_c and d_t range between 0 (no damage) and 1 (complete damage). The energies per unit area and unit volume are related by $g_c = G_{ch}/l_{eq}$ and $g_t = G_F/l_{eq}$, where G_{ch} and G_F are material parameters defined as crushing and fracture energies, and l_{eq} is the characteristic length of the element (Alfarah et al., 2017).

The relation between compressive stress σ_c and crushing strain ε_c^{ch} And the relation between tensile stress σ_t and cracking strain ε_t^{ck} are (Lubliner et al., 1989):

$$\sigma_c = f_{c0}[(1 + a_c) \exp(-b_c \varepsilon_c^{ch}) - a_c \exp(-2b_c \varepsilon_c^{ch})] \quad (2.35)$$

and,

$$\sigma_t = f_{t0}[(1 + a_t) \exp(-b_t \varepsilon_t^{ck}) - a_t \exp(-2b_t \varepsilon_t^{ck})] \quad (2.36)$$

In Eqs. (2.35) and (2.36), f_{c0} and f_{t0} are the compressive and tensile stresses that correspond to zero crushing ($\varepsilon_c^{ch} = 0$) and to onset of cracking ($\varepsilon_t^{ck} = 0$), respectively; As well, a_c, a_t, b_c and b_t are dimensionless coefficients to be determined. Substituting Eqs. (2.35) and (2.36) into Eq. (2.34), results in:

$$g_c = \frac{f_{c0}}{b_c} \left(1 + \frac{a_c}{2}\right), \quad g_t = \frac{f_{t0}}{b_t} \left(1 + \frac{a_t}{2}\right) \quad (2.37)$$

Using the definition $g_c = G_{ch}/l_{eq}$ and $g_t = G_F/l_{eq}$ in Eq. (2.37) leads to:

$$b_c = \frac{f_{c0} l_{eq}}{G_{ch}} \left(1 + \frac{a_c}{2}\right), \quad b_t = \frac{f_{t0} l_{eq}}{G_F} \left(1 + \frac{a_t}{2}\right) \quad (2.38)$$

By substituting results (2.35) to (2.37) in Eq. (2.33), the compressive and tension damage functions per unit length are:

$$d_c = 1 - \frac{1}{2+a_c} [2(1 + a_c) \exp(-b_c \varepsilon_c^{ch}) - a_c \exp(-2b_c \varepsilon_c^{ch})] \quad (2.39)$$

and

$$d_t = 1 - \frac{1}{2+a_t} [2(1 + a_t) \exp(-b_t \varepsilon_t^{ck}) - a_t \exp(-2b_t \varepsilon_t^{ck})] \quad (2.40)$$

For a_c and a_t not equal to zero, these equations can be re-written as:

$$\exp(-b_c \varepsilon_c^{ch}) = \frac{1}{a_c} [1 + a_c - \sqrt{1 + a_c(2 + a_c)d_c}] \quad (2.41)$$

and,

$$\exp(-b_t \varepsilon_t^{ck}) = \frac{1}{a_t} [1 + a_t - \sqrt{1 + a_t(2 + a_t)d_t}] \quad (2.42)$$

By zeroing derivatives of σ_c and σ_t (Eqs. (2.35) and (2.36), respectively) with respect to, respectively, crushing and cracking strain, the maximum values f_{cm} and f_{tm} (Figure 2.11) are obtained:

$$f_{cm} = \frac{f_{c0}(1+a_c)^2}{4a_c}, \quad f_{tm} = \frac{f_{t0}(1+a_t)^2}{4a_t} \quad (2.43)$$

From Eq. (2.43), one has,

$$a_c = 2(f_{cm}/f_{c0}) - 1 + 2\sqrt{(f_{cm}/f_{c0})^2 - (f_{cm}/f_{c0})} \quad (2.44)$$

$$a_t = 2(f_{tm}/f_{t0}) - 1 + 2\sqrt{(f_{tm}/f_{t0})^2 - (f_{tm}/f_{t0})} \quad (2.45)$$

The above shows that the parameters a_c, a_t, b_c and b_t can be determined based on $f_{cm}, f_{c0}, f_{tm}, f_{t0}, l_{eq}, G_{ch}$ and G_F . Once these parameters are known, the damage functions that are defined in Eqs. (2.39) and (2.40) can be evaluated.

Before explaining the use of the damage functions, a few words on the compressive and tensile model presented in Figure 2.11 and its relation to the damage-plasticity behavior presented in Figure 2.8c is in order. Thick solid lines in Figure 2.11 display the constitutive laws, and the thin dashed lines represent the unloading/reloading branches. The ascending compressive segments in Figure 2.11a follows CEB-FIP (Model Code 2010), and the descending segment is the one described in Krätzig et al. (2004). Tensile stress-strain relation consists of an initial linear segment and a nonlinear descending branch, as shown in Figure 2.11b. Both compressive and tensile descending branches are generated to ensure nearly mesh-independency.

The application of the CPDM proposed by Alfarah et al. (2017) was extensively discussed in their study. In Figure 2.11, f_{cm} and f_{tm} represent predicted compressive and tensile strengths, respectively; corresponding strains are ε_{cm} and ε_{tm} , respectively.

The first segment in Figure 2.11a is linear, $\sigma_{c(1)} = E_0 \varepsilon_c$, reaching $0.4 f_{cm}$; second (ascending) segment (in between $0.4 f_{cm}$ and f_{cm}) is quadratic:

$$\sigma_{c(2)} = \frac{E_{ci}(\varepsilon_c/f_{cm}) - (\varepsilon_c/\varepsilon_{cm})^2}{1 + (E_{ci}(\varepsilon_{cm}/f_{cm}) - 2)(\varepsilon_c/\varepsilon_{cm})} f_{cm} \quad (2.46)$$

where E_{ci} is the modulus of deformation of concrete for zero stress, in which $E_{ci} = 10000 f_{cm}^{1/3}$ and $E_0 = (0.8 + 0.2 f_{cm}/88) E_{ci}$ (MPa). In the initial linear branch, E_0 is the secant modulus that corresponds to $0.4 f_{cm}$ stress.

The third (descending) segment is given by:

$$\sigma_{c(3)} = \left(\frac{2 + \gamma_c f_{cm} \varepsilon_{cm}}{2 f_{cm}} - \gamma_c \varepsilon_c + \frac{\varepsilon_c^2 \gamma_c}{2 \varepsilon_{cm}} \right)^{-1} \quad (2.47)$$

and,

$$\gamma_c = \frac{\pi^2 f_{cm} \varepsilon_{cm}}{2 [G_{ch}/l_{eq} - 0.5 f_{cm} (\varepsilon_{cm} (1-b) + b (f_{cm}/E_0))]^2}, \quad b = \frac{\varepsilon_c^{pl}}{\varepsilon_c} \quad (2.48)$$

G_{ch} and l_{eq} depend on the mesh size, the type of finite element, and the crack direction. By assuming the behavior of a single band of cracks, the characteristic length can be determined after the mesh size is defined.

Based on experimental observations, b in Eq. (2.28) can be initially assumed to be equal to 0.9. After calculating the damage variables, the average value of b along with the relevant strain range is obtained; iterative calculations are performed until convergence is achieved. The final value of b affects the softening branch of the compressive stress-strain relation (Eqs. (2.47) and (2.48)). Eq. (2.47) shows that the descending branch approaches asymptotically zero; therefore, a fictitious maximum strain should be selected for calculation purposes. The maximum strain value should fulfill the crushing energy in

Eq. (2.52) is equal to the area under the corresponding compressive stress-strain law multiplied by the characteristic length.

Regarding tensile behavior, given a crack width ω , the ratio between tensile stress $\sigma_t(\omega)$ and maximum tensile strength f_{tm} , is given (Hordijk, 1992):

$$\frac{\sigma_t(\omega)}{f_{tm}} = \left[1 + \left(c_1 \frac{\omega}{\omega_c} \right)^3 \right] e^{-c_2 \frac{\omega}{\omega_c}} - \frac{\omega}{\omega_c} (1 + c_1^3) e^{-c_2} \quad (2.49)$$

where $c_1 = 3$, $c_2 = 6.93$, and ω_c is the critical crack opening. Eq. (2.49) shows that $\sigma_t(0) = f_{tm}$ and $\sigma_t(\omega_c) = 0$. Therefore, ω_c can be considered as the fracture crack opening. ω_c is related to G_F per unit area (Hordijk, 1992):

$$\omega_c = 5.14 G_F / f_{tm} \quad (2.50)$$

According to CEB-FIP (Model Code, 2010), G_F (N/mm) can be calculated using,

$$G_F = 0.073 f_{cm}^{0.18} \quad (2.51)$$

where f_{cm} is in MPa. The ratio between crushing and fracture energies can be assumed proportional to the square of the ratio between compressive and tensile strengths (Oller, 1988):

$$G_{ch} = (f_{cm}/f_{tm})^2 G_F \quad (2.52)$$

In the present study, the actual crack spacing is not investigated. It has been assumed that there is a single crack per element. This assumption is considered to be adequate for assessing the overall concrete gravity dams (Alfarah et al., 2017). Based on this assumption, for the descending segment of the tensile stress-strain curve (Figure 2.11b), the strain can be obtained in terms of the crack opening from the following kinematic relation: (Alfarah et al., 2017))

$$\varepsilon_t = \varepsilon_{tm} - \omega / l_{eq} \quad (2.53)$$

Following the formulation described above, the implementation of the CPDM, according to Alfarah et al. (2017), can be carried out by using the following steps (the stress is in MPa):

1) Provide the concrete compressive strength f_{ck} , the parameters in Table 2.3, the mesh size l_{eq} , and the ratio b (Eq. (2.48)), which is initially assumed to be 0.9;

2) Calculate the compressive and tensile stress strength;

$$f_{cm} = (f_{ck} + 8) \text{ and } f_{ct} = 0.3016 f_{ck}^{2/3} \quad (2.54)$$

3) Assign $\varepsilon_{cm} = 0.0022$, and calculate the initial tangent modulus of deformation of concrete E_{ci} and the undamaged modulus of deformation $E_0 = E_{ci} (0.8 + 0.2 f_{cm}/88)$;

4) Calculate $G_F = 0.073 f_{cm}^{0.18} / G_{ch} = (f_{cm}/f_{tm})^2 G_F$, (N/mm), and the critical crack opening $\omega_c = 5.14 G_F / f_{tm}$;

5) Define the first, second, and third segments of the concrete uniaxial compressive law for compression (i.e., $\sigma_{c(1)} = E_0 \varepsilon_c$, Eq. (2.46), and Eq. (2.47)). In Eq. (2.47), a strain is bounded; the selected upper bound should fulfill the condition that the crushing energy G_{ch} (Eq. (2.52)) is reached;

6) Define the first and second segments of the concrete uniaxial tensile law for tension (i.e., $\sigma_{t(1)} = E_0 \varepsilon_t$, Eqs. (2.49) and (2.53)).

7) Calculate the damage parameters according to equations (2.39), (2.40), (2.44) and (2.45);

8) Calculate the damage functions d_c and d_t (Eqs. (2.39) and (2.40));

9) Calculate the compressive and tensile plastic strains (i.e., $\varepsilon_c^{pl} = \varepsilon_c^{ch} - \sigma_c d_c / (1 - d_c) E_0$, and $\varepsilon_t^{pl} = \varepsilon_t^{ck} - \sigma_t d_t / (1 - d_t) E_0$);

10) Calculate the average value of ratio $b = \varepsilon_c^{pl} / \varepsilon_c^{ch}$ and compare it with its previous value. Repeat until an adopted convergence criterion is achieved.

Note that the sophisticated stress-strain model described above is already built-in in ABAQUS. The model parameters are to be provided by the user. These parameters are to be calibrated for the concrete gravity dam in the following chapters and used for numerical analysis to be carried out.

2.9 Summary

The literature review carried out on the analysis of the dam indicates that the aging effects of a concrete dam are not considered in the simple traditional static analysis. The simple design procedure cannot take into account the magnitude of the uncertainty in the random variables involved in concrete gravity design. The finite element method could be considered to overcome some of the simplifying assumptions adopted in the simple design procedure. The essentially theoretical background to analyze concrete gravity dams by using the finite element model found in the literature is reviewed, summarized, and to be applied in the subsequent chapters.

Aging affects the safety of dams. Major aging scenarios of concrete dams are identified. A proper evaluation of the concrete capacity of an aging dam is essential. It was pointed out that the previous seismic analysis of concrete gravity dams often neglects the time-varying deterioration of the concrete strength. The strength degradation of concrete is a very complex process. A damage assessment model of the concrete strength by considering both the concrete crushing and cracking is assembled based on the nonlinear material behavior and concrete plasticity damage model (CPDM). Specific formulations to assess the damage (i.e., damage functions) (i.e., the model is given by Alfarah et al. 2017) are summarized. The steps for their implementation are given and to be employed in the following chapters for the numerical analysis.

It was pointed out that the sophisticated model given in Alfarah et al. (2017) does not consider the gain and reduction of the concrete strength due to aging and degradation. These aspects are to be discussed in the following chapter, and their effects are to be incorporated in this concrete plastic damage model for the numerical analysis to be carried out in the present thesis.

Chapter 3

3 Degradation Modeling of Concrete in Concrete Gravity Dam and Its Application

3.1 Introduction

A concrete gravity dam is generally constructed crossing a river to sustain a considerable amount of water in the upstream face for the purpose of irrigation and power generation. Dams have excellent durability and the capacity to retain their operational requirements. However, concrete does suffer deterioration over time, causing a reduction in its strength. The deterioration of a dam is interpreted as any change in dam properties with the passage of time if these changes affect dam safety. The entire life of a dam might be divided into periods of young, medium, and old age.

The first years, which are called a young age, are characterized by irreversible deformations, high plastic deformations, and lower material parameters (modulus of elasticity, compressive, and tensile strength). Due to the amount of creep present during the first years, stress concentrations are reduced, and stress redistribution takes place in the dam. During the medium age, dam behavior is characterized by a stable condition. An improvement in the material strength is expected due to hydration during the periods of young and medium ages. Old age is associated with strength degradation affecting structural safety. The aging of a dam includes the dam structure together with grouting works, joints, etc. (Zenz, 2008). According to ICOLD (1993), aging is defined as a class of deterioration associated with time-related changes in the properties of the materials of which the structure and its foundation are constructed. The degradation due to aging is of concern for the design, construction, and operation of dams. This concern extends over the entire life of the dam from construction until the safe abandonment or demolition, as illustrated in Figure 3.1, which identifies the aging effects. Major aging scenarios identified by ICOLD (1993) are summarized in Table 3.1 (see further discussion in Chapter 2). Although these cases do not necessarily represent the aging of concrete dams, the statistics could be used as a guide in selecting the major aging scenarios for concrete dams.

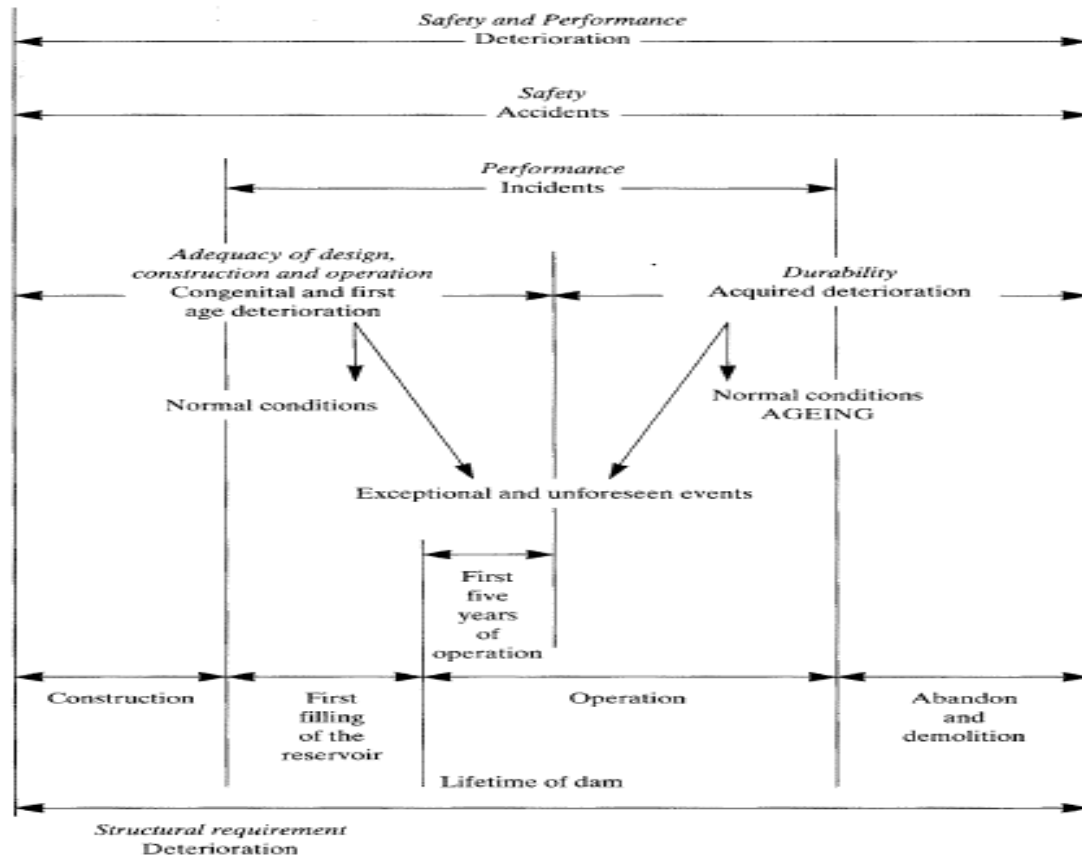


Figure 3.1. Deterioration process with time (after ICOLD 1993).

Table 3.1. Major aging scenarios for concrete dams.

Aging scenarios	Total No.	Cases No.	Description
Foundation (Rock mass)	72 (15%)	37 (8%)	Loss of strength
		11 (2%)	Erosion and solution
		24 (5%)	Aging of grout curtains and of drainage systems
Dam body (concrete)	372 (77%)	45 (9%)	Chemical reactions resulting in swelling
		23 (5%)	Shrinkage, creep, and reaction
		142 (29%)	Degradation due to chemical reactions of material with the environment
		75 (16%)	Loss of strength
		87 (18%)	Poor resistance to freezing and thawing
other	38 (8%)	9 (2%)	Aging of structural joint
		26 (5%)	Aging of upstream facings
		3 (1%)	Aging of pre-stressed structures
482 (100%)			The number of case histories

There are a number of chemical and environmental actions that aggressively attack cement concrete and cause degradation: sulfate, alkali-silica or alkali-carbonate, freezing and thawing, acid, chloride, wetting and drying environment. The three most critical deterioration mechanisms affecting hydraulic structures are sulfate attack, alkali-silica reaction, and freezing-thawing attack. Internal sulfate attack (ISA) is a chemical degradation of cement paste caused by high concentrations of sulfates in soils and groundwater. ISA is caused by chemical interactions between sulfate ions and constituents of the cement paste. The disintegration appears to be caused by chemical reactions with cement hydration products and the formation of a secondary compound, accompanied by a large volumetric expansion and cracking of the concrete. Alkali aggregate reactions (AAR) are the chemical reactions between certain specific mineralogical types of aggregates (sand or gravel) and the alkali compounds (generally less than 2 percent of the cement composition) of cement in the presence of moisture. The reaction products have a swelling nature, leading to tensile stresses that cause micro-cracking within the concrete. Freezing and thawing (FT) deterioration is the deleterious expansion of water within the cement paste, destroying the concrete matrix. When confined within a rigid, the expanding ice crystals can exert pressures far exceeding the tensile capacity of the paste, causing cracking and, ultimately, the disintegration of the concrete.

A literature review of degradation modeling for structures and infrastructure indicates that the modeling is often carried out based on physical models or probabilistic models (Frangopol et al., 2004; Nicolai, 2008). The degradation caused by different mechanisms may share the same time-varying functional form (Pantazopoulou and Papoulia, 2001; Castanier et al., 2005; Ching and Leu, 2009). The degradation could generally be broken down into two phases, an initiation phase, where degradation is unobservable on the surface, and a propagation phase during which the default is observable on the surface. Physics-based models are models based on the simulation of the physics of deterioration and failure (Nicolai et al., 2007; Vaidya and Rausand, 2011; Rakotovo et al., 2015). One of the difficulties of using a physics-based model is associated with the calibration of model parameters and computation effort. A probabilistic model could be a simple data-driven empirical model with uncertainty model parameters, allowing modeling the evolution of the degradation using observations (Singpurwalla, 1995). A probabilistic model can also

be based on a stochastic process with its model parameters estimated from experimental results. Some of the stochastic processes adopted to model the degradation include the Markov chains (Welte et al., 2006; Besnard and Bertling, 2010; Sun et al., 2012; Bastidas-Arteaga and Schoefs, 2012; O'Connor and Kenshel, 2013), Gaussian or Wiener process (Whitmore, 1995; Nicolai et al., 2007; Wang et al., 2011; Si et al., 2013; Guo et al., 2013), and the gamma process (Abdel-Hameed, 1975; Singpurwalla, 1995; Nicolai et al., 2007; Van Noortwijk, 2009; Vatn, 2012). The use of the gamma process is preferred for its monotonically increasing property and infinitesimal divisibility.

In this Chapter study, we focus on modeling the deterioration of the concrete strength of the aging dam by considering both the gain and degradation due to concrete aging. For modeling, we adopt the gamma process. We consider the reactions between materials and the environment (i.e., the degradation due to chemical reactions of material with the environment) and the loss of strength under permanent and repeated actions. In the following section, we first summarized the properties of the gamma process. We then discuss how the gamma process could be used to cope with very limited available experimental results of aging and degrading concrete strength models.

3.2 Modeling Time-Varying Concrete Strength

3.2.1 Modeling Degradation Using Gamma Process

The gamma process is a stochastic process with independent non-negative increments having a gamma distribution with identical scale parameters. It was used by Abdel-Hameed (1975) to model the degradation of wear. It is also used to model corrosion, erosion wear, and creep of materials (Van Noortwijk, 2009). The gamma process is described in the following mathematical terms. Consider a random variable, X , that is gamma distributed with the shape parameter $\nu > 0$ and scale parameter $u > 0$. The probability density function of X is given by (Benjamin and Cornell, 1970),

$$\text{Ga}(x|\nu, u) = \frac{u^\nu}{\Gamma(\nu)} x^{\nu-1} \exp\{-ux\} 1_{(0,\infty)}(x) \quad (3.1)$$

where $1_A(x) = 1$ for $A \ni x$ and $1_A(x) = 0$ for $A \not\ni x$, and $\Gamma(a) = \int_{z=0}^{\infty} z^{a-1} e^{-z} dz$ is a Gamma function for $a > 0$. Furthermore, let v be a function of time t , $v(t)$, and let $v(t)$ be a non-decreasing, right continuous, real-valued function for $t \geq 0$ with $v(0) \equiv 0$. The gamma process with shape function $v(t) > 0$ and scale parameter $u > 0$ is a continuous-time stochastic process $\{X(t), t \geq 0\}$ with the following properties:

- (1) $X(0) = 0$ with probability one,
- (2) $X(\tau) - X(t) \sim Ga(x(\tau) - x(t) | v(\tau) - v(t), u)$ for all $\tau > t \geq 0$,
- (3) $X(t)$ has independent increments.

If $X(t)$ denotes the decrement of concrete strength by degradation at time $t, t \geq 0$, and the probability density function $X(t)$, which is represented by the gamma process, $f_{X(t)}(x)$ is given by,

$$f_{X(t)}(x) = Ga(x | v(t), u) \quad (3.2)$$

where the mean of the process is given by $E(X(t)) = \mu = v(t)/u$ and the variance of the process is given by $\text{Var}(X(t)) = \sigma^2 = v(t)/u^2$.

If the initial strength is denoted by f_{co} , the strength at time t , $f_D(t)$, by only considering the degradation is given by $f_{co} - X(t)$ in Figure 3.2. The degradation increment from time $t_i - h$ to t_i , $X(t_i) - X(t_i - h)$, is a non-negative value that is independent of the cumulative degradation at the time $t_i - h$, $X(t_i - h)$. The increment is gamma distributed with shape parameter $v(t_i) - v(t_i - h)$ and scale parameter u . The degradation increment from any time $X(t)$ is an independent random variable. The path of the gamma process is monotone in Figure 3.2. In the following, the normalized degradation, $DI(t)$,

$$DI(t) = \frac{f_{co} - f_D(t)}{f_{co}} = \frac{X(t)}{f_{co}} = \frac{\Sigma(X(t_i) - X(t_i - h))}{f_{co}}, i = 1, 2, \dots, t, h > 0 \quad (3.3)$$

is referred to as the damage index function, where $t_1-h = 0$. $DI(t)$ is a monotonic increasing function and varies from 0 (undamaged) to 1 (completely damaged), $f_D(t)$ is the concrete strength at time t by taking into account the strength degradation but without considering the strength gain due to aging, which is discussed in the following.

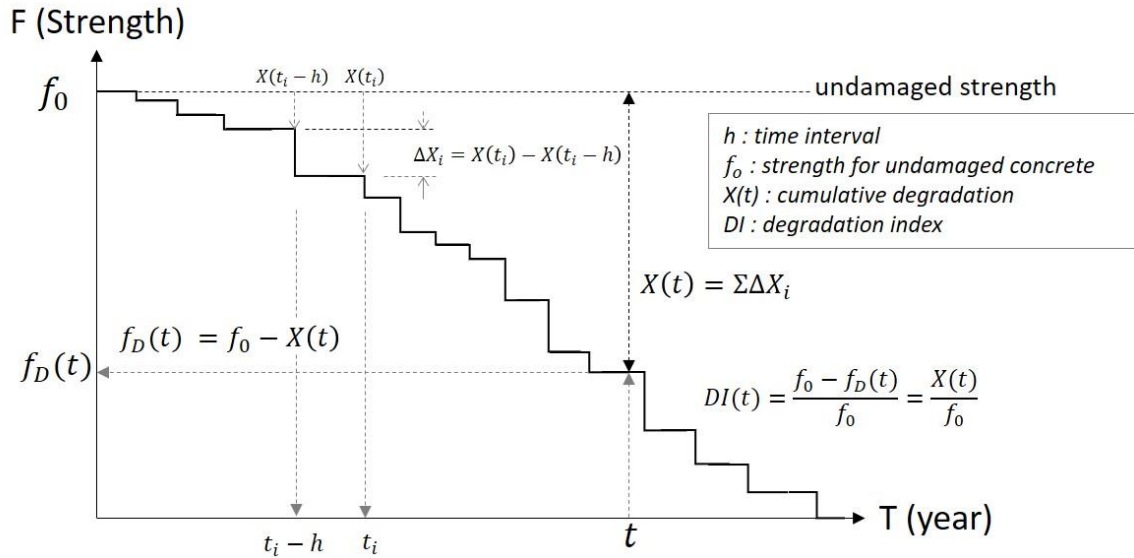


Figure 3.2. Continuous Gamma degradation process.

3.2.2 Modeling Degradation of Concrete based experimental

It has been reported that the degradation of the concrete strength occurs due to some Physico-chemical reactions that arises from the continuous contact of the reservoir water with the upstream face of the concrete gravity dam (Dolen et al., 2003). This leads to the reduction of the net load supporting area of the concrete. A discussion on the estimation of parameters based on experimental results for the constitutive modeling, evaluation of the degradation index, and estimation of the modulus of the elasticity value over time are discussed below.

According to Ghrib and Tinawi (1995), the orthotropic index for measuring the extent of damage in concrete could be expressed as:

$$DI_i = \frac{\Omega_i - \Omega_i^d}{\Omega_i} = 1 - \frac{\Omega_i^d}{\Omega_i} \quad (3.4)$$

where Ω_i is the tributary area of the surface in the ' i^{th} ' direction and Ω_i^d is the area affected by degradation. The scale of degradation lies between 0 and 1, in which $DI_i = 0$ represents no degradation and $DI_i = 1$ signifies completely degraded material. The index i for $i = 1, 2$ corresponds to the Cartesian axes system. In this case, the ratio of the net area over the geometrical area may be different for each direction. The plane strain constitutive material matrix, $[D_d]$, can be expressed as (Ghrib and Tinawi, 1995):

$$[D_d] = \frac{E_d}{(1+\nu)(1-2\nu)} \begin{bmatrix} (1-\nu)\Lambda_1^2 & \nu\Lambda_1\Lambda_2 & 0 \\ \nu\Lambda_1\Lambda_2 & (1-\nu)\Lambda_2^2 & 0 \\ 0 & 0 & (1-2\nu)\Lambda_1^2\Lambda_2^2/(\Lambda_1^2 + \Lambda_2^2) \end{bmatrix} \quad (3.5)$$

where $\Lambda_1 = (1 - d_1)$ and $\Lambda_2 = (1 - d_2)$, E_d is the modulus of elasticity of concrete without degradation. If $d_1 = d_2 = d$, $[D_d]$ becomes,

$$[D_d] = (1 - d)^2 [D] \quad (3.6)$$

in which $[D]$ is the constitutive material matrix without material degradation that was discussed extensively in Chapter 2.

Existing literature (Carde et al., 1996; Carde and Francois, 1997) revealed that one of the main measuring parameters of the concrete degradation index is the total porosity in concrete. According to Kuhl et al. (2004), the total porosity, ϕ , is defined as the sum of the initial porosity, ϕ_0 , the chemical porosity resulting from skeleton dissolution, ϕ_c and the apparent mechanical porosity, ϕ_m . This can be expressed as,

$$\phi = \phi_0 + \phi_c + \phi_m \quad (3.7)$$

The apparent mechanical porosity arises due to the opening and propagation of micro-cracks in the concrete material. ϕ_m is defined as

$$\phi_m = [1 - \phi_0 - \phi_c] * DI \quad (3.8)$$

where DI is defined as the scalar degradation parameter, which is given by,

$$DI = \alpha_s - \frac{K^0}{K} \{1 - \alpha_c + \alpha_c \exp[\beta_c(K^0 - K)]\} \quad (3.9)$$

in which K^0 and K are the variables that correspond to the initial degradation and the current degradation status, respectively. The internal variable K depends on the loading history of the material, whereas K^0 is determined by f_t/E_0 , where f_t is the static tensile strength and E_0 is the elastic modulus without material degradation. β_c in Eq. (3.9) is estimated experimentally. It is well established from several studies (Pan et al., 2013a,b) that one of the significant factors for premature concrete deterioration is AAR. Pan et al. (2013a, 2013b, 2014) considered the effect of AAR on aged concrete gravity dam and arch dam. They concluded that by assuming that ϕ_c is solely due to the alkali-aggregate reaction (AAR), one has:

$$\phi_c = d_{aar} \quad (3.10)$$

where, d_{aar} is the degradation factor. This degradation factor is generally expressed in terms of the expansion strains caused by the AAR effect. This d_{aar} could be determined by using the following expression Pan et al. (2013a):

$$d_{aar} = \frac{\varepsilon_{aar}}{\varepsilon_{aar} + 0.003} \quad (3.11)$$

The degradation of the modulus of elasticity E and the tensile strength f_t are considered based on the AAR degradation factor as follows (Pan et al. .2014):

$$E = E_0(1 - d_{aar}) \quad (3.12)$$

and,

$$f_t = f_{t_0}(1 - d_{aar}) \quad (3.13)$$

where E_0 and f_{t_0} are the elastic modulus and tensile strength of the un-degraded concrete. According to Gogoi and Maity (2007), the degradation index with respect to time, $DI_p(t)$ (i.e., the ratio of the strength reduction $X(t)$ to the initial characteristics strength), may be expressed as,

$$DI_p(t) = 1 - \frac{E_m}{E_0} \quad (3.14)$$

where $E_0 = 4773\sqrt{f_H(t)}$ and an empirical equation for the modulus of elasticity of the degraded concrete over time E_m is,

$$E_m = 0.0175 t^3 - 3.4054 t^2 + 29.807 t + E_i \quad (3.15)$$

In this equation, t is exposure to time in years, E_i is the initial value of the modulus of elasticity, and $f_H(t)$ is the compressive strength at time t by considering the strength gain due to aging but without the degradation effect.

3.2.3 Model for Aged Concrete Strength

If the strength degradation of the concrete gravity dam is not considered, the estimated performance, the fragility curve, and the annual failure probability of the dam are time-invariant for time-invariant loads. However, the assumption that the strength of the concrete gravity dam remains unchanged could not be justified based on the previous sections.

In standard practice, it is assumed that all the cement particles in concrete get hydrated within 28 days, and the concrete obtains its full compressive strength. In reality, concrete gains additional compressive strength after 28 days. Also, the durability of concrete is considerably affected due to damage resulting from time-varying external loads, moisture, heat transport, freeze-thaw actions, chemically expansive reaction, and chemical dissolution. The changes in the strength of the concrete dam over time due to the aging effect and gain of the concrete strength were not considered simultaneously in the literature to form the degradation model.

Estimation of the aged concrete is related to the two main factors. On one side, the concrete gains compressive strength with its age. On the other side, the properties of concrete get deteriorated due to chemical and mechanical actions. In order to predict the properties of the aged concrete, these two factors need to be appropriately considered (see Figure 3.3).

$$f(t) = f_H(t) + f_D(t) - f_0 \quad (3.16)$$

where $f_H(t) - f_0$ represents the compressive strength gain at time t due to aging, f_0 is the initial compressive strength.

The degradation process of concrete shown in Figure 3.3 can be divided into three phases. The ascent phase of concrete strength is characterized by the hydration reaction in concrete. The hydration reaction is a continuing process. So, the concrete strength goes on increasing rapidly in the early stage and very slow in later days. The steady phase of concrete strength is dominated by the time of balancing a rate between increasing strength and degraded strength. The trend of concrete strength becomes flat because the increment of concrete strength due to hydration reaction is as same as the reduction of it by deterioration at this phase. Finally, the descent phase lies in the excessive accumulation of deterioration. This generates decreasing concrete capacity and results in the performance degradation of concrete.

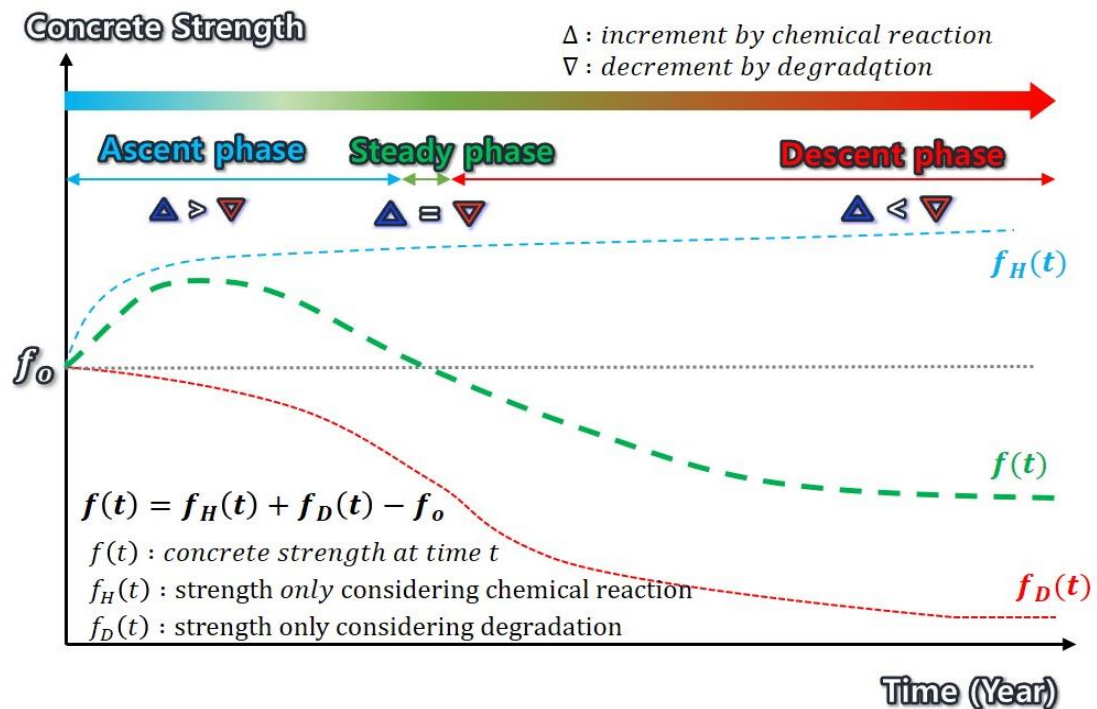


Figure 3.3. Change of concrete strength over time.

In predicting the change of the concrete strength with time, it should be noted that the gain of compressive strength of concrete could be predicted by fitting experimental data published by Washa et al. (1989). At the same time, the concrete strength decreases due

to the degradation process may be assessed based on experimental data, or the parameters of the degradation model could be estimated using the experimental data. A literature review indicates that full-scale data for the gain and degradation is rarely published in the literature. This is partly due to collecting such data is extremely expensive. This underlines the need for additional full-scale experimental data in assessing time-varying concrete strength under realistic environmental conditions. This is especially the case since the accurate prediction of the time-varying concrete strength is essential for the durability assessment or structural service life prediction. The long-term concrete strength under a real service environment is an important parameter when evaluating existing concrete dams, which should also be appropriately considered in structural design as well.

3.2.4 Proposed Model for Time-Varying Compressive Strength

In general, given a set of experimental results, one could judiciously select a parametric model and carry out the curve fitting to determine the model parameters. The mathematical parametric model should be selected based on the physical ground whenever possible, and the model parameters should lend themselves to an easy interpretation. Gogoi and Maity (2007) proposed an equation to predict the gain of concrete compressive strength with the passage of time (in terms of years) based on the test results reported in Washa et al. (1989). In the present study, the experimental studies reported by Washa et al. (1989) and Dolen (2005) on the compressive strength of concrete gain over the duration of 50 years and 60 years, respectively, have been considered. Dolen (2005) suggested that the mean concrete compressive strength at time t without degradation but with chemical reaction $f_H(t)$ is,

$$f_H(t) = 2.54 \ln(t) + f_{ck} = 2.54 \ln(t) + f_0 - 8 \text{ (MPa)}, t > 0 \quad (3.17)$$

where t is the age of concrete expressed in years ($t > 0$), and f_{ck} is the characteristic strength of concrete at 28 days. $f_{ck} = f_0 - 8 \text{ (MPa)}$ suggested by the Korean Design Standard (MOCT, 2016) is used in Eq. (3.17). This proposed expression may be used for predicting the compressive strength of concrete at any later stage.

The evaluation of concrete strength with t by considering both the increment due to chemical reaction and decrement due to degradation can be expressed as

$$f(t) = f_H(t) + f_D(t) - f_o \quad (3.18)$$

As mentioned previously, there are essentially two approaches to model the degradation, namely the probabilistic approach and the physical (or deterministic experimental results-based) approach that can be used to model the concrete strength by considering degradation. If the stochastic model (see Eq. (3.3)) and the gain in concrete strength due to aging are considered, the concrete compressive strength at time t can be expressed as,

$$f(t) = 2.54 \ln(t) + f_{ck} - X(t) = 2.54 \ln(t) + f_o - 8 - X(t) \quad (3.19)$$

If instead of the stochastic model, the “physical-based” (or experimental based) deterministic model shown in Eq. (3.14) is considered,

$$f(t) = 2.54 \ln(t) + f_o - 8 - f_o * (1 - E_m/E_o) \quad (3.20)$$

The long-term tensile strength of concrete was scarcely discussed in the literature. The correlation between the compressive and tensile strength of concrete by considering aging was also scarcely discussed. Yao et al. (2017) indicated that all the compressive-tensile strength relationships for fresh concrete do not apply to the environmentally deteriorated concrete with satisfactory accuracy. They investigated the correlation between the compressive and tensile strength of concrete by using the compressive and tensile strength of concrete under the real marine environment for an extended period (up to 61 years). Their study, based on 48 compressive and splitting tensile strength specimens, indicated that as the compressive strength increases, the tensile strength of concrete increases as well. According to the test results, the function that best represents the relationship between the compressive strength and tensile strength under the marine environment is,

$$f_{ts}(t) = 1.02 \cdot (f(t))^{0.36} \quad (3.21)$$

In summary, the procedure to evaluate the time-varying concrete strength is obtained by using the degradation model or experimental results, as illustrated in Figure 3.4. The

stochastic model is adopted in the present study in the following chapters for the numerical analysis.

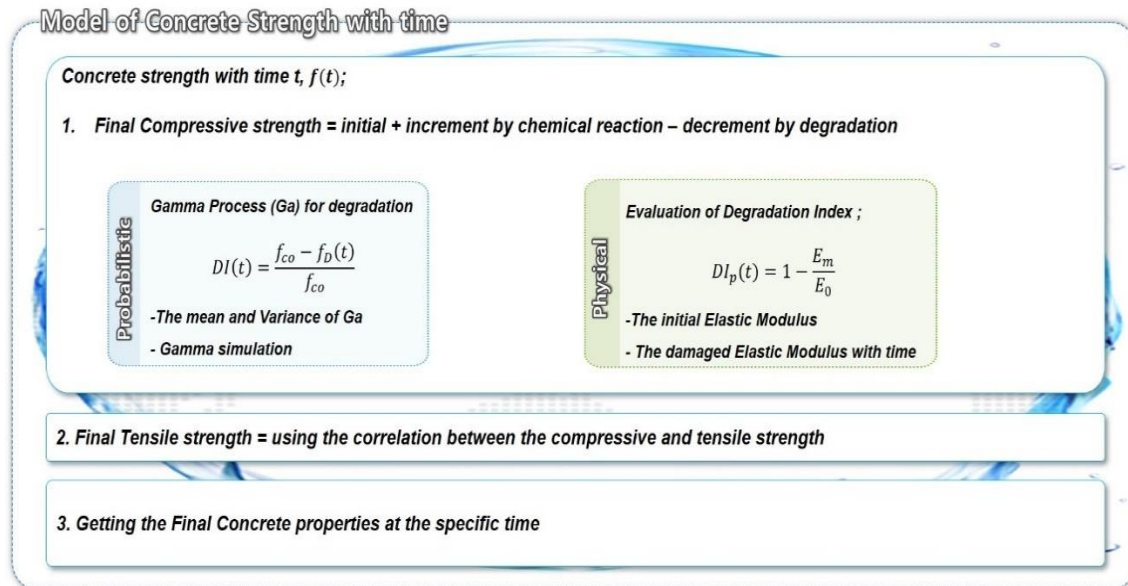


Figure 3.4. Procedure to model the concrete strength with time t .

3.3 Application to Time-Varying Concrete Strength Model to Chungju dam

The model described in the previous section is applied to Chungju dam, which is located in the middle of Korea (more information on this dam is given in Chapter 4).

If sufficient statistical data on the time-varying concrete strength is available, the model or model parameter calibration is not difficult. For example, one could select the preferred model based on the regression analysis results. The purpose of model selection should consider simplicity and its practical application. It should take into account the errors associated with the prediction (Nguyen et al., 2017).

Figure 3.5 shows the procedure of model selection adopted in the present study. The first step is to obtain data of concrete strength, which is recorded at the inspection times. Step 2) is to assign the likely model parameters. By using the assigned model parameters for the stochastic degradation process, samples of the degradation can be simulated and compared with observed time-varying degradation strength in Step 3). In Step 4), the root

mean square error (RMSE) can be evaluated. Steps 2) to 4) may need to be carried out iteratively to find the model or model parameters that lead to the lowest root mean square error (RMSE). Note that for simple models, Steps 2) to 4) can be carried out easily and without iteration.

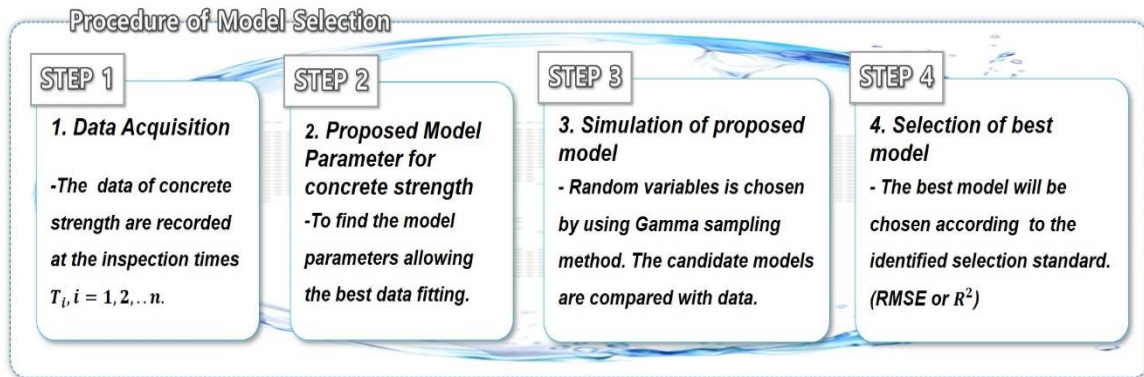


Figure 3.5. Procedure to find model parameters

For the model fitting using the procedure described in Figure 3.5, the data of concrete strength for the considered dam is obtained at the inspection times (i.e., at every five years). This inspection interval was stipulated by Korea Infrastructure Safety and Technology Corporation (KISTEK) for Chungju dam. The inspection schedule and obtained concrete compressive strength for three types of concrete used for the dam (see Figure 4.2) are given in Table 3.2. The compressive strength of the outer dam body (Type B) increased until 2002. A decreasing trend can be observed after 2002. The time-varying concrete strength for the weir (Type F) follows a similar trend. Although the concrete strength for the inner dam body (Type A concrete) is available for the construction stage, no samples were available at each inspection time since the inner dam body is not accessible without a damaging and costly sampling process. Therefore, it is assumed that the degradation of the inner dam body (Type A) is similar to that of the outer dam body (Type B).

Note that the values given in Table 3.2 are obtained from several internal proprietary reports. There is a large number of samples available during the construction stage. However, for the existing dam (i.e., during the dam's operation), the number of samples is small or unavailable. In a few cases, only the mean value is reported while the standard deviation is unavailable.

Table 3.2: Experimental Data of Concrete Compressive Strength for Chungju Dam

Concrete strength		1985	1997	2002	2007	2012	2017
Type A	Sample Numbers	1,259	-	-	-	-	-
	Mean (MPa)	12.71	-	-	-	-	-
	Standard Deviation	0.8					
Type B	Sample Numbers	860	-	-	47	55	59
	Mean (MPa)	18.52	24.2	27.4	25.5	25.2	24.3
	Standard Deviation	1.078	-	-		2.2	1.5
Type F	Sample Numbers	346	-	-	47	55	59
	Mean (MPa)	22.31	28.5	28.8	30.8	27.2	24
	Standard Deviation	1.195	-	-	-	1.2	1.2

More specifically, to obtain the model parameters, the concrete strength at time t (Eqs. (3.19) and Eq. (3.20)) can be re-written as ($i = 1, 2, \dots, t$ and $h > 0$);

$$f(t) = 2.54 \ln(t) + f_{ck} - \Sigma[X(t_i) - X(t_{i-h})] \quad (3.22)$$

As previously mentioned, the degradation at time t , $X(t)$, is gamma process with shape function $v(t) > 0$ and scale parameter $u > 0$. The gamma process $X(t)$ is gamma distributed with shape function $v(t)$ and scale parameter u , which could be calculated based on the distribution fitting method such as the like maximum likelihood method and moments method if the parametric form of $v(t)$ is given. In the modeling of degradation, the trend of the expected degradation over time is important. Empirical studies show that the expected degradation at time t is often represented by a power-law parameter form (Ellingwood and Mori, 1993; van Noordwijk and Klatter, 1999),

$$E(X(t)) = \frac{v(t)}{u} = \frac{at^b}{u} \quad (3.23)$$

where $v(t) = at^b$ for some physical constant $u > 0$, $a > 0$, and $b > 0$. To model the deterioration as a gamma process with shape function $v(t) = at^b$ and scale parameter u , the parameters a , b , and u should be estimated in Eq. (3.23) based on statistical data. The parameter b could be assumed constant. For example, it was considered that $b = 1, 2$,

and 0.5 are considered for the degradation of concrete, sulfate attack, and diffusion-controlled aging (Ellingwood and Mori, 1993). We assume that the expected degradation of concrete is linear degradation, but a and u are unknown, which are estimated using statistical methods (Cinlar et al. 1977; van Noordwijk and Pandey, 2003; Mahmoodian and Alani, 2014).

In particular, assuming a typical data set consists of the inspection time t_i , $i = 1, \dots, n$ ($0 < t_1 < \dots < t_n$), times between inspections $h_i = t_i^b - t_{i-1}^b$, $i = 1, \dots, n$, corresponding observation of the cumulative amount of degradation x_i , $i = 1, \dots, n$ ($0 < x_1 < \dots < x_n$), observed degradation increment $\Delta x_i = x_i - x_{i-1}$, $i = 1, \dots, n$. The use of the method of moment leads to the estimated a and u given by (van Noordwijk and Pandey, 2003),

$$\frac{\hat{a}}{\hat{u}} = \frac{\sum_{i=1}^n \Delta x_i}{\sum_{i=1}^n h_i} = \frac{x_n}{t_n^b} = \widetilde{\Delta x} \quad (3.24)$$

$$\frac{x_n}{\hat{u}} \left[1 - \frac{\sum_{i=1}^n h_i^2}{[\sum_{i=1}^n h_i]^2} \right] = \sum_{i=1}^n (\Delta x_i - \widetilde{\Delta x} \cdot h_i)^2 \quad (3.25)$$

However, as the experimental data is rare and difficult to obtain for a dam, the dam subject to continuous degradation in assessing its seismic capacity is rarely discussed in the context of using actual data. It is noted that in an illustrative example, Iervolino et al. (2013) considered that the degradation could be modeled as a gamma process with a mean equal to $10^{-3}t$, and variance of $10^{-4}t$, respectively. This implies that b equal to one (see Eq. (3.1)) is considered in their model. A simple calculation shows that the use of $b=1$ does not match the trend degradation tend provided by the available data for Chungju Dam shown in Table 3.2. Consequently, these values are not used.

Ideally, if sufficient experimental data points are available and the strength gain due to aging is confirmed, one could minimize the error between the predicted time-varying mean and observed concrete strength defined as

$$Error = \sum \left(at_i^b/u - (f(t_i) - 2.54 \ln(t_i) - f_{ck}) \right)^2 \quad (3.26)$$

Unfortunately, the available data sample size is too small to provide a meaningful statistical inference. Therefore, the values of the parameters a , b , and u for the gamma process used to model the degradation are assigned by trial and error.

Essentially, this involves assigning the value of b , and the parameter a and u are obtained by the moment method (Eq. (3.24) and (3.25)) and the degradation $X(t)$ is obtained by using the parameter a , u , and b . The degradation $X(t)$ is simulated and compared with the observed values shown in Table 3.2. The root mean square error (RMSE) and R-squared (R^2) are then calculated. The R^2 and RMSE values are reported. The values of shape and scale parameters of degradation with time t . that results in the highest R^2 and lowest RMSE, which is reported in Table 3.3, are adopted. It must be emphasized that this is not as rigorous as minimizing the error defined in Eq. (3.26) because the tiny sample size is considered, and a rigorous minimization approach may not be warranted. Note also that the b value obtained is much different from that considered in Iervolino et al. (2013) (i.e., $b = 1$) for their illustrative example. The use of $b = 1$ results in a much sharp degradation, which is not adequate for the data presented in Table 3.2.

Table 3.3: Shape and scale parameters of degradation for Chungju Dam

Parameter	Dam Body (Type A, B)	Weir (Type F)
Shape, $\nu(t) = at^b$	$0.21441 \cdot t^{0.0446}$	$0.25402 \cdot t^{0.0655}$
Scale, u	0.03733	0.02675

Figure 3.6 shows a comparison of simulation concrete strength according to the adopted gamma degradation model, the strength predicted by Eq. (3.20), and the experimental data presented in Table 3.2. The concrete strength by physical approach (i.e., Eq. (3.20)) and without considering other modeling error does not match well the observation. On the other hand, the concrete strength by considering the stochastic degradation model could cope with the observed concrete strength variation. This is because the use of an uncertain degradation model could lead to different time-varying strength paths. The plots also show that the assigned model parameters could be considered adequate for the considered samples. The developed degradation model presented in this chapter is adopted in the following Chapters for the fragility analysis of dam subjected to seismic ground motions.

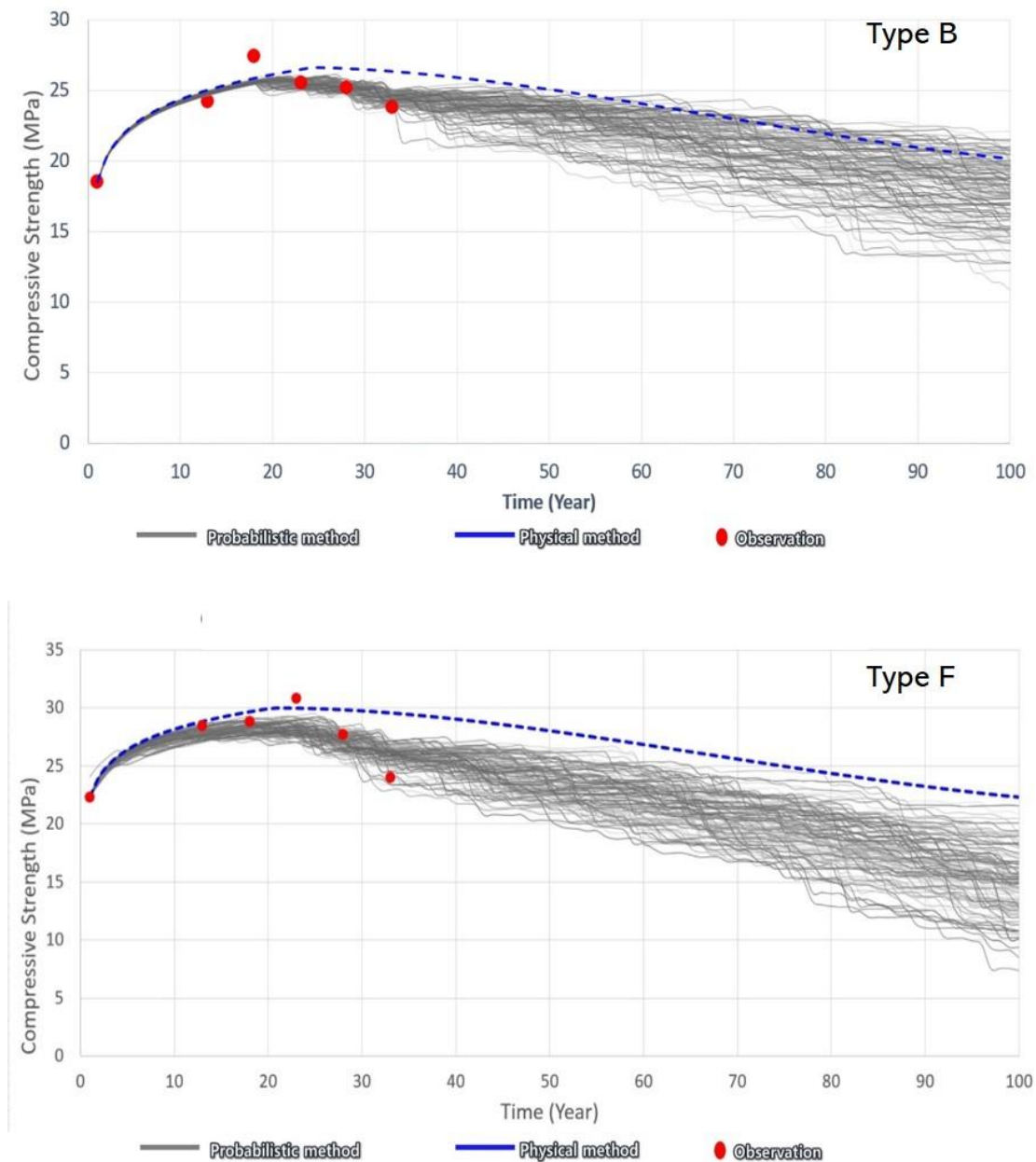


Figure 3.6: Comparison of the models and observed time-varying concrete strength.

3.4 Summary

In this chapter, a review of the modeling of the time-varying concrete strength is presented. The review is focused on the modeling of the aging and degradation effect on concrete strength. It was pointed that an empirical model could be developed if sufficient samples of concrete strength at different ages during the service are available. Also, the

degradation of concrete strength can be modeled using the gamma process. Unfortunately, data for in-service structures such as the concrete dam are extremely scarce.

By using very limited samples from the Chungju Dam, model parameters for two degradation models are estimated by “trial and error.” No rigorous statistical test was carried out because of the unavailability of sufficient samples. The use of the model parameters obtained in such a manner is for necessity as well be see in the following chapters; the model could only be considered as models based on engineering judgment. It is suggested for assessing existing structures and infrastructure systems and for asset management, more experimental data are to be collected and to be used to calibrate concrete degradation models.

Chapter 4

4 Finite Element Modeling of a Concrete Gravity Dam: a Case Study

4.1 Introduction

In this chapter, the Chungju Multi-Purpose Dam (Chungju dam) in Korea is considered as a case study to describe and demonstrate the application of the proposed degradation model in Chapter 3 for aged concrete gravity dams subjected to seismic excitation. The dam is located in the middle of Korea, as shown in Figure 4.1a. A photo of the dam is presented in Figure 4.1b.



Figure 4.1: Location of Chungju Dam and a photo of the dam: (a) Location of Chungju dam, (b) photo of the dam.

Chungju Dam is a concrete gravity dam. It has a 464.0 m crest length. The tallest overflow section shown in Figure 4.2 is considered for the finite element (FE) modeling. The dimensions and material properties of the dam, reservoir, and rock foundation are given in Figure 4.2 and Table 4.1. The dynamic elastic moduli of the dam for the concrete and foundation rock are increased by 15% as compared to the static elastic moduli, according to U.S. Army Corps (EM 1110-2-6053, 2007). The dynamic tensile and compressive strengths of concrete are obtained by applying a dynamic magnification factor of 1.5 and 1.15 to the static strength, respectively. The material damping for the dam-reservoir-foundation system is considered via the Rayleigh damping assumption with a damping ratio of 5%. The value of the damping ratio is selected according to the current seismic codes in Korea (Korean Design Standard, 2018).

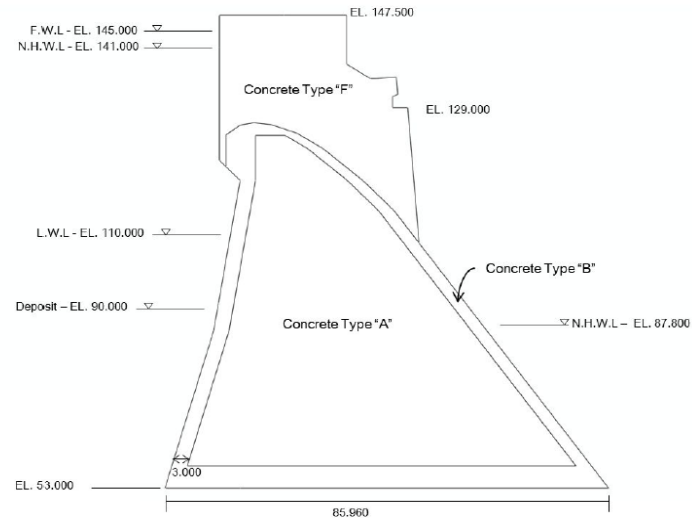


Figure 4.2. Dimensions of Chungju dam (Block #10).

Table 4.1. Material properties of Chungju dam.

Dam	Modulus of Elasticity (GPa)	Compressive strength (MPa)	Poisson's Ratio	Mass Density (kg/m ³)	Sonic Velocity (m/s)	Wave Reflection Coefficient
Dam Body(internal) [Type A]	22.25	11.8	0.117	2226	-	-
Dam Body (external) [Type B]	25.47	17.6	0.117	2226	-	-
Weir [Type F]	26.81	20.6	0.117	2226	-	-
Foundation	53.5	-	0.2	2690	-	-
Reservoir	-	-	-	1000	1440	0.7

4.2 Developed the Finite Element Model of a Dam

For the modeling of the dam-foundation-reservoir system, the computer program ABAQUS is used in this study. Two-dimensional CPS4R, CINPS4, and AC2D4 elements in ABAQUS are used to model the solid and fluid (i.e., dam and foundation and reservoir). The CPS4R element has four nodes with two degrees of freedom at each node, namely translation in x and y directions. The CINPS4 element has four nodes and is a one-way continuum infinite element, which can prevent reflection of the outgoing wave into the system again by using an appropriate boundary condition for the far-end node. The AC2D4 element has four nodes and is an acoustic element. In an acoustic fluid

system, the fluid field is of constant volume. The acoustic element has a degree of freedom in terms of pressure at the nodes of the element. A non-reflecting boundary condition is also used at the upstream face of the reservoir to enable energy dissipation in the reservoir.

Zero pressure is applied at the truncated boundary and at the top of the reservoir to consider the damping effect arising from the propagation of pressure waves. For the static analysis, zero displacements are imposed on the horizontal translation degrees of freedom at the dam-foundation interface. For the dynamic analysis, the horizontal and vertical translation degrees of freedom are not fixed, but the interface of the dam and foundation are connected by the tie element. The dam is assumed to be homogenous, nonlinear, isotropic. The foundation is assumed to be homogeneous, elastic, and isotropic, and the fluid is assumed to be compressible and inviscid. Figure 4.3 shows the mesh of the developed FE model. The dam and rock foundation are modeled with 1140 CPS4R and CINPS4 elements, and the reservoir is modeled with 400 AC2D4 elements. The comparisons between the results obtained using the developed FE model and those published results by K-water (Korea Water Resources Corporation, 2013) are used to validate the developed model in the following sections.

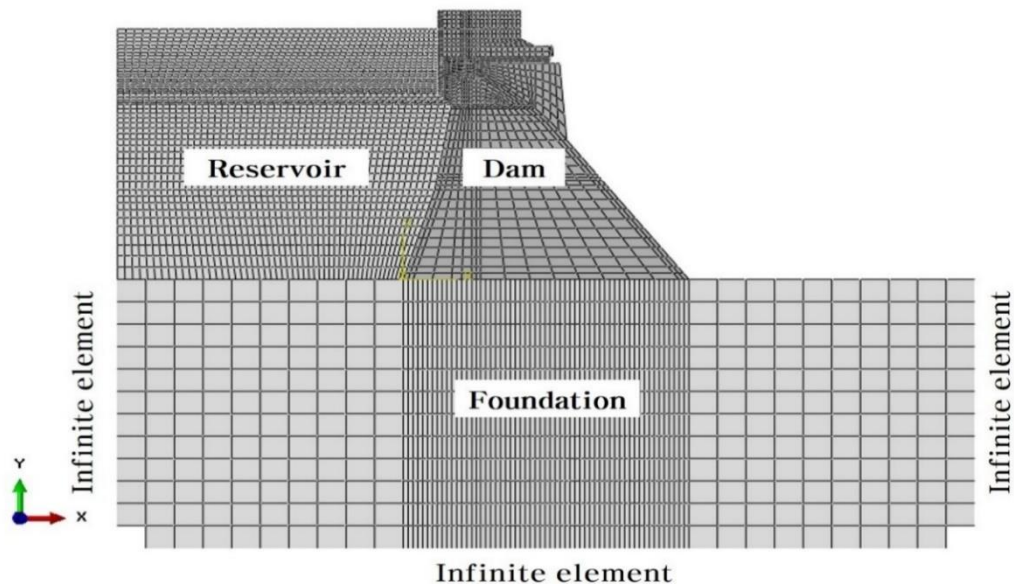


Figure 4.3. The Model of a dam-reservoir-foundation system in ABAQUS.

4.3 Validation of the developed FE Model

4.3.1 Forces acting on a Concrete Gravity Dam and Static Analysis

To validate the developed FE model, first, a comparison is made between the static results obtained by using a proprietary analytical method used in K-water (Seismic performance evaluation report by K-water, 2013) and by using the developed FE model in ABAQUS.

For the static analysis, the forces acting on the gravity dam, including the seismic force, are illustrated in Figure 4.4. The main stabilizing force for a gravity dam is its weight. It comprises the weight of the concrete along with the weight of the appurtenances (gates, piers, etc.). The weight of the dam per unit length is equal to the product of the area of the dam and the specific weight of the material. The total weight of the dam acts at the center of the geometry of the section. The specific weight of concrete is usually taken 24 kN/m^3 . However, the actual specific weight may vary depending upon the water-cement ratio, compaction of concrete, and the unit weight of the aggregate used. In this study, the weight of concrete is considered 22.246 kN/m^3 .

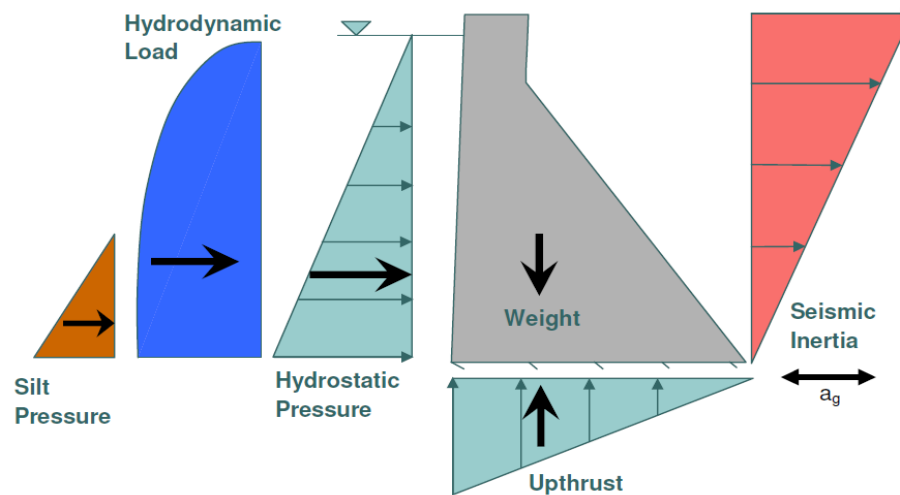


Figure 4.4. Forces acting on a gravity dam.

The water pressure intensity (i.e., hydrostatic pressure per unit width of the dam), P , (kN/m^2) varies linearly with the depth of the water h measured below the free surface and is expressed as:

$$P = \gamma_w h \quad (4.1)$$

where γ_w is the specific weight of water (9.81 kN/m³). The water pressure always acts normal to the surface. In the case of the inclined face of the dam, the pressure is decomposed into vertical and horizontal components. The horizontal pressure, P_H , (kN/m), is given by,

$$P_H = \frac{1}{2} \gamma_w H^2 \quad (4.2)$$

where H (m) is the total depth of the water. Moreover, it acts horizontally at a height $H/3$ above the base of the dam. The vertical component is equal to the weight of the water column above the inclined portion of the upstream face of the dam and will act through the centroid of the area associated with the water column.

Water tends to seep through the pores and fissures of the foundation material. The seeping water exerts pressure and should be included in the stability calculations. The uplift pressure is defined as the upward pressure of water as it flows or seeps through the dam or its foundation. A portion of the dam weight will be adequately supported by this uplift, thus reducing the net vertical force.

According to the Dam Design Criteria in Korea (Korean Design Standard, 2016), the uplift pressure is illustrated in Figure 4.5. The uplift pressure distribution in the dam body shall have an intensity at the line of the drains exceeding the tailwater pressure by one-third the differential of the reservoir level and the tailwater level. The pressure gradient shall extend linearly to heads corresponding to reservoir level and tailwater level, the uplift acting over 100% area. In case of the absence of the line of drains and for extreme loading conditions, the uplift pressure shall be varying linearly from the reservoir water pressure at the upstream to tailwater pressure downstream. If the reservoir water pressure exceeds the normal vertical stress, then a crack will be assumed from the upstream face to the point where the normal vertical stress is equal to the reservoir pressure at the elevation. The uplift pressure shall be equal to the reservoir pressure throughout the assumed crack length and then vary linearly to the tailwater pressure level downstream.

Based on the above, the uplift pressure at the full reservoir for the considered dam is distributed at the bottom of the dam, as shown in Figure 4.6. The drainage is located 14.55m away from the upstream of the dam.

Commonly, parts of the dams are in contact with soil, and this could be due to soil backfill or in a case where a concrete dam is connected to an earth. According to the Dam Design Criteria in Korea, the horizontal silt pressure is calculated by the below equation:

$$p_s = \frac{1}{2} C_\varepsilon \gamma' g H_s^2 \quad (4.3)$$

where C_ε is the coefficient of soil pressure, γ' is effective mass under the water, g ($=9.81 \text{ m/sec}^2$) is the gravitational acceleration, H_s is the soil depth. In this study, the coefficient of soil pressure (C_ε) is taken equal to 0.5, the effective mass under the water (γ') is taken equal to 800 kg/m^3 . The hydrostatic pressure function in ABAQUS is used.

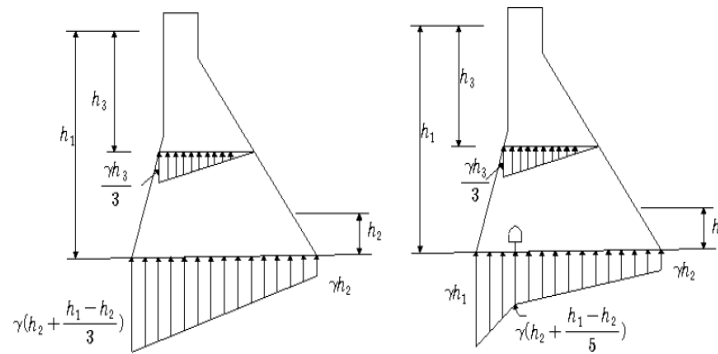


Figure 4.5. Distribution of uplift pressure on a gravity dam.

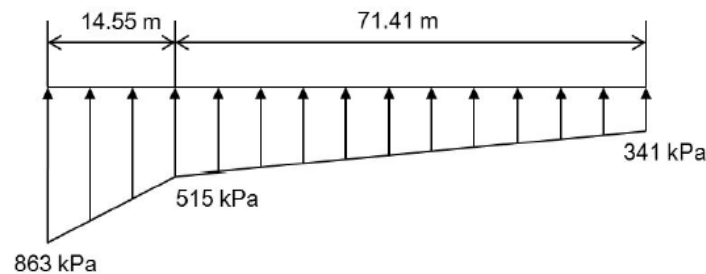


Figure 4.6. Distribution of uplift pressure on the Chungju dam.

The seismic load is primarily accounted for as a coefficient along with the weight of the dam for preliminary analysis. This load, represented by the seismic inertia force, is illustrated in Figure 4.4, which is a very simplified treatment. For more accurate analysis, the response spectrum method or time history analysis is required (Malm 2016). The dam also experiences inertia force exerted by the mass of water, termed as the hydrodynamic interaction effect. The hydrodynamic interaction effect of the water adjacent to the upstream face of the dam is expressed by an equivalent added mass of water. An approach to take into account the added mass is based on the approach developed by Westergaard (1933). This approach assumes that the dam is rigid, the water can be considered as an incompressible fluid, and it is only developed for a vertical upstream face. Further development of this approach for non-vertical upstream faces is, for instance, described in Goldgruber (2015). The hydrodynamic pressure, in this case, is given by (Korean Design Standard, 2016),

$$p = \frac{7}{8} \rho \sqrt{h(h-z)} \ddot{u} \quad (4.4)$$

where p is the hydrodynamic pressure at height z above the reservoir bottom, h is the depth of the reservoir, ρ is the mass density of water and \ddot{u} is the horizontal ground acceleration. From the above equation, it follows that the hydrodynamic pressure is maximum at the reservoir bottom (where $z = 0$) and decreases parabolically to zero at the reservoir surface (where $z = h$).

However, the fluid is compressible (density changes due to pressure variations). The influence of the incompressible and compressible fluid assumption on the response of the dam was studied by Chopra (1968). It was found that the key parameter controlling whether the compressibility of the reservoir has to be taken into account is the ratio between the natural frequency of the reservoir and the natural frequency of the dam. The frequency of the reservoir could be calculated using (Malm, 2016);

$$f_e = \frac{c_w}{4h} \quad (4.5)$$

where f_e is the natural frequency of the reservoir (Hz). c_w is the wave propagation velocity (m/s), and h is the water depth (m). The ratio of the natural frequencies is defined as follows;

$$\Omega_r = \frac{f_e}{f_u} \begin{cases} < 2.0 \text{ compressible reservoir} \\ > 2.0 \text{ incompressible reservoir} \end{cases} \quad (4.6)$$

where f_u is the natural frequency of the dam [Hz]. As will be discussed, the above criteria indicate that the compressibility of the water needs to be considered for the Chungju dam.

Other forces that may need to be considered include ice pressure, wind pressure, wave pressure, etc. For the considered dam, the ice pressure is assumed to be equal to 75 kN/m (per unit width of the dam), while the eave pressure and wind pressure are neglected.

Based on the described static forces described in the previous section, static analysis is carried out using the developed FE model. The results are presented in Figures 4.7 and 4.8. For comparison purposes, the stress distribution given by the K-water (Seismic performance evaluation report by K-water, 2013) is included in Figure 4.7. As can be observed, the stress distributions obtained by using the developed FE model and K-water have similar trends, and the location of the maximum principal stress is consistent. For the developed FE model, the maximum principal stress is 1.14 MPa, which is located at the bottom upstream of the concrete gravity dam, and the minimum principal stress is 1.79 MPa, which is shown at the bottom of downstream of the concrete dam. Figure 4.8 shows that large horizontal displacement is expected at the top of the dam, while a large vertical displacement is expected at the bottom of the dam.

4.3.2 Modal Analysis results

A modal analysis is carried out using the developed FE model by considering a full reservoir. The results are presented in Figure 4.9 and Table 4.2 and compared with those reported by the K-water water (Seismic performance evaluation report by K-water, 2013). The frequencies of the first, second, and third models are 3.8237, 10.079, 10.773 Hz,

respectively. In all cases, they compare favorably to those given by K-water. The results also show that the first and second modes are the most important modes for horizontal and vertical vibration, respectively, since they are associated with significant modal participation.

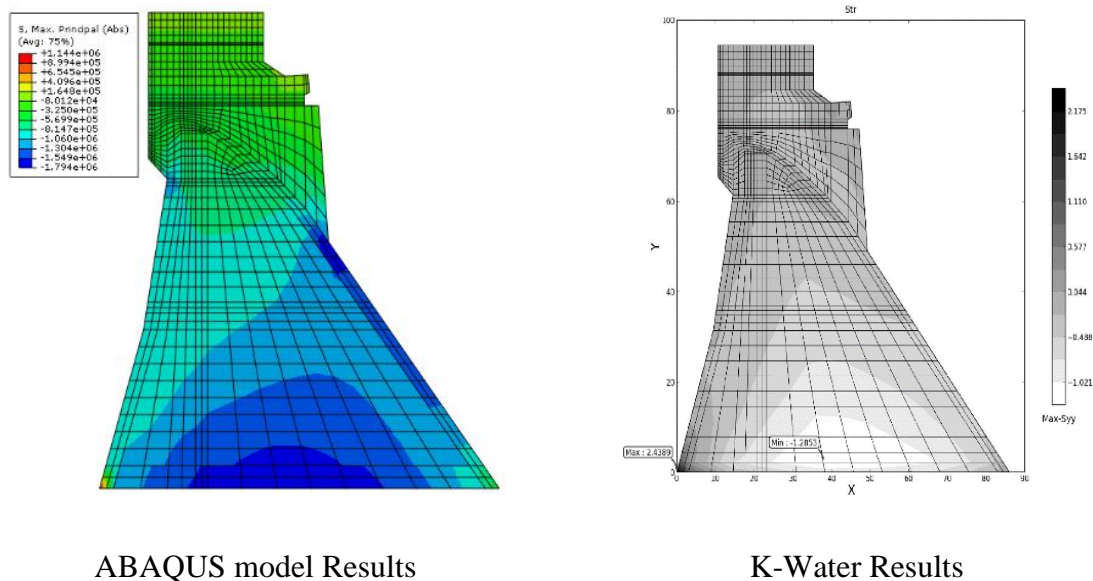


Figure 4.7. Stress contour of analysis results from the developed FE model and from K-water.

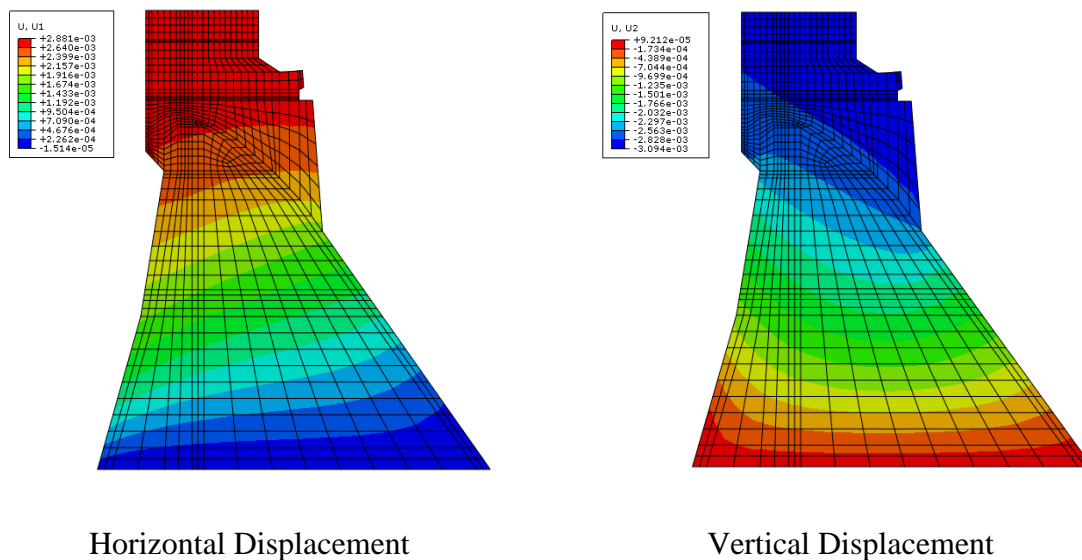


Figure 4.8. Horizontal and vertical displacement obtained from the developed FE model.

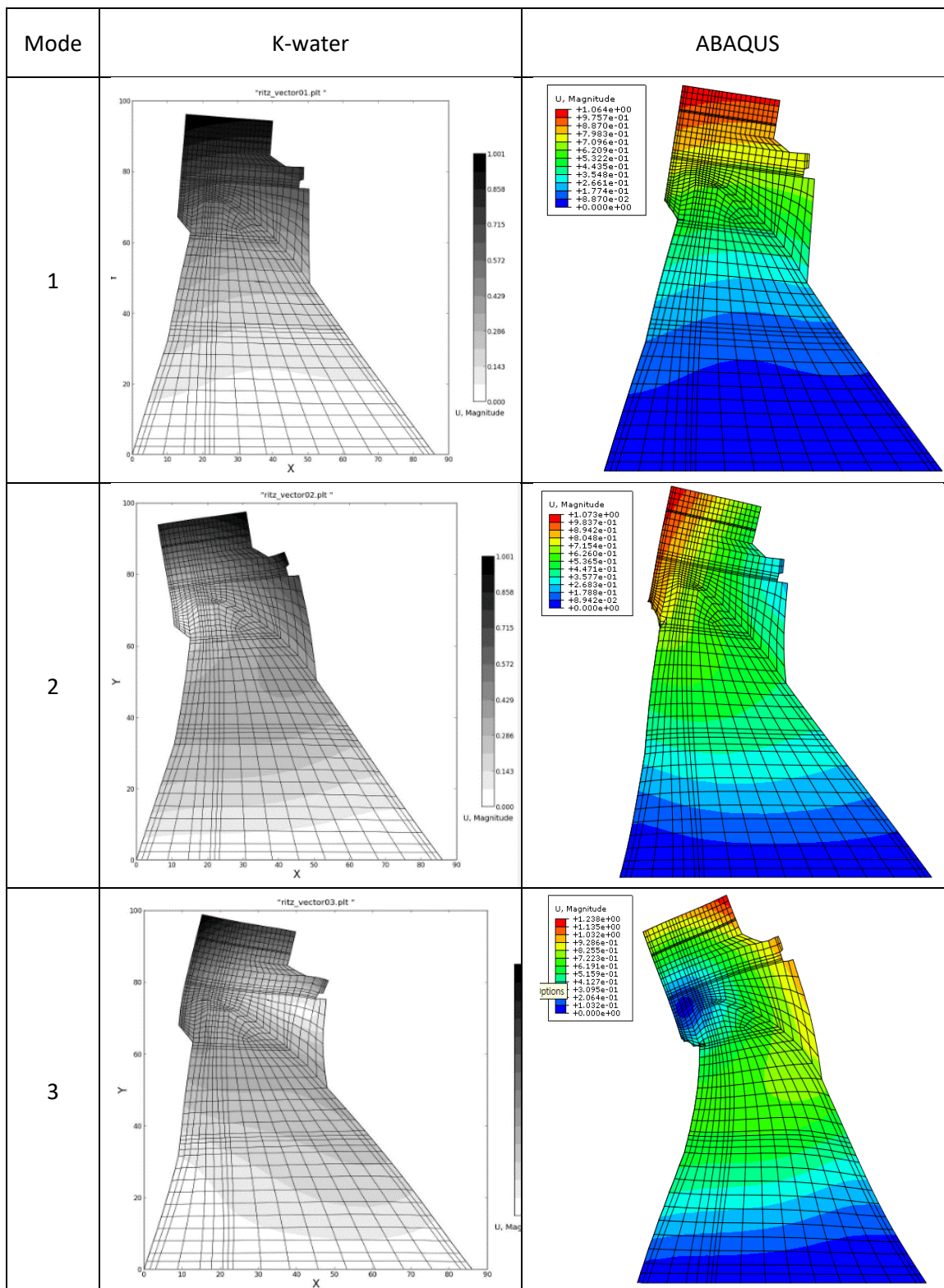


Figure 4.9. Mode shapes of Chungju dam obtained from different models.

Table 4.2. Modal frequencies of Chungju dam from different models.

Mode	Natural Frequency (Hz)		Natural Period (sec)		Horizontal direction (x-direction)				Vertical direction (Y-direction)			
	K-water	ABAQUS	K-water	ABAQUS	K-water		ABAQUS		K-water		ABAQUS	
					Mass (%)	SUM (%)	Mass (%)	SUM (%)	Mass (%)	SUM (%)	Mass (%)	SUM (%)
1	4.9259	3.8237	0.2030	0.2615	37.6	37.6	45.8	45.8	0.9	0.9	0.8	0.8
2	11.2880	10.079	0.0886	0.0992	13.4	51.0	16.1	61.9	26.5	27.4	47.7	48.4
3	12.5905	10.773	0.0794	0.0928	3.1	54.1	17.0	78.9	35.7	63.1	28.8	77.3
4	18.7931	19.506	0.0532	0.0513	28.6	82.7	13.2	92.2	2.0	65.1	0.1	77.3
5	20.0976	19.964	0.0498	0.0501	0.1	82.8	0.0	92.2	11.6	76.7	0.0	77.3
6	25.9002	22.883	0.0386	0.0437	0.6	83.4	0.0	92.2	3.7	80.4	0.0	77.3
7	27.2390	25.909	0.0367	0.0386	2.6	86.0	0.1	92.3	0.0	80.4	17.6	94.9
8	29.1722	26.559	0.0343	0.0377	1.0	87.0	0.0	92.3	0.8	81.1	0.0	94.9
9	33.1923	28.547	0.0301	0.0350	0.5	87.6	3.7	96.0	5.2	86.3	0.0	95.0
10	35.9891	30.626	0.0278	0.0327	3.4	91.0	0.0	96.0	0.3	86.6	0.0	95.0
11	41.0721	31.588	0.0243	0.0317	0.1	91.1	0.4	96.4	2.7	89.3	0.2	95.2
12	48.8173	33.647	0.0205	0.0297	0.3	91.4	0.7	97.0	0.1	89.5	0.0	95.2
13	58.7557	36.641	0.0170	0.0273	0.4	91.8	0.0	97.0	0.1	89.5	0.0	95.2
14	78.2390	37.09	0.0128	0.0270	0.5	92.3	0.6	97.6	0.0	89.6	2.5	97.7
15	123.913	37.754	0.0081	0.0265	0.5	92.8	0.0	97.6	2.5	92.1	0.0	97.7

4.4 Time-history response of Dam subjected to ground motions: Parametric Investigation

In this section, a parametric investigation of the characteristics of the dam is carried out using the developed FE model described in previous sections. The objective of the parametric investigation is to assess the sensitivity of the dynamic characteristics of the dam to some of the input variables listed in Table 4.1.

For the parametric investigation, the value shown in Table 4.1 for the modulus of elasticity and compressive strength (for Type A, B, and F) is varied one at a time, and the corresponding cases are listed in Table 4.3. The considered variation equals one standard deviation of the variable, which will be discussed in Chapter 5. The modal analysis that was carried out for the results presented in Table 4.2 is repeated for each of the cases listed

in Table 4.4 for the first three modes. The change of the concrete strength does not affect the initial dynamic characteristics of the dam. This is expected since the strength does not affect linear elastic dynamic characteristics. However, the change of the elastic modulus of concrete affects the vibration frequency of the structure. The results show that the vibration frequency is most sensitive to the variation of the elastic modulus of concrete used for the dam body (i.e., Type A). The variability of the elastic modulus of concrete for the weir (i.e., Type F) does not lead to a significant change in the vibration characteristics.

Table 4.3. Cases for Parametric Analysis

Dam Body			Cases for Parametric Analysis (C : Compressive Strength / E : Elastic Modulus)											
			1	2	3	4	5	6	7	8	9	10	11	12
Type A	E	22.25	24.48	20.03	22.25	22.25	22.25	22.25	22.25	22.25	22.25	22.25	22.25	22.25
	C	11.8	11.80	11.80	12.60	11.00	11.80	11.80	11.80	11.80	11.80	11.80	11.80	11.80
Type B	E	25.47	25.47	25.47	25.47	25.47	27.71	23.23	25.47	25.47	25.47	25.47	25.47	25.47
	C	17.6	17.60	17.60	17.60	17.60	17.60	17.60	18.68	16.52	17.60	17.60	17.60	17.60
Type F	E	26.81	26.81	26.81	26.81	26.81	26.81	26.81	26.81	26.81	29.49	24.13	26.81	26.81
	C	20.6	20.60	20.60	20.60	20.60	20.60	20.60	20.60	20.60	20.60	20.60	21.80	19.40

Table 4.4. Modal frequencies for the considered cases shown in Table 4.3.

Case	Natural Frequency (Hz) for the first free modes			Natural vibration period (Sec) for the first three modes		
	1	2	3	1	2	3
1	3.82	10.17	10.93	0.262	0.098	0.091
2	3.60	9.44	10.24	0.278	0.106	0.098
3	3.71	9.82	10.60	0.270	0.102	0.094
4	3.71	9.82	10.60	0.270	0.102	0.094
5	3.76	9.91	10.69	0.266	0.101	0.094
6	3.66	9.72	10.50	0.273	0.103	0.095
7	3.71	9.82	10.60	0.270	0.102	0.094
8	3.71	9.82	10.60	0.270	0.102	0.094
9	3.73	9.84	10.68	0.268	0.102	0.094
10	3.70	9.80	10.51	0.270	0.102	0.095
11	3.71	9.82	10.60	0.270	0.102	0.094
12	3.71	9.82	10.60	0.270	0.102	0.094

Also, a dynamic analysis is carried out by considering a selected ground motion record with a horizontal component and the vertical component of San Fernando (RSN-80) earthquake shown in Figure 4.10. By applying the selected ground motion record, the obtained time histories of the displacement at the top of the dam, the stress at the upper stream and downstream of the toe are presented in Figure 4.11 by considering the concrete strength as defined in Table 4.1. The fact that the displacement is not equal to zero for increased time indicates that there is a permanent displacement. Consequently, there is a permanent “damage” to the structure, although it is negligible. The maximum displacement at the top of the dam that is identified from the time history is 0.017 m. The maximum stress at the toe of upstream is 1.44 MPa, and the maximum stress is at the toe of downstream is 0.43 MPa. These values are much smaller than the minimum of the compressive and tensile strengths of the concrete, indicating that the dam is safe for the considered ground motion excitation and without considering the strength degradation.

As part of the sensitivity analysis, this dynamic analysis is repeated for each of the cases tabulated in Table 4.3. The maximum absolute values of the displacement at the top of the dam and the stress at the upper stream and downstream of the toe are summarized in Table 4.5 for each of the cases. The results presented in the table indicate that the elastic modulus affects the maximum displacement at the top of the dam and the stresses at the toe. Also, the compressive strength is less sensitive to the elastic modulus. It must be emphasized that the observed low stress level caused by the seismic ground motion is attributed to the moderate to low ground motion intensity used for the analysis. The variation of the stress versus the ground motion intensity measure is to be discussed in Chapter 5. In addition, it was observed that a single time history analysis is in the order of about 20 minutes using a desktop computer. This runtime needs to be considered in the design of the fragility analysis methodology.

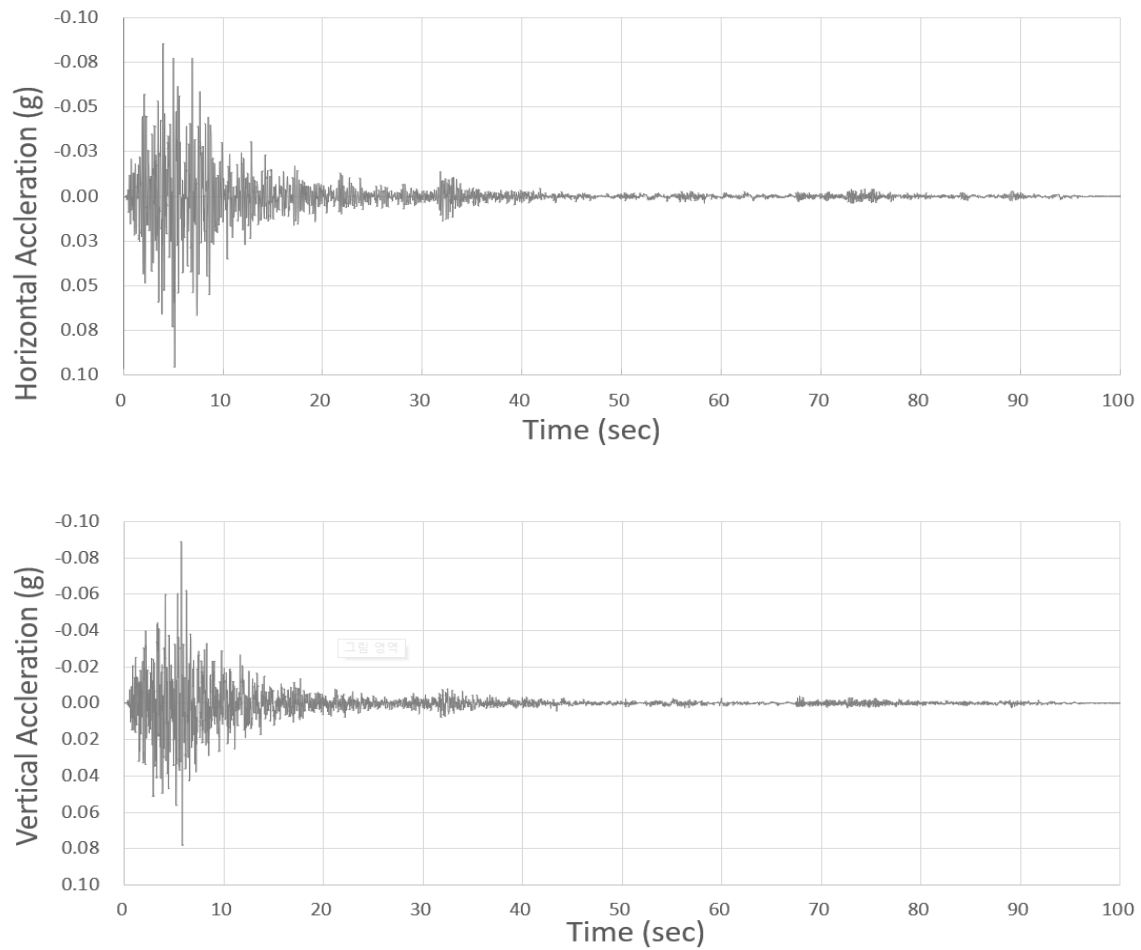
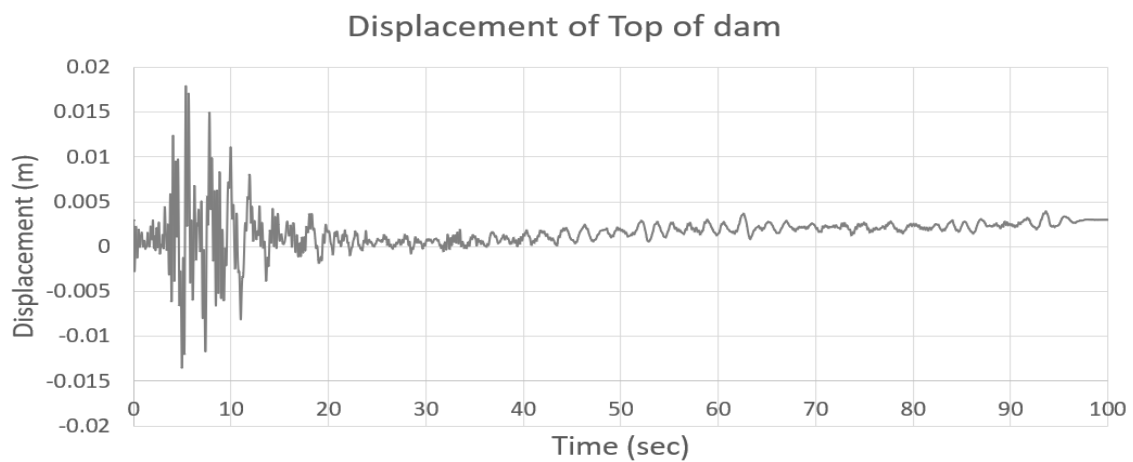


Figure 4.10. Horizontal ground motion record from San Fernando earthquake (RSN-80) of moment magnitude 6.61. The record is recorded at an epicentral distance of 21.5 km.



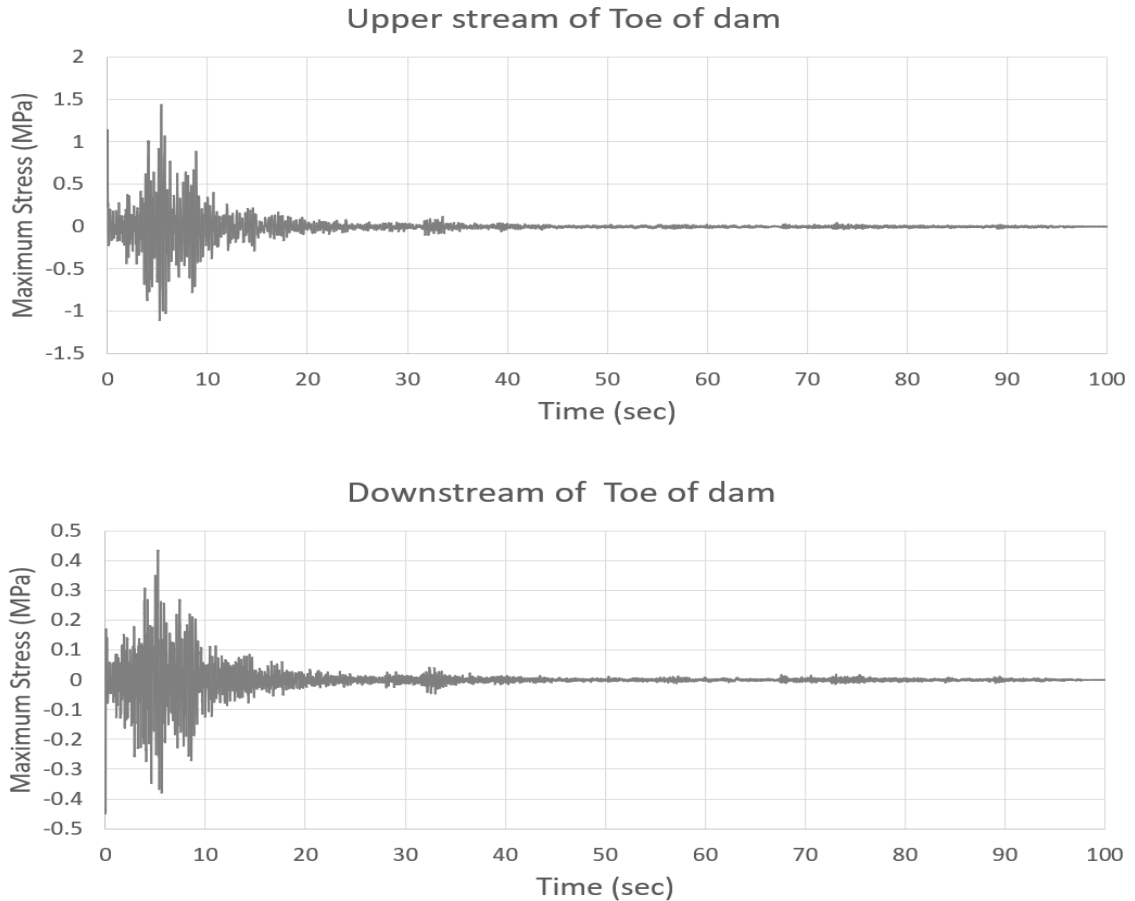


Figure 4.11. Time histories the displacement at the top of the dam, the stress at the upper stream and downstream of the toe

Table 4.5. Result of dynamic Analysis.

Case	Top Displacement (m)	Max Stress at Upper stream of Toe (MPa)	Max Stress at Downstream of Toe (MPa)
1	0.0176	1.489	0.419
2	0.0177	1.360	0.399
3	0.0179	1.441	0.433
4	0.0179	1.441	0.433
5	0.0177	1.582	0.473
6	0.0178	1.311	0.391
7	0.0179	1.441	0.433
8	0.0179	1.440	0.433
9	0.0176	1.437	0.412
10	0.0179	1.422	0.425
11	0.0179	1.441	0.433
12	0.0179	1.441	0.433

4.5 Summary and conclusion

Modeling and analysis of an actual concrete gravity dam - Chungju Multi-Purpose Dam (Chungju dam) in Korea - is presented in this chapter. The model is developed in ABAQUS. The analysis results obtained from the implemented model are compared with those obtained from proprietary software (K-water). The comparison shows that they are in very good agreement and consistent.

In addition, a simple sensitivity analysis is carried out by varying the concrete properties. The sensitivity analysis indicates that the natural vibration frequency is sensitive to the elastic modulus of concrete used for the dam body. The variability of the elastic modulus of concrete for the weir does not lead to a significant change in the vibration characteristics.

As part of the sensitivity analysis, this dynamic analysis is repeated by using a single ground motion record with a horizontal component and vertical component. The results indicate that the variability of concrete properties affects the estimated compressive stress as well as tensile stress.

Chapter 5

5 Probabilistic analysis and development of fragility curve of a Concrete Gravity Dam

5.1 Introduction

Dams are some of the critical energy-generating infrastructures for our society. Existing dams have been in service for some time; they are aging and deteriorating. Few new dams are built due to social, economic, and environmental constraints. There is a necessity for extending the service life of the existing dams beyond their design working life. The decision on the extension should take the potential seismic risk into account for dams located in the seismic hazard-prone region.

The fragility curve represents the estimated failure probability conditioned on the seismic intensity measure, such as the peak ground acceleration. The use of the fragility curve effectively separates the seismic hazard modeling and estimation of the failure probability conditioned on given seismic ground motion intensity, facilitating its practical applications. The fragility curve could be determined based on the empirical approach, heuristic approach, and analytical approach. The empirical approach is carried out based on historical data, while the heuristic approach is carried out based on expert opinion. The analytical approach is based on formal probabilistic structural analysis results that could overcome the data limitation problem associated with the empirical approach and the subjectivity related to the heuristic approach. The fragility curve can also be estimated based on the combinations of the mentioned approaches.

One of the earlier fragility assessments of the concrete gravity dam was presented by Tekie and Ellingwood (2003). For their assessment, the simple simulation technique (or crude Monte Carlo technique) was considered. A disadvantage of using the simple simulation technique is that it is computing time-intensive if a detailed finite element model of a concrete dam is employed for nonlinear dynamic analysis. For improved computational efficiency, Ghanaat et al. (2012) proposed the application of the Latin hypercube sampling (LHS) technique (Iman and Conover 1982) to assess the seismic fragility analysis of the gravity dam. The use of the LHS technique is subsequently considered by others,

including Segura et al. (2020). The limit state function or performance function often considered include the concrete cracking of the neck, foundation material compressive failure at the toe, sliding at the dam-foundation interface, and deflection at the crest with respect to hell. For a detailed review of the fragility assessment of concrete gravity dam, the reader is referred to Hariri-Ardebili and Saouma (2016). Note that many of the probabilistic analysis of concrete gravity dam is focused on the effect of the ground motion record-to-record variability on the estimated responses, while others are focused on the detailed finite element modeling of dams subjected to a single or multiple selected ground motions. However, none of the available assessments considered the effect of aging and degradation of the concrete when assessing the fragility curve. The fact that the combined effect of aging and degradation of concrete can affect the time-varying concrete strength was described and presented in Chapters 3 and 4.

The main objective of this chapter is to carry out the fragility curve assessment by considering the time-varying concrete properties. The evaluation follows the steps illustrated in Figure 5.1. It includes the finite element modeling of the concrete dam, the selection of uncertain model parameters and ground motion records, the nonlinear seismic response analyses, the definition of limit states, and the construction of fragility curves. The uncertainty in material parameters and uncertainty in earthquake ground motions are taken into account using the Monte Carlo simulation. The material properties, such as the elastic modulus of concrete, concrete strength, damping ratio, foundation parameters, are assumed uncertain. The samples of the random variables are to be generated by using the LHS technique. For the numerical analysis, only 12 sets of samples (i.e., surrogates of the dam) are generated. A detailed finite element model for each of the 12 surrogates is implemented and used to evaluate the dynamic responses subjected to the seismic ground motions. By considering the uncertainty in ground motions, twelve ground motions are selected from the Pacific Earthquake Engineering Research Center (PEER) ground motion database. Following Ghanaat et al. (2012) and Segura et al. (2020), the analysis for each surrogate is paired with the 12 selected ground motion records. It is acknowledged that the number of samples may not be entirely justified theoretically, but it is practical considering that the records must be scaled to a set of specified ground motion intensities and the computing time-consuming nonlinear dynamic analysis is to be carried out. In

total, there are 864 nonlinear time-history analyses by considering 12 intensity levels and six age instances of the dam. The estimated computing time, including the preprocessing and postprocessing, using a single desktop is about three months. The obtained time history responses are used as the basis to develop fragility curves. The details of the considered probabilistic models, the analysis procedure and results, the considered limit state functions, and the developed fragility curve are described in the following sections in this chapter.

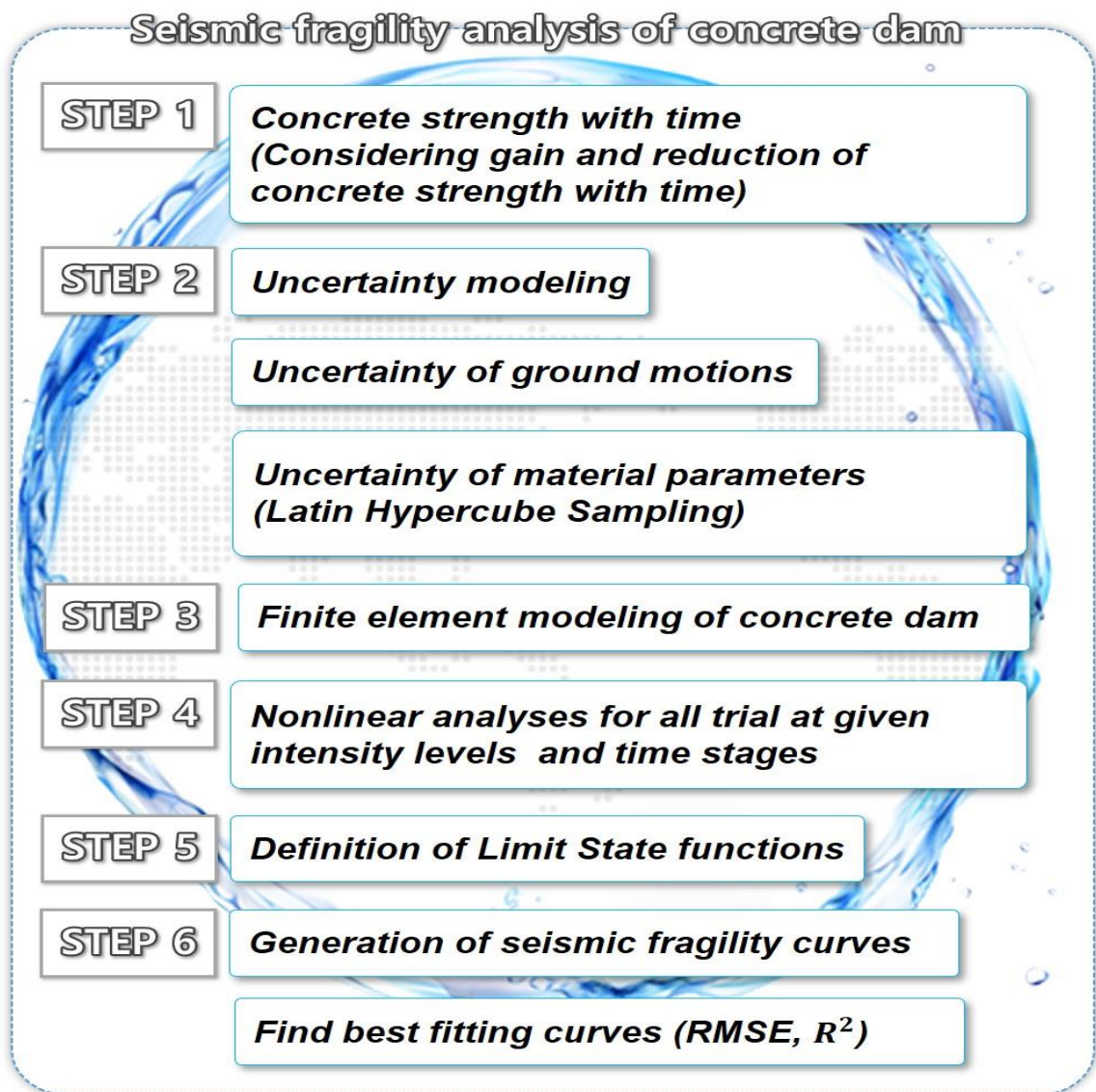


Figure 5.1: Procedures of seismic fragility analysis of concrete dam

5.2 Probabilistic models

5.2.1 Probabilistic models for material properties

For the reliability analysis of the concrete gravity dam, the uncertainty in the material properties and geometric variables as well as in the external loading, such as the seismic ground motions, need to be considered. The considered random variables for the material properties are listed in Table 5.1 for the reliability analysis of Chungju dam. Since the uncertainty in the self-weight of the dam is generally small in comparison to other types of loads (JCSS probabilistic model code, 2001), its variability is neglected.

The modeling of the degradation was discussed in Chapter 3. The concrete compressive strength with degradation effect is assumed to have a lognormal distribution, and the elasticity modulus is assumed to have a normal distribution (Mirza et al., 1979). The coefficient of variation of elasticity modulus is assumed to be equal to 0.1. The coefficient of variation of the tensile strength is assumed to be 0.3 (Probabilistic model code for concrete dams 2016). The coefficient of variation of the compressive strength at each type of concrete is assumed to be 0.063, 0.058, and 0.054, respectively (Korea Infrastructure Safety and Technology Corporation report, 1985). The statistics of the remaining variables shown in Table 5.1 are based on the information suggested in K-water (Seismic performance evaluation report by K-water, 2013). They are explained in the following.

Table 5.1: Statistics for the considered random variables

Uncertainty		Distribution	Parameter	
Dilation Angle		Log-Normal	$\mu = 0.268$	$\sigma = 0.0524$
Friction Angle (°)		Normal	$\mu = 0.7$	$\sigma = 0.031$
Elasticity Modulus of concrete (GPa)	Type A	Normal	$\mu = 22.25$	$\sigma = 2.225$
	Type B	Normal	$\mu = 25.47$	$\sigma = 2.447$
	Type F	Normal	$\mu = 26.81$	$\sigma = 2.681$
Concrete compressive strength (MPa)	Type A	Log-Normal	$\mu = 11.8$	$\sigma = 0.8$
	Type B	Log-Normal	$\mu = 17.6$	$\sigma = 1.078$

Uncertainty		Distribution	Parameter	
	Type F	Log-Normal	$\mu = 20.6$	$\sigma = 1.196$
Concrete tensile strength (MPa)	Type A	Log-Normal	$\mu = 2.480$	$\sigma = 0.744$
	Type B	Log-Normal	$\mu = 2.864$	$\sigma = 0.859$
	Type F	Log-Normal	$\mu = 3.031$	$\sigma = 0.909$
Parameters for damping coefficient α		Uniform	$L = 0.253$	$U = 0.310$
Parameter for damping Coefficient β		Uniform	$L = 0.006$	$U = 0.008$

It must be emphasized that some of the mentioned random variables shown in Table 5.1 could be correlated. Such a correlation is not considered because there is no information available for the considered dam to assess such a correlation. This is a simplifying assumption which deserves further investigation.

In general, the concrete-rock interface can exhibit a relatively high cohesion and tensile strength if the bond is intact. For an interface with cohesion, the failure occurs as a brittle failure without any sliding. At the point of failure, the shear strength can be described with the Mohr-Coulomb failure criterion with cohesion, c_c and an internal friction angle, $\phi_{i,c}$. If no bond exists or the intact bond is broken, no cohesion exists, and the total friction angle can be expressed as the sum of two components, a friction angle from a macroscopic smooth but microscopic rough surface, $\phi_{b,c}$ and a dilation angle, i_c which originates from the inclination of larger asperities in the concrete-rock interface. This means that failure can occur at different degrees of deformation, without any relative deformations (failure of the intact bond) and with a relative deformation within from a few millimeters to a few centimeters if no intact bond exists.

The shear strength can, therefore, be divided into two separate cases. The first one considers that an intact bond exists, and cohesion is included. The second one considers that the bond is broken, and no cohesion is included. Even though cohesion may exist in the interface, the uncertainty associated with this parameter is significant.

For a broken concrete rock interface, the total friction angle, ϕ_{tot} , can be described as,

$$\phi_{tot,c} = \phi_{b,c} + i_c \quad (5.1)$$

where $\phi_{b,c}$ is the primary friction angle for a macroscopic smooth but microscopic rough surface and i_c is the contribution from the large-scale asperities in the interface. According to Westberg Wilde, M, and F. Johansson (2016), if the project-specific tests are not performed $\tan(\phi_{b,c})$ could be assumed to be normally distributed with a mean of 0.7 and a standard deviation of 0.031 (i.e., $N(0.7, 0.031)$). i_c for a blasted rough surface can be assumed to have a mean value of 15° and a standard deviation of 3° . This value has to be supported by measurements of the inclination of larger asperities at the rock surface. If the dam is founded on smooth surfaces, or if it cannot be verified that the dam is founded on a blasted rough surface, i_c may be assumed to have a mean value of 5° and a standard deviation of 1° . Since the actual test results are unavailable for the considered dam, it is considered that $\tan(i_c)$ could be assumed to be lognormally distributed with a mean of 0.268 and a standard deviation of 0.0524 (i.e., $LN(0.268, 0.0524)$) for a blasted rough surface, and $\tan(i_c)$ could be assumed to be lognormally distributed with a mean of 0.087 and a standard deviation of 0.0175 (i.e., $LN(0.087, 0.0175)$) for a smooth surface. For practical applications, $\tan(\phi_{b,c} + i_c)$ could be calculated by using,

$$\tan(\phi_{b,c} + i_c) = \frac{\tan(\phi_{b,c}) + \tan(i_c)}{1 - \tan(\phi_{b,c}) \cdot \tan(i_c)} \quad (\text{trigonometry identity}) \quad (5.2)$$

For the reliability analysis to be carried out, it is assumed that $\tan(\phi_{b,c}) \in N(0.7, 0.031)$. and $\tan(i_c) \in LN(0.268, 0.0524)$ (Probabilistic model code for concrete dams. 2016).

Given the characteristic value of compressive strength f_{ck} (MPa), according to the Korean Design Standard (MOCT, 2016), the mean of the concrete compressive strength for undamaged concrete, f_0 , can be estimated:

$$f_0 = f_{ck} + 8, \text{ (MPa), for } f_{ck} < 40 \text{ MPa} \quad (5.2a)$$

The mean of the tensile strength of concrete f_{ta} (MPa) can be calculated using,

$$f_{ta} = 0.57 \times \sqrt{f_{ck}} \quad (5.2b)$$

and the mean of the elastic modulus of concrete E_c (GPa) can be calculated using,

$$E_c = 8,500 \times \sqrt[3]{f_0} \quad (5.3)$$

Those parameters could vary with time because of aging and degradation, as discussed in the previous chapter.

It is considered that the Rayleigh damping is applicable, and the damping coefficient matrix C can be expressed as,

$$C = \alpha M + \beta K \quad (5.4)$$

where M and K are the mass and stiffness matrices, and α and β could be determined based on

$$\alpha = \frac{2\omega_1\omega_3}{\omega_1+\omega_3} \xi, \quad \beta = \frac{2}{\omega_1+\omega_3} \xi \quad (5.5)$$

which ξ is assumed to be 5%. The calculated α and β are treated as their mean values. α and β are assumed to be independent uniformly distributed with upper and lower bounds equal to 0.9 and 1.1 of their corresponding mean values.

5.2.2 Simulation of the random variables for the concrete dam

Given the random variables that are defined according to their probability distribution, their samples can be generated using the crude or simple simulation technique. As mentioned in the introduction in this chapter, such an approach could be very computing-time consuming for the analysis of the dam subjected to ground motions and considering the nonlinear inelastic behavior. To improve efficiency, the LHS technique (Iman and Conover, 1982; Olsson et al., 2003) is considered in the following. In simple terms, to generate m_s samples by considering n_{rv} random variables, the range of each variable is divided into m_s equally probable intervals. m_s samples for each random variable are mixed such that no one sample from a random variable is used twice. An advantage of this

sampling scheme is that the required samples do not increase with the increased number of random variables.

The use of the LHS technique to evaluate the fragility curve for the concrete gravity dam was considered by, amount other, by Ghanaat et al. (2012) and Segura et al. (2020). It was claimed in Ghanaat et al. (2012) that a sample size of 10 could be adequate. In this chapter, a sample size of 12 is considered for the concrete gravity dam modeling. Again, it is emphasized that the use of only 12 samples to develop the fragility curve is usually small but is accepted in the literature for dam safety assessment (for a review, see Hariri-Ardebili and Saouma 2016). However, it is adequate to illustrate the overall procedure to assess the fragility curve by considering the time-varying concrete degradation. A detailed finite element model, similar to that described in Chapter 4, for each Latin hypercube sample (i.e., a sampled dam) is implemented and used to evaluate the dynamic responses subjected to the seismic ground motions. Based on the LHS techniques, the simulated 12 samples are listed in Table 5.2.

Table 5.2: Case study for the considered random variables

case	1	2	3	4	5	6	7	8	9	10	11	12	
Dilation Angle	52.49	52.62	53.26	51.09	53.33	52.38	51.88	52.19	54.88	51.94	53.23	51.51	
Friction Angle	34.76	35.05	34.74	36.11	35.30	34.35	34.13	36.78	36.44	34.81	35.46	34.38	
Elastic Modulus (GPa)	Type A	19.69	22.02	22.48	22.96	24.06	26.10	23.47	21.54	24.81	21.03	18.40	20.44
	Type B	28.29	27.46	26.25	21.23	22.66	23.48	26.81	29.71	25.21	24.69	25.73	24.13
	Type F	23.73	28.99	24.63	26.53	31.45	25.34	27.66	28.28	25.96	27.09	22.17	29.89
Compressive Strength (MPa)	Type A	11.86	11.68	12.42	11.75	12.50	13.36	11.34	11.85	12.42	10.88	10.68	10.86
	Type B	18.04	18.39	17.57	15.85	16.94	16.53	18.55	18.88	17.71	18.43	18.49	15.85
	Type F	18.71	20.77	21.09	20.73	23.03	19.86	20.50	19.87	20.89	20.62	19.07	22.06
Tensile Strength (MPa)	Type A	2.56	2.72	1.62	2.89	2.40	1.19	2.07	2.24	3.08	3.34	1.88	3.77
	Type B	1.38	2.39	2.59	3.14	2.17	3.56	1.88	2.95	2.77	3.85	3.34	4.35
	Type F	2.74	4.61	3.13	1.46	2.29	3.77	3.32	1.99	2.94	3.53	2.53	4.08
Damping coefficient α (10^{-1})	2.79	3.00	2.99	3.03	2.65	3.02	2.66	2.78	2.78	2.87	2.66	2.78	
Damping coefficient β (10^{-3})	6.6	7.3	6.9	6.9	6.6	6.4	6.8	6.4	6.3	6.5	6.3	6.9	

For the numerical analysis, 12 ground motion records are selected, as described in the next section. For each of the sampled dam, nonlinear inelastic dynamic analysis is to be carried out. If 12 seismic intensity levels (e.g., 12 peak ground acceleration level or 12 spectral acceleration (*SA*) level) are considered, and six ages of the concrete dam are considered, the total number of required nonlinear dynamic analysis of the dam is 864.

5.2.3 Seismic Loading Consideration

The uplift pressure, silt pressure, and ice load are treated deterministically since their variability is usually small for the considered scenario. Their calculation is explained in the previous chapters. The hydrodynamic pressure is calculated based on the ratio between the natural frequency of the reservoir and the natural frequency of the dam (Chopra 1968). For the Chungju dam, the natural frequency of the reservoir is 4.09 Hz (see Eq. (4.5)), and the natural frequency of the dam is 3.82 Hz (see Table 4.2). Thus, the ratio of these two natural frequencies for the considered dam is less than 2 (see Eq. (4.6)), and the acoustic element should be applied, and the water is considered compressible. The acoustic elements in the ABAQUS are used to describe the pressure distribution over time in acoustic media such as water (ABAQUS analysis user's manual).

According to the Korean seismic design standard (2019), the standardized design response spectrum for the location of the considered dam is shown in Figure 5.2 with the parameters given in Table 5.3. The design spectrum has three segments corresponding to the acceleration, velocity, and displacement sensitivity ranges. In the acceleration sensitivity range, the spectral acceleration remains to be constant. In the velocity sensitivity range and the displacement sensitivity range, S_a is proportional to $1/T$ and $1/T^2$ respectively, where T in here represents the natural vibration period of a single-degree-of-freedom system.

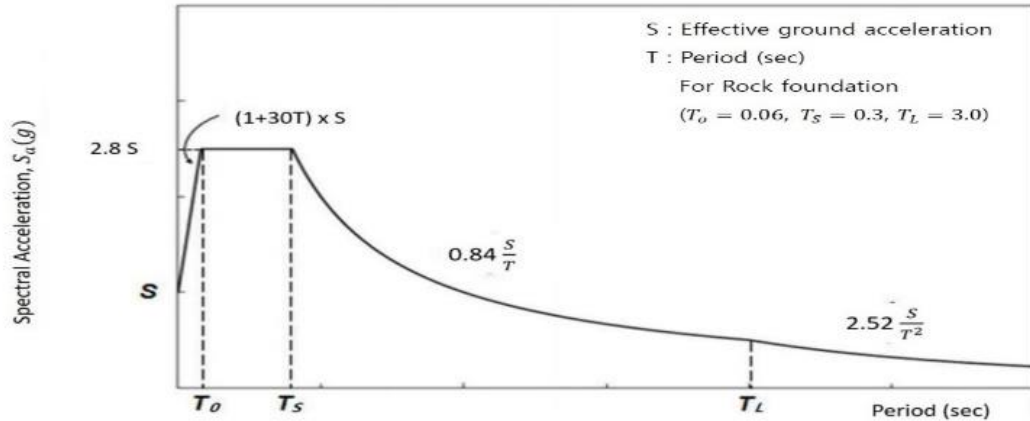


Figure 5.2: Design response spectrum characterization (Korean seismic design guideline, 2019)

Table 5.3: Spectrum parameters (Korean seismic design guideline, 2019)

Short Period Amplification Factor	Transition Period (second) for Rock foundation		
	T_0	T_S	T_L
2.8	0.06	0.3	3.0

The effective ground acceleration S shown in Figure 5.2 can be determined based on the Korea seismic design standard (MOCT, 2019). It is determined by multiplying the seismic zone factor and hazard coefficient shown in Table 5.4. There are two Seismic Zone I and II with the seismic zone factor that equals $0.11g$ and $0.07g$, respectively, for the return period of 500 years, where g is the gravitational acceleration. Since the Chungju dam, which is built on the rock foundation, is located in Seismic zone I, and requires the consideration of a 2400 year return period for selecting the hazard coefficient, the resulting in S equals $0.22g$ (i.e., $0.11g \times 2$). The use of this S value and Figure 5.2 leads to the design spectrum to be considered, as shown in Figure 5.3, where the horizontal axis is in logarithmic scale.

Table 5.4: Seismic risk factor (Korean seismic design guideline, 2019)

Mean Return Period (Year)	50	100	200	500	1,000	2,400	4,800
Hazard Coefficient	0.40	0.57	0.73	1	1.4	2.0	2.6

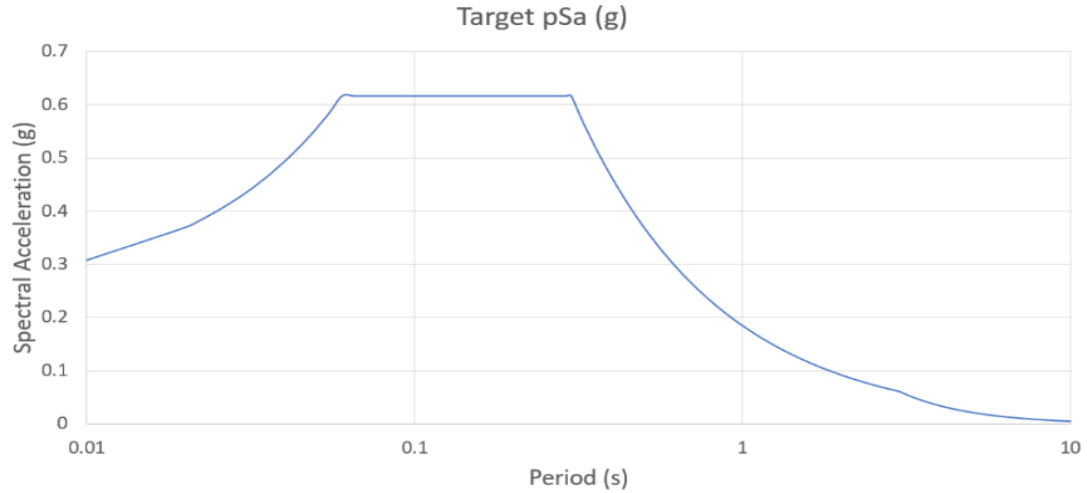


Figure 5.3: Target Spectrum of Chungju dam

Based on the information given in Table 5.3, and considering that the annual maximum effective ground acceleration S follows the lognormal distribution,

$$F_s(S) = \Phi \left(\frac{\ln S - \ln(\mu/\sqrt{1+v^2})}{\sqrt{\ln(1+v^2)}} \right) \quad (5.6)$$

where μ and v are the mean and coefficient of variation of x . By considering that x represents the “hazard coefficient” (as shown in Table 5.4), and carrying out the least-squares fit based on the values shown in Table 5.4, it was concluded that μ equals 0.0643 and v equals 1.977. In other words, the annual maximum effective ground acceleration S can be modeled using the lognormal distribution with the mean equal to 0.0643g and the coefficient of variation of 1.977. Based on this fitted distribution, the 1000-, 2500-, 5000-, 10000-, 50000- and 100000-year return period value of S is 0.157g, 0.219g, 0.278g, 0.348g, 0.568g, and 0.693g, respectively. Since the spectral acceleration equals 2.8 S (see Figure 5.2), the 1000-, 2500-, 5000-, 10000-, 50000- and 100000-year return period value of SA equals 0.441g, 0.614g, 0.777g, 0.974g, and 1.59g, and 1.94g, respectively.

The seismic ground motions are uncertain and nonstationary. Ideally, one should consider many ground motions to assess the linear and nonlinear seismic responses and to develop fragility curves. However, such an analysis is prohibitive expensive for the current project since a single analysis for a selected ground motion record is computing time-consuming

for a well-equipped desktop computer. As the objective is to show the overall analysis procedure to develop the time-dependent fragility curve, only 12 records are considered and scaled.

For the record selection, it was considered that the record must be recorded at the rock site, with an epicentral distance less than 60 km and an earthquake moment magnitude between 6.0 to 7.5. In setting this criterion, it was considered that the epicentral distance from the dam to Hongsung Earthquake (1987) is about 25 km. By adopting the mentioned criteria, the selected 12 records from PEER Strong Ground Motion Data Base are shown in Table 5.5. For each selected record, the first horizontal component and the vertical component could be considered for the dynamic analysis (MOCT, 2019).

To show the characteristics of the selected records, the spectral acceleration (SA) for the horizontal component of each record by considering a damping ratio of 5% is calculated and shown in Figure 5.4. For the plot, SA is normalized such that the SA at the fundamental vibration period of the dam (see Chapter 4) is equal to 1g. Similarly, SA for the vertical component of each record is calculated and depicted in Figure 5.5. Again, the SA is normalized for the plot. It must be emphasized that the normalization is done to illustrate their characteristics. Figures 5.4 and 5.5 show that there is a significant record to record variability.

Table 5.5: Selected ground motions

No	Year	Event	Station	Moment magnitude, M	Epicentral distance, R (km)
1	1971	"San Fernando"	"Pasadena - Old Seismo Lab"	6.61	21.5
2	1984	"Morgan Hill"	"Gilroy Array #1"	6.19	14.9
3	1989	"Loma Prieta"	"Gilroy Array #1"	6.93	8.84
4	1992	"Landers"	"Lucerne"	7.28	2.19
5	1994	"Northridge-01"	"LA - Wonderland Ave"	6.69	15.11
6	1994	"Northridge-01"	"Vasquez Rocks Park"	6.69	23.1

No	Year	Event	Station	Moment magnitude, M	Epicentral distance, R (km)
7	1995	"Kobe_ Japan"	"Kobe University"	6.9	0.9
8	1999	"Chi-Chi_ Taiwan-05"	"HWA003"	6.2	49.84
9	1999	"Chi-Chi_ Taiwan-06"	"HWA003"	6.3	52.33
10	1989	"Loma Prieta"	"Los Gatos - Lexington Dam"	6.93	3.22
11	2000	"Tottori_ Japan"	"SMNH10"	6.61	15.58
12	2003	"San Simeon_ CA"	"Diablo Canyon Power Plant"	6.52	37.92

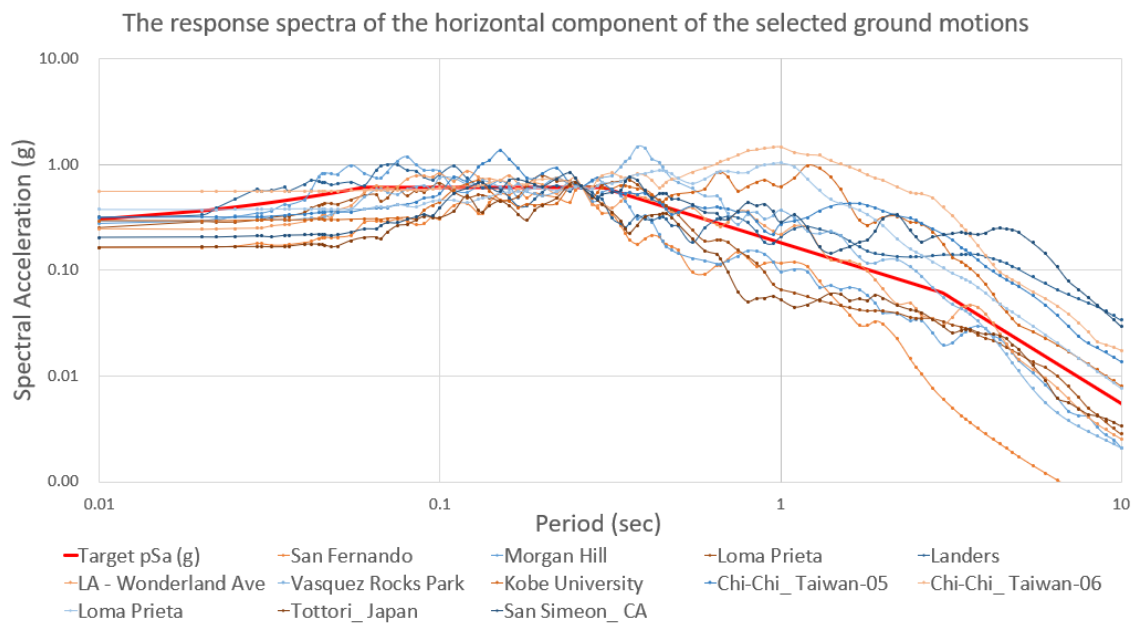


Figure 5.4: Response spectra of the horizontal component of selected ground motions (SA are normalized such that their values are equal to 1g at the natural fundamental vibration period).

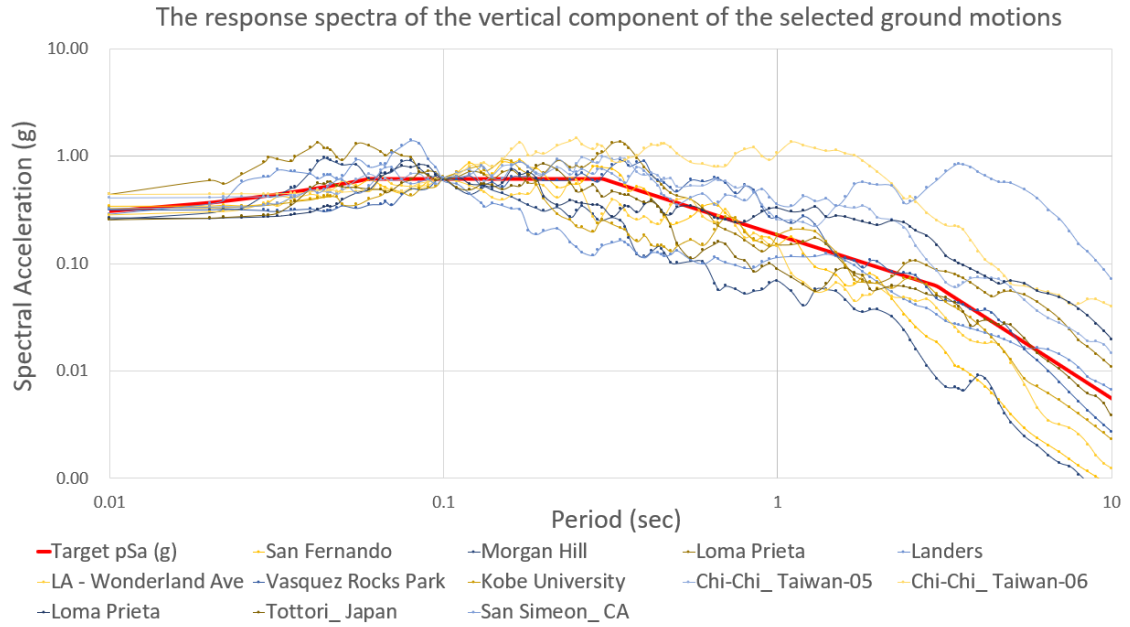


Figure 5.5: Response spectra of vertical components of selected ground motions (SA are normalized such that their values are equal to 1g at the first vibration period in the vertical direction).

5.3 Consideration of Limit State Functions

Several limit states are considered for the fragility analysis to be carried out based on the results from the rigid body analysis and the nonlinear inelastic dynamic analysis by using the model developed in Chapter 4. These limit state functions are established based on:

- 1) Resultant force outside of kern (rigid body analysis) or tension at the heel (FE);
- 2) Resultant force outside of middle-half of a base of the dam;
- 3) Material failure of concrete at the toe or at the upstream face;
- 4) Material failure of concrete at the neck of the dam;
- 5) Material failure of foundation at the toe;
- 6) Sliding at the dam-foundation interface, and

7) Deflection of the top of the dam relative to the heel.

The limit state functions established based on the above condition are named as g_i , $i=1, \dots, 7$. $g_i < 0$ indicates that failure for the i -th limit state is observed. g_1 and g_2 are used to assess the stability of the monolith. In the rigid body analysis, $g_1 > 0$ is achieved if the eccentricity of the resultant vertical force is less than 1/3 of the width of the base or greater than 2/3 of the base, i.e., if the resultant lies outside of the middle third of the dam. It is usually associated with the onset of tension cracks at the heel of the dam and is thus considered analogous to observing tensile stresses at the heel of the dam in the FE analyses. Similarly, in the rigid body analysis, if the resultant force is outside of the middle half, i.e., eccentricity, e , is less than 1/4 of base or greater than 3/4 of the base, then $g_2 < 0$ occurs. In the linear FE analysis, this would be analogous to having 1/6 of the base of the dam in tension. In the nonlinear FE analysis, this limit state function is characterized by the formation of a significant crack by tensile forces at the dam-foundation interface, which is assumed to have no cohesion. However, the cracking responses related to the resultant force (g_1 and g_2) are not meaningful performance states in seismic analyses. These two limit state functions are not considered in the following fragility curve analysis.

The limit state functions g_3 to g_5 are related to material failures. The crack formation due to tensile stress at the dam is checked in terms of maximum tensile stress caused by earthquakes. When the maximum tensile stress by earthquakes exceeds the tensile strength of concrete, the cracking of a concrete dam occurs. The tensile stresses at the toe or at the upstream face could exceed the concrete tensile strength, resulting in $g_3 < 0$. The limit state $g_4 < 0$ occurs if the stress in the concrete at the neck exceeds the concrete strength. These two limit state functions g_3 and g_4 are considered for the fragility curve analysis. The mathematical equations for these two limit state functions are expressed as,

$$g_{3,4} = \sigma_{ta} - \sigma_{max} \quad (5.7)$$

where is σ_{ta} the tensile strength of concrete at a dam, σ_{max} is the maximum tensile stress due to earthquakes by ABAQUS. Further discussion of these two limit state functions is given in the subsequent sections.

By using the results from the rigid body analysis, $g_5 < 0$ occurs if the compressive stresses at the foundation around the toe or the upstream face of the dam are more significant than the bearing capacity of the foundation material. By assuming that the foundation is homogeneous, elastic, and isotropic, the dam-foundation interface is subjected to intermittent opening and closure but with no residual cracks formed due to seismic ground motions. Moreover, our experience indicates that the magnitude of the opening or closure is negligible has safety significance.

The limit state $g_6 < 0$ represents the sliding failure at the interface between the dam and the foundation. This occurs when the total horizontal force is greater than the resisting frictional force developed at the interface. The potential base sliding under seismic ground motions depends on the friction angle and cohesion between the interface of the dam and foundation. Often the possibility of the base sliding for the concrete gravity dam is very slight. This is verified using some preliminary analysis results. For this reason, the limit state g_6 is not considered in the following for developing the fragility curve. This is further justified since the objective of this chapter is focused on the effect of the age and degradation of concrete strength.

The excessive deformation g_7 of the dam body is checked in terms of relative deformation between the crest of a dam and the base of a dam. The excessive deformation of the dam body can impair the internal drainage system or cause service limitation for equipment. In the present study, the difference between the horizontal displacements of nodal points (toe and crest point) are considered. The fragility curves are obtained based on the 1.323 cm and 2.646 cm relative displacements, which are calculated as 0.014% and 0.028% of the dam height, respectively (Tekie and Ellingwood 2003). A relative deformation of 0.014% (1.323 cm) may affect the performance of the dam drainage system, which can increase the uplift pressure at the base interface. A relative deformation of 0.028% (2.646 cm) could be used to indicate differential movements between adjacent monoliths in the dam, which causes the eventual loss of pool control. Based on these assumed relative deformation thresholds, the limit state functions can be written as,

$$g_7(a) = (\delta_x^{Crest} - \delta_x^{Toe}) - 1.323 \text{ cm} \quad (5.8a)$$

and,

$$g_7(b) = (\delta_x^{Crest} - \delta_x^{Toe}) - 2.646 \text{ cm} \quad (5.8b)$$

where δ_x^{Crest} is the horizontal displacement at the crest of the dam and δ_x^{Toe} is the horizontal displacement at the toe of the dam.

5.4 Developed Fragility curves

The seismic fragility is defined as the conditional probability of failure or exceedance of a certain limit state at a given intensity measure such as earthquake spectral acceleration (SA). As mentioned earlier, the fragility analysis for the considered concrete dam can be carried out based on the simulation technique. For the analysis, the adopted ground motion intensity measure is the spectral acceleration (SA) at the fundamental natural vibration period

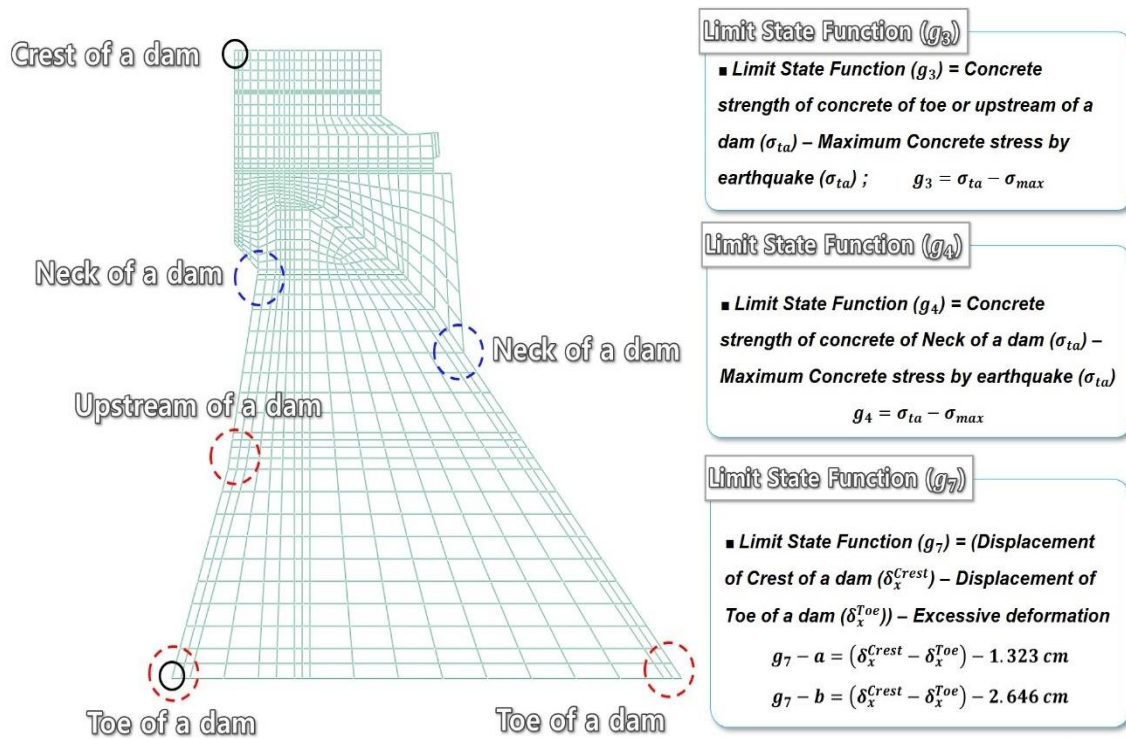


Figure 5.6: Limit State Function of Chungju Dam.

The considered intensities are 0.1g to 1.2g with a 0.1g increment. The scaling factor used to scale the horizontal component is also applied to the vertical component. The 12 selected ground motion records in Table 5.4. were randomly paired with the 12 prepared finite element models at a specific time. The ages since the construction of the dam equal to 1, 25, 36, 50, 75, and 100 years are considered to investigate the effect of aging and degradation

5.4.1 Tensile Cracking at the toe or upstream face of the dam

The crack formation of a dam is induced under cyclic or dynamic loads. The main failure mechanisms are cracking in tension and crushing in compression. The concrete is designed to resist compression; the tensile strength of concrete is comparatively less than its compressive strength. When the maximum tensile stress (σ_{max}) due to earthquake ground motions exceed the tensile strength of concrete at toe or upstream face (σ_{ta}), the cracking of concrete should occur. The tensile cracking at the toe or at the upstream face of the dam, according to g_3 defined in Eq. (5.7), is checked by the maximum tensile stress caused by earthquakes and the tensile strength of concrete. For completeness, the samples are presented in Appendix A.

Before carrying out the estimation of the conditional failure probability, a few observations are in order. From the analysis results, it was found that the failure mechanism of tensile cracking is formed of three main damage zones, one at the neck of the upstream direction, the second one at the neck of the downstream direction, and the last one at the upstream face, as shown in Figure 5.7. In most cases, the cracking profile in the neck of the dam at the upstream direction initiates at the point of slope discontinuity on the upstream face. After the neck cracking of the upstream direction has occurred, the cracking of the upstream face is initiated in the horizontal direction. In the last stage, the neck cracking of the downstream direction occurs.

It should be noted that most of the studies focused on dam safety directly uses the ratio of the number of failure events divided by the total number of sampled events (referred to as based on counts) in assessing the conditional probability and fragility curve (Hariri-Ardebili and Saouma 2016). The calculated conditional failure probability, according to

the count, is presented in Figure 5.8a. Unfortunately, the number of samples is too limited to provide a sufficient adequate estimate for the conditional probability of failure. In order to take advantage of the value of the limits state function, a probability distribution fitting based on 12 samples for the given year and seismic intensity level is carried out by using the normal distribution and the Gumbel distribution. The selection of these distributions is based on the consideration that they are defined for positive and negative values. By using the fitted distributions, the obtained conditional probability of failure is plotted in Figure 5.8b if the normal distribution is used and in Figure 5.8c if the Gumbel distribution is used. The fitting and extrapolation are extremely important for cases only very limited samples are available. This is because one is focused on the overall failure probability in the order of less than 10^{-3} in the structural reliability analysis.

The mathematical form of the normal probability distribution function is,

$$F(x) = \Phi\left(\frac{x-m}{\sigma}\right) \quad (5.9)$$

and the Gumbel probability distribution is,

$$F(x) = \exp(-\exp(-(x-u)/a)) \quad (5.10)$$

where m and σ are two parameters (i.e., mean and standard deviation) of the normal distribution, $\Phi(\cdot)$ is the standard normal distribution function, u and a are two parameters of the Gumbel distribution function.

The results presented in Figures 5.8a to 5.8c indicate that the calculated conditional failure probability depends on the adopted option. It must be emphasized that this simply indicates the problem associated with a very limited number of samples rather than the problem of the methodology. The conditional probability increases with increasing seismic intensity and with increasing time after 25 years. The latter can be explained by noting that the concrete strength by considering both the aging and degradation is an increase and then decreasing function of time (see Chapter 4).

The results presented in Figure 5.8 are to be used to assess the parametric model for the fragility curves. For developing the time-dependent fragility curve, a curve fitting based

on the least-squares method is carried out. For the fitting, it is considered that the fragility curve could be represented by using the mathematical form representing the normal, lognormal, or Weibull distribution. The best fit curve is judged based on the coefficient of determination R^2 , the root-mean-square error (RMSE) and the visual inspection of the plot. It was concluded that the fragility curve could be represented by the curve representing the Weibull distribution

$$F_x(S_a) = 1 - e^{-\left(\frac{S_a}{\alpha}\right)^\gamma} \quad (5.11a)$$

or by curves representing the lognormal distribution (see Eq. (5.6)), which is re-written as,

$$F(x) = \Phi\left(\frac{\ln S_a - m_{\ln x}}{\sigma_{\ln x}}\right) \quad (5.11b)$$

Where S_a denotes the spectral acceleration, α and γ are parameters for the Weibull distribution, and $m_{\ln x}$ and $\sigma_{\ln x}$ are two parameters for this fragility curve. Note that while the lognormal distribution is frequently employed to fit the fragility curve, the use of the Weibull distribution is much less frequent. It was found that there is no unique distribution that is preferred for all cases. By considering all cases and for consistency, the Weibull distribution is preferred. The fitted Weibull distribution parameters are shown in Table 5.6, and the fitted curves are also presented in Figure 5.8. Again, it must be emphasized that due to limited samples, although the fit may be questionable, it does show that the seismic fragility curve is time-dependent.

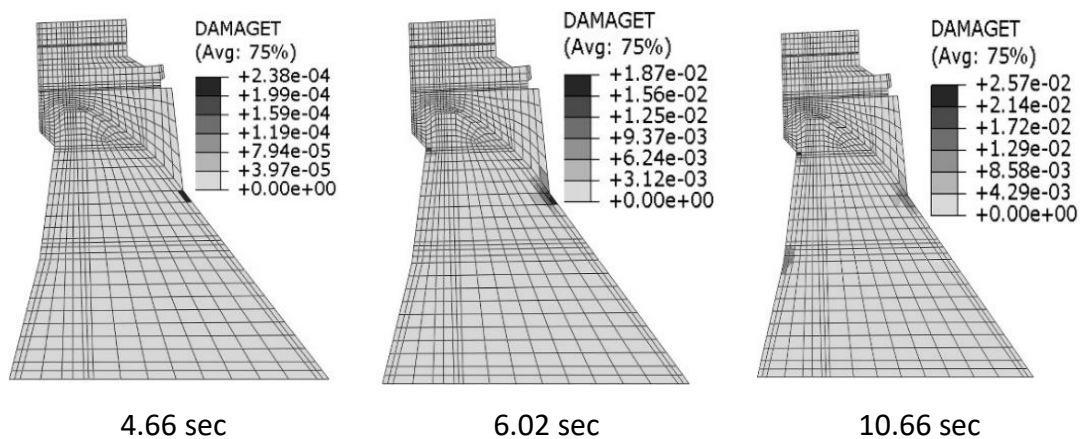


Figure 5.7: Cracking profiles based on limit state g_3

Table 5.6: Fitted model parameters by considering limit state function g_3 .

Year	Based on results shown in Figure 5.8a		Based on results shown in Figure 5.8b		Based on results shown in Figure 5.8c	
	α	γ	m	σ	u	a
1	1.743	4.686	1.817	4.599	1.394	4.508
25	1.620	7.719	1.883	5.565	1.405	7.952
36	1.528	7.041	1.736	5.659	1.403	5.332
50	1.361	10.124	1.786	4.527	1.362	4.395
75	1.283	5.814	1.437	4.657	1.223	3.542
100	1.245	4.153	1.536	3.168	1.143	2.863

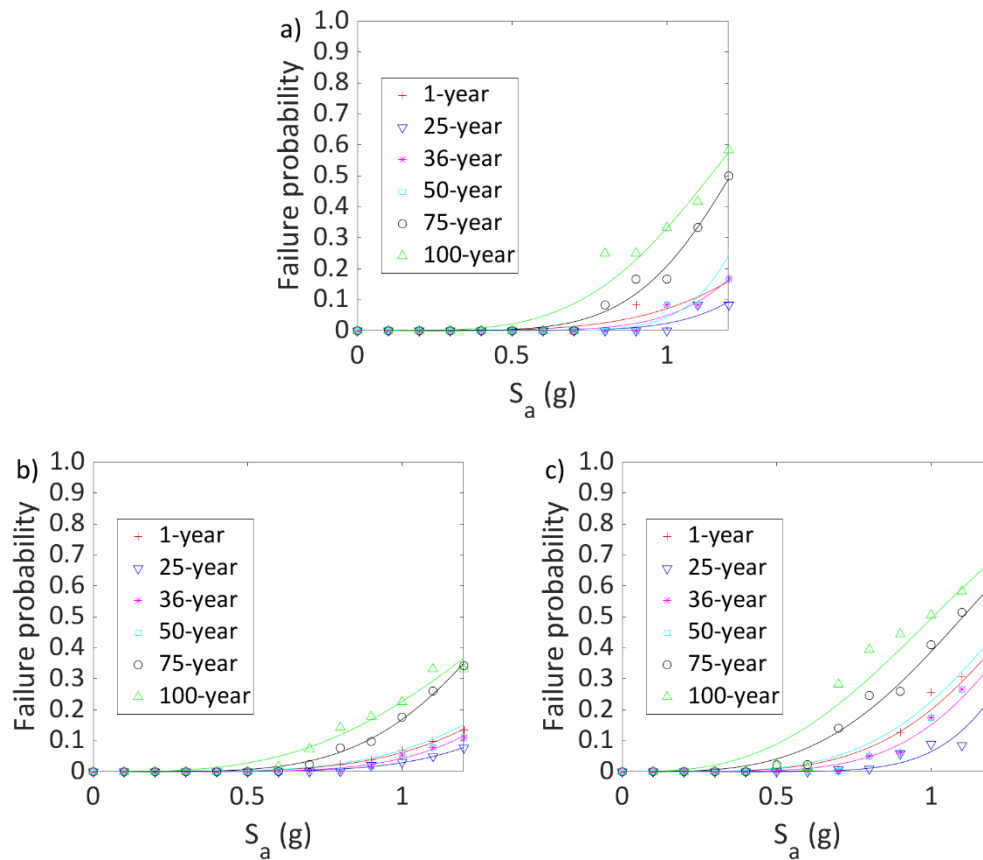


Figure 5.8: Estimated conditional failure probability by considering the tensile cracking at toe or upstream face (i.e., limit state function g_3): a) Based on the ratio of failed events, b) Based on the fitted Normal distribution, and c) Based on the fitted Gumbel distribution.

5.4.2 Tensile Cracking at the Neck of the Dam

The tensile cracking at the neck of the dam occurs following the same mechanism of tensile cracking at a toe or an upstream face of the dam. The tensile cracking at the neck of the dam is defined based on g_4 , as described in Eq. (5.7), which depends on the maximum tensile stress σ_{max} and tensile strength of concrete at the neck of a dam σ_{ta} .

Inspection of the simulation results indicates that the failure mechanism of tensile cracking is formed of two main damage zones, one at the neck of the downstream direction and one in the neck of the upstream direction of the dam. In most cases, the cracking in the upstream neck of the dam initiates first. It is followed at the point of slope discontinuity on the upstream face, as illustrated in Figure 5.9.

Values of the limit state function g_4 are calculated by considering the combinations of the 12 surrogates of the dam (i.e., obtained from Latin hypercube sampling), 12 seismic intensity levels, and six ages since the construction of the dam. These values are given in Appendix A for completeness. Similar to the previous section, the conditional failure probability is calculated using the number of failed events or the probability distribution fitting to each set of 12 samples (conditioned on the seismic intensity and age). The obtained conditional failure probability based on the ratio of failed events or the fitted distribution is shown in Figures 5.10a to 5.10c. Again, it must be emphasized that the estimated conditional failure probability depends on the adopted option because of the very small sample size. Also, there is inconsistency in the estimated failure probability for the age of 100 years because of the increased failure probability at a low SA value. This is attributed to the problem of using a small sample size rather than the problem of the methodology.

The figure shows that the conditional failure probability of tensile cracking at the neck of the dam increases with the increasing seismic intensity. The lowest conditional failure probability is associated with age equal to 25 years. This is because, at this age, the average concrete strength tends to be maximum due to the combined effect of aging and degradation. The degradation influenced the conditional failure probability of tensile cracking of the neck as the age increases beyond 25 years.

A similar analysis for developing the fragility curve that was carried out by considering g_3 in the previous section is repeated by considering g_4 with the results presented in Figure 5.10. The fitted parameters for the fragility models are presented in Table 5.7, and the fitted curves are shown in Figure 5.10. In all cases, the trends are similar to those by considering g_3 shown in the previous section.

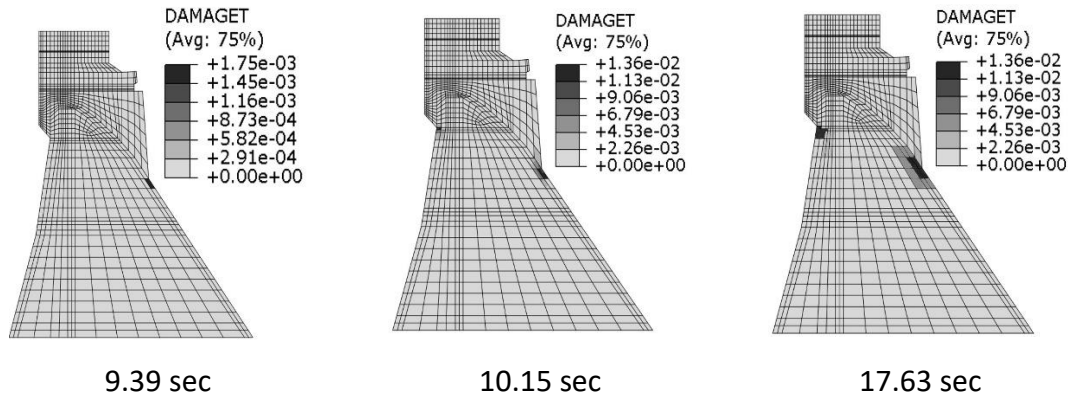


Figure 5.9: Cracking profiles based on limit state g_4

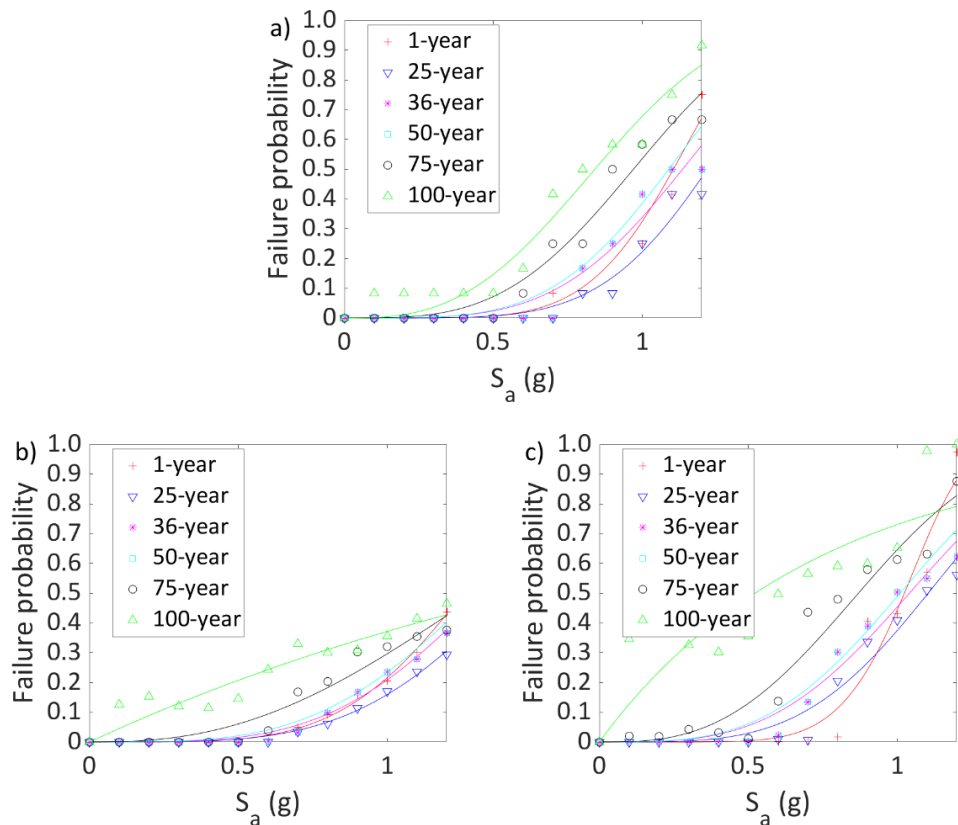


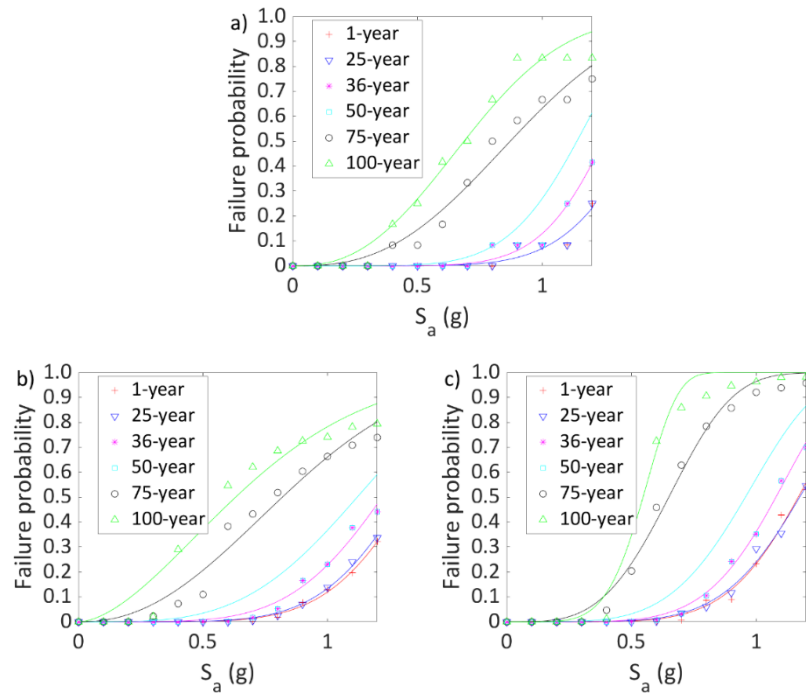
Figure 5.10: Estimated conditional failure probability by considering the tensile cracking at the neck of the dam (i.e., using the limit state function g_4): a) Based on the ratio of failed events, b) Based on the fitted Normal distribution, and c) Based on the fitted Gumbel distribution.

Table 5.7: Fitted model parameters by considering limit state function g_4 .

Year	Based on results shown in Figure 5.10a		Based on results shown in Figure 5.10b		Based on results shown in Figure 5.10c	
	α	γ	m	σ	u	a
1	1.178	5.723	1.360	4.592	1.078	7.065
25	1.309	5.117	1.534	4.085	1.211	3.943
36	1.242	4.072	1.456	3.855	1.159	3.410
50	1.189	4.152	1.438	3.634	1.124	3.403
75	1.082	3.352	1.523	2.482	0.987	2.897
100	0.957	2.835	2.150	1.000	0.759	0.983

5.4.3 Excessive Deformation of the Dam

The maximum relative displacements associated with the limit state function shown in Eq. (5.8) were extracted from the simulation analysis from 864 finite element runs. The values of $\delta_x^{Crest} - \delta_x^{Toe}$ are included in Appendix A. A probability distribution fitting to the values of the limit state functions $g_7(a)$ and $g_7(b)$ (see Eq. (5.8)) is carried out following the similar steps presented in the previous sections by using the normal and Gumbel model. The estimated conditional probability based on the fitted distributions is shown in Figures 5.11 and 5.12. Fragility curves are developed based on these results by fitting the Weibull distribution. The obtained Weibull distribution parameters are shown in Table 5.8 and the fitted curves are shown in Figures 5.11 and 5.12. Note that since the conditional failure probability for all the considered age, no fragility curve fitting is carried out for such cases.



**Figure 5.11: Conditional probability of failure estimated based on simulation and distribution fitting by considering the limit state function shown in Eq. (5.8a) $g_7(a)$:
a) Based on the ratio of failed events, b) Based on the fitted Normal distribution, and c) Based on the fitted Gumbel distribution.**

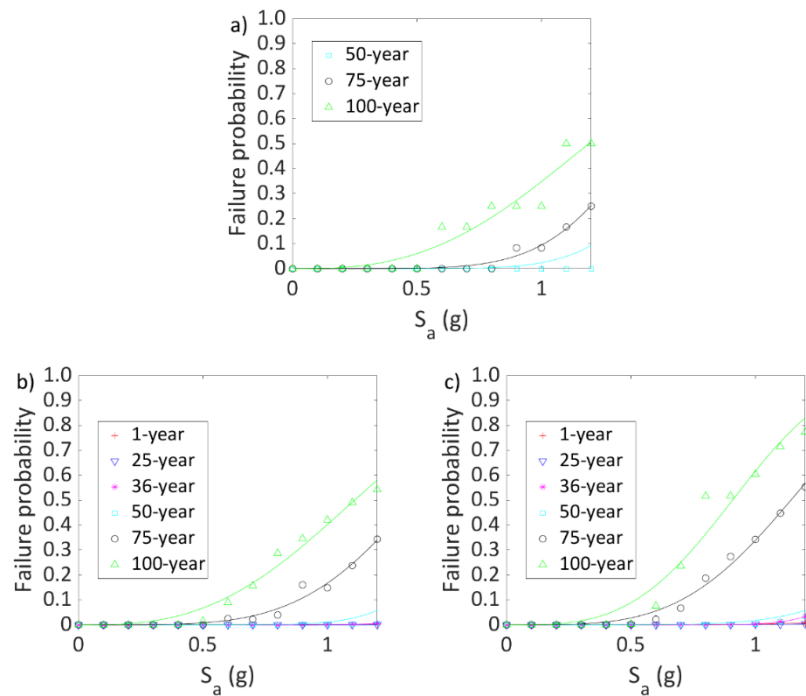


Figure 5.12: Conditional probability of failure estimated based on simulation and distribution fitting by considering the limit state function shown in Eq. (5.8b) $g_7(b)$:
a) Based on the ratio of failed events, b) Based on the fitted Normal distribution, and c) Based on the fitted Gumbel distribution.

Table 5.8a: Fitted model parameters by considering limit state function $g_7(a)$.

Year	Based on results shown in Figure 5.11a		Based on results shown in Figure 5.11b		Based on results shown in Figure 5.11c	
	α	γ	m	σ	u	a
1	1.450	7.062	1.401	6.116	1.240	6.165
25	1.450	7.062	1.384	5.971	1.251	5.762
36	1.308	7.344	1.313	4.954	1.150	5.722
50	1.210	6.061	1.237	3.676	1.034	4.700
75	1.000	2.673	0.965	2.221	0.718	3.642
100	0.795	2.504	0.781	1.711	0.584	5.510

Table 5.8b: Fitted model parameters by considering limit state function $g_7(b)$.

Year	Based on results shown in Figure 5.12a		Based on results shown in Figure 5.12b		Based on results shown in Figure 5.12c	
	α	γ	m	σ	u	a
1	0	0	8.919	3.736	2.869	5.466
25	0	0	4.531	5.839	2.945	6.074
36	0	0	2.702	6.548	1.601	11.676
50	1.620	7.719	1.640	9.013	1.863	6.415
75	1.476	5.935	1.459	4.491	1.256	3.866
100	1.358	2.776	1.259	2.876	1.012	3.360

5.5 Use of the fragility curves for reliability analysis

As mentioned in the previous sections, the fragility curve represents the failure probability conditioned on a given seismic intensity measure, such as the annual maximum effective ground acceleration S . Since the annual maximum effective ground acceleration S is uncertain for the considered site and is described by the lognormal distribution shown in Eq. (5.6), the annual maximum spectral acceleration (SA), according to Figure 5.2, equals $2.8S$. By taking this uncertainty into account, the failure probability at age t year (given the structure is safe before $t-1$ year), $P_{f|t}$, can be calculated by using

$$P_{f|t} = \int_0^{\infty} F_c(y) f_S(y) dy \quad (5.12a)$$

where y represents the SA, $F_c(y)$ denotes the fragility curve developed in the previous sections, and $f_S(y)$ denote the probability density function of the annual maximum SA whose corresponding probability distribution function is given by

$$F_S(y) = \Phi \left(\frac{\ln y - \ln(\mu/\sqrt{1+v^2})}{\sqrt{\ln(1+v^2)}} \right) \quad (5.12b)$$

in which $\mu = 2.8 \times 0.0643g = 0.18g$ and the coefficient of variation $v = 1.977$.

By considering the developed fragility curves with the parameters shown in Table 5.6 to 5.8 and solving Eq. (5.12b) using the simple simulation technique, the obtained $P_{f|t}$ are shown in Table 5.9. Table 5.9 indicates that $P_{f|t}$ is consistently greater than 10^{-2} . Based on the limit state functions g_3 , g_4 , $g_7(a)$ and $g_7(b)$. This value is much greater than the tolerable annual failure probability often encountered for the normal buildings, which is in the order of 10^{-4} to 10^{-5} . Based on these values alone, retrofitting must be considered for it to be acceptable.

Table 5.9: Estimated failure probability at a given year, $P_{f|t}$, by considering different limit state functions.

Year	Based on the ratio of failed events				Based on the fitted normal distribution				Based on the fitted Gumbel distribution			
	g3	g4	g7(a)	g7(b)	g3	g4	g7(a)	g7(b)	g3	g4	g7(a)	g7(b)
1	0.033	0.050	0.039	0.000	0.032	0.045	0.041	0.003	0.044	0.054	0.047	0.017
25	0.034	0.046	0.039	0.000	0.029	0.040	0.042	0.008	0.040	0.052	0.047	0.016
36	0.037	0.050	0.044	0.000	0.032	0.043	0.046	0.017	0.042	0.056	0.052	0.033
50	0.040	0.052	0.049	0.034	0.033	0.044	0.052	0.033	0.045	0.058	0.059	0.029
75	0.046	0.060	0.068	0.039	0.042	0.047	0.073	0.042	0.053	0.067	0.084	0.050
100	0.050	0.069	0.083	0.051	0.043	0.057	0.091	0.054	0.059	0.105	0.094	0.064

5.6 Summary

In this chapter, an overall framework to assess the fragility of the concrete dam is presented and illustrated. The framework is the first of its kind in that it incorporates the stochastic degradation and aging effect in defining the concrete strength for the time-dependent fragility curve assessment of the dam by considering different limit state functions. The assessment is carried out using the nonlinear inelastic finite element model, time history analysis, and Latin hypercube sampling. In addition, the use of the fragility curve for reliability analysis is presented.

It is shown that the fragility curve is sensitive to the year since the dam has been put into service. The fragility curve is an increasing function of the spectral acceleration, which is expected. It must be emphasized that, in all cases, the number of samples is too small to provide a very good smoothed estimate of the fragility curves, even though such a small number of samples are employed in the literature. It is suggested that an increased number of samples are be considered for a refined assessment.

The reliability analysis results indicate that in all cases, the failure probability is too large. Such a large estimated failure probability deserves further scrutiny, especially a site-specific seismic hazard assessment must be carried out to justify the considered probability distribution of spectral acceleration derived from the design code.

Chapter 6

6 Conclusions and Future Research

6.1 Summary and Conclusions

The present thesis is focused on the development of an overall framework to assess the seismic fragility curves and reliability of concrete gravity dams. The framework emphasizes the need to consider the time-dependent material properties for assessing the seismic fragility curves and reliability of the dam. The main tasks consist of the nonlinear inelastic finite element modeling and dynamic analysis, the modeling of time-dependent concrete strength due to aging and degradation, and the development of probabilistic analysis procedure leading to the time-dependent seismic fragility curves and reliability.

Through a literature review, it was shown that the design of the dam, following codes or standards, is often carried out following very simplified procedure, and nonlinear inelastic behavior of the dam subjected to seismic excitations is neglected. The review also indicates that the available seismic fragility and reliability analysis of the concrete gravity dam neglects the time-dependent effects of concrete material strength.

It was suggested that the strength of concrete could be modeled by considering both the strength gain due to aging and the strength reduction due to degradation, where the gain is modeled using an empirical function and the degradation is modeled using the gamma process. The model is validated using valuable time-dependent samples taken from a concrete gravity Chungju dam. It is acknowledged that the statistical criterion could not be used confidently for such a validation because of the scarce of data from the in-service dam. However, it is shown that the assumed parameters used in the literature for degradation may be questionable.

The sensitivity analysis results by using the developed finite element models indicate that the results from the proprietary software (Seismic performance evaluation report by K-water, 2013) are consistent with those obtained from the commercially available ABAQUS. Moreover, the sensitivity analysis results indicate that the dynamic characteristics in the linear elastic range are not very sensitive to the concrete properties.

The developed time-dependent seismic fragility curves of Chungju dam indicate that the consideration of the time-dependent effect is extremely important. This suggests that an effort in collecting the data from the in-service dam for developing the time-dependent concrete strength model is extremely important if one wants to gain confidence in the estimated seismic fragility curves and reliability. Moreover, it is acknowledged that the sample size used to develop the fragility curves is small (even it is consistent with those used in the literature). More extensive sampling is recommended based on the developed framework if the results are to be used for decision making in extending the working life of a dam.

It must be emphasized that, in all cases, the number of samples for the development of the is too small to provide a very good smoothed estimate, even though such a small number of samples are employed in the literature. It is suggested that an increased number of samples are to be considered for a refined assessment. Also, the reliability analysis results indicate that in all cases, the failure probability is large for the considered dam. Given there is no observed seismic event near the considered dam site since its construction, it is prudent to carry out a site-specific seismic hazard assessment. When such a site-specific seismic hazard becoming available, a re-evaluation of the reliability is recommended.

6.2 Future research

A few research topics are suggested below:

1. The first and most important aspect is collecting data on the time-dependent concrete strength from the in-service concrete gravity dam. This suggested topic may not be very scholastic but can have significant practical consequences. The fact that the limit state design code calibration results is well accepted is because it contains extensive statistical data and probabilistic models supported by data.
2. The nonlinear inelastic dynamic analysis is time-consuming, and the data processing is not very user friendly. A better user interface would be desirable for pre- and post-processing for the simulation analysis. Most importantly, the use of newly developed

popular simulation techniques such as subset simulation may be considered in estimating the seismic fragility curves and reliability

3. It is well-known that the ground motions at spatially distributed points are not identical. This spatial coherence on the seismic response of the dam needs to be investigated to see if neglecting the coherence is a conservative or unconservative measure for the concrete gravity dam.

4. No detailed site-specific seismic hazard assessment is carried out for the present study. For the decision making concerning a multi-million dollar project such as extending, retrofitting, or decommissioning a concrete gravity dam, detailed seismic hazard assessment results could be used to guide and constrain the selection or simulation of the ground motion records to be used for seismic fragility assessment.

References

- ABAQUS analysis user's Manual version 6.11.3. (2013). Pawtucket (RI): Hibbitt, Karlsson and sorenson.
- Abdel-Hameed, M. (1975). A gamma wear process. *IEEE transactions on Reliability*, 24(2), 152-153.
- Alfarah, B., López-Almansa, F., & Oller, S. (2017). New methodology for calculating damage variables evolution in Plastic Damage Model for RC structures. *Engineering Structures*, 132, 70-86.
- Bastidas-Arteaga, E., & Schoefs, F. (2012). Stochastic improvement of inspection and maintenance of corroding reinforced concrete structures placed in unsaturated environments. *Engineering Structures*, 41, 50-62.
- Benjamin, J. R., & Cornell, C. A. (1970). *Probability, Statistics, and Decision for Civil Engineers*. MacGraw-Hill Book Company.
- Besnard, F., & Bertling, L. (2010). An approach for condition-based maintenance optimization applied to wind turbine blades. *IEEE Transactions on Sustainable Energy*, 1(2), 77-83.
- Blind, H. (1983). The safety of dams. *International Water Power and Dam Construction*, vol. 35: 17-21
- Carde, C., & Francois, R. (1997). Effect on the leaching of calcium hydroxide from cement paste on mechanical properties. *Cement and Concrete Research* 27, 539–550.
- Carde, C., Francois, R., & Torrenti, J.-M., (1996). Leaching of both calcium hydroxide and C–S–H from cement paste: modelling the mechanical behavior. *Cement and Concrete Research* 22, 1257–1268.
- Castanier, B., Grall, A., & Bérenguer, C. (2005). A condition-based maintenance policy with non-periodic inspections for a two-unit series system. *Reliability Engineering & System Safety*, 87(1), 109-120.
- CEB-FIP, C. E. B. F. I. P. "Model code (2010)." Comite Euro-International du beton.
- Chávez, J. W., & Fenves, G. L. (1995). Earthquake response of concrete gravity dams including base sliding. *Journal of Structural Engineering*, 121(5), 865-875.
- Cheng, S. T. (1993). *Statistics of dam failure. Reliability and uncertainty analysis in hydraulic design*. ASCE, New York, 97-105.
- Ching, J., & Leu, S. S. (2009). Bayesian updating of reliability of civil infrastructure facilities based on condition-state data and fault-tree model. *Reliability Engineering & System Safety*, 94(12), 1962-1974.
- Chopra, A. K. (1968). Earthquake behavior of reservoir-dam systems. *Journal of the Engineering Mechanics Division*, 94(6), 1475-1500.
- Chopra, A. K., & Chakrabarti, P. (1981). Earthquake analysis of concrete gravity dams including dam-water-foundation rock interaction. *Earthquake engineering & structural dynamics*, 9.4 (1981): 363-383.

- Cinlar, E., Bazant, Z. P., & Osman, E. (1977). Stochastic process for extrapolating concrete creep. *J. Engrg. Mech. Div.*, 103(6), 1069–1088
- Corns, I. G. (1988). Compaction by forestry equipment and effects on coniferous seedling growth on four soils in the Alberta foothills. *Canadian Journal of Forest Research*, 18(1), 75-84.
- De Boer, R., & Ehlers, W. (1990). The development of the concept of effective stresses. *Acta Mechanica*, 83(1-2), 77-92.
- Dewey, R. R., Reich, R. W., & Saouma, V. E. (1994). Uplift modeling for fracture mechanics analysis of concrete dams. *Journal of Structural Engineering*, 120(10), 3025-3044.
- Dolen, T. P. (2005). Material properties model of aging concrete, Dam safety technology development program, U.S. Department of the Interior Bureau of Reclamation, Report DSO-05-05. Colorado.
- Dolen, T. P., Scott, G. A., von Fay, K. F., & Hamilton, B. (2003). Effects of Concrete Deterioration on Safety of Dams. US Department of Interior, Bureau of Reclamation.
- Douglas, K., Spannagle, M., & Fell, R. (1999). Analysis of concrete and masonry dam incidents. *International Journal on Hydropower & Dams*, 6(4), 108-115.
- Duffaut, P. (1986). Ruptures de barrages et incidents a ravers le monde. *Trevaux*, No 607: 55-57
- Ellingwood, B. R., and Mori, Y. (1993). "Probabilistic methods for condition assessment and life prediction of concrete structures in nuclear power plants." *Nucl. Eng. Des.*, 142, 155–166.
- Fahjan, Y. M., Börekçi, O. S., & Erdik, M. (2003). Earthquake-induced hydrodynamic pressures on a 3D rigid dam–reservoir system using DRBEM and a radiation matrix. *International journal for numerical methods in engineering*, 56(10), 1511-1532.
- Federal Energy Regulatory Commission. (2002). Engineering guidelines for the evaluation of hydropower projects, chapter III: gravity dams. Federal Energy Regulatory Commission, Washington.
- FEMA, FEMA. (2006). "445. Next-Generation Performance-Based Seismic Design Guidelines Program Plan for New and Existing Buildings." Redwood City.
- Frangopol, D. M., Kallen, M. J., & Noortwijk, J. M. V. (2004). Probabilistic models for life-cycle performance of deteriorating structures: review and future directions. *Progress in structural engineering and Materials*, 6(4), 197-212.
- Ghanaat, Y., Patev, R. C., & Chudgar, A. K. (2012, September). Seismic fragility analysis of concrete gravity dams. In *Proceedings of the 15th world conference on earthquake engineering*, Lisbon, Portugal (pp. 24-28).

- Ghrib, F., & Tinawi, R. (1995). An application of damage mechanics for seismic analysis of concrete gravity dams. *Earthquake engineering & structural dynamics*, 24(2), 157-173.
- Gogoi, I., & Maity, D. (2007). Influence of sediment layers on dynamic behavior of aged concrete dams. *Journal of engineering mechanics*, 133(4), 400-413.
- Goldgruber, M. (2015). Nonlinear seismic modelling of concrete dams.
- Guo, C., Wang, W., Guo, B., & Si, X. (2013). A maintenance optimization model for mission-oriented systems based on Wiener degradation. *Reliability Engineering & System Safety*, 111, 183-194.
- Gustafsson, A., Johansson, F., & Stille, H. (2008). *Betongdammas glidstabilitet: Förslag på nya riktlinjer*.
- Hariri-Ardebili, M. A. (2018). Risk, Reliability, Resilience (R3) and beyond in dam engineering: A state-of-the-art review. *International journal of disaster risk reduction*, 31, 806-831.
- Hariri-Ardebili, M. A., & Saouma, V. E. (2016). Seismic fragility analysis of concrete dams: A state-of-the-art review. *Engineering structures*, 128, 374-399.
- Hordijk, D. A. (1992). Tensile and tensile fatigue behaviour of concrete; experiments, modelling and analyses. *Heron*, 37(1).
- ICOLD. "inspection of dams after earthquakes -Guidelines." *Bulletin 62* (1988).
- ICOLD. "Internal Erosion at Existing Dams: an Outline of a Proposed ICOLD Bulletin."(1976).
- ICOLD. "Quality Control of Concrete, Report for the Committee on Materials for Dams." *Bulletin 47* (1983).
- ICOLD. "Reinforced rockfill and reinforced fill for dams - State of the art State of the art." *Bulletin 89* (1993)
- Iervolino, I., Chioccarelli, E., & Giorgio, M. (2013). Gamma modeling of continuous deterioration and cumulative damage in life-cycle analysis of earthquake-resistant structures.
- Iman, R. L., & Conover, W. J. (1982). A distribution-free approach to inducing rank correlation among input variables. *Communications in Statistics-Simulation and Computation*, 11(3), 311-334.
- JCSS Probabilistic Model. "Joint committee on structural safety." URL: www.jcss.ethz.ch (2001).
- Johnson, F. A. (1976). A classification of dam failures.
- Korea Ministry of Land . (2011). Korean dam design standard.
- Korea Ministry of Land, (2011). design of concrete dam,119-142
- Krätzig, W. B., & Pölling, R. (2004). An elasto-plastic damage model for reinforced concrete with minimum number of material parameters. *Computers & structures*, 82(15-16), 1201-1215.

- Kuhl, D., Bangert, F., & Meschke, G. (2004). Coupled chemo-mechanical deterioration of cementitious materials. Part I: Modeling. *International Journal of Solids and Structures*, 41(1), 15-40.
- K-water, (2013). Report for seismic performance evaluation considering the fluid-structure interaction of concrete dam.
- Lubliner, J., Oliver, J., Oller, S., & Oñate, E. (1989). A plastic-damage model for concrete. *International Journal of solids and structures*, 25(3), 299-326.
- Lupoi, A., & Callari, C. (2012). A probabilistic method for the seismic assessment of existing concrete gravity dams. *Structure and Infrastructure Engineering*, 8(10), 985-998.
- Madsen, H. O., Krenk, S., and Lind, N.C. (2006). *Methods of structural safety*. Courier Corporation.
- Mahmoodian, M., and Alani, A. (2014). "Modeling deterioration in concrete pipes as a stochastic gamma process for time-dependent reliability analysis." *Journal of pipeline systems engineering and practice* 5.1 (2014): 04013008.
- Malm, R. (2016). *Guideline for FE analyses of concrete dams*.
- McKay, M. D., Conover, W. J., & Whiteman, D. E. (1976). Report on the application of statistical techniques to the analysis of computer codes (No. LA-NUREG--6526-MS). Los Alamos Scientific Lab..
- Mirza, S. A., MacGregor, J. G., & Hatzinikolas, M. (1979). Statistical descriptions of strength of concrete. *Journal of the Structural Division*, 105(6), 1021-1037.
- Mirza, S. A., MacGregor, J. G., & Hatzinikolas, M. (1979). Statistical descriptions of strength of concrete. *Journal of the Structural Division*, 105(6), 1021-1037.
- Mridha, S., & Maity, D. (2014). Experimental investigation on nonlinear dynamic response of concrete gravity dam-reservoir system. *Engineering Structures*, 80, 289-297
- Nguyen, G. D., & Korsunsky, A. M. (2008). Development of an approach to constitutive modelling of concrete: isotropic damage coupled with plasticity. *International Journal of Solids and Structures*, 45(20), 5483-5501.
- Nguyen, K. T., Fouladirad, M., & Grall, A. (2018). Model selection for degradation modeling and prognosis with health monitoring data. *Reliability Engineering & System Safety*, 169, 105-116.
- Nicolai, R. P. (2008). *Maintenance models for systems subject to measurable deterioration* (No. 420). Rozenberg Publishers.
- Nicolai, R. P., Dekker, R., & Van Noortwijk, J. M. (2007). A comparison of models for measurable deterioration: An application to coatings on steel structures. *Reliability Engineering & System Safety*, 92(12), 1635-1650.
- Nowak, A. S. (2003). Calibration of the design code for concrete structures. In *Reliability and Optimization of Structural Systems: Proceedings of the 10th IFIP WG7. 5 Working Conference, Osaka, Japan, 25-27 March 2002* (p. 1). CRC Press.

- O'Connor, A. J., & Kenshel, O. (2013). Experimental evaluation of the scale of fluctuation for spatial variability modeling of chloride-induced reinforced concrete corrosion. *Journal of Bridge Engineering*, 18(1), 3-14.
- Oller, S. (1988). A continuous damage model for frictional materials. Technical University of Catalonia, Barcelona, Spain.
- Oller, S. (2014). *Nonlinear dynamics of structures*. Cham: Springer International Publishing.
- Olsson, A., Sandberg, G., & Dahlblom, O. (2003). On Latin hypercube sampling for structural reliability analysis. *Structural safety*, 25(1), 47-68.
- Olsson, A., Sandberg, G., & Dahlblom, O. (2003). On Latin hypercube sampling for structural reliability analysis. *Structural safety*, 25(1), 47-68.
- Pan, J., Feng, Y., Jin, F. and Zhang, C. (2013a), Numerical prediction of swelling in concrete arch dams affected by alkali-aggregate reaction, *European Journal of Environmental and Civil Engineering*, 17(4), 231-247.
- Pan, J., Feng, Y., XU, Y., Jin, F., Zhang, C. and Zhang, B. (2013b), Chemo-damage modeling and cracking analysis of AAR-affected concrete dams, *Science China Tech Science*, 56(6), 1449-1457.
- Pan, J., Xu, Y., Jin, F., & Zhang, C. (2014). A unified approach for long-term behavior and seismic response of AAR-affected concrete dams. *Soil Dynamics and Earthquake Engineering*, 63, 193-202.
- Pantazopoulou, S. J., & Papoulia, K. D. (2001). Modeling cover-cracking due to reinforcement corrosion in RC structures. *Journal of engineering mechanics*, 127(4), 342-351.
- Pebesma, E. J., & Heuvelink, G. B. (1999). Latin hypercube sampling of Gaussian random fields. *Technometrics*, 41(4), 303-312.
- Rakotovoava Ravahatra, N., De Larrard, T., Duprat, F., Bastidas-Arteaga, E., & Schoefs, F. (2015). Sensitivity Analysis and Ranking of Simplified Models of Concrete Carbonation. *Construction & Building Materials*.
- Reinius, E. (1962/1982) Vattenbyggnad del 3 – Dambyggnader. In Swedish.
- Segura, R. L., Padgett, J. E., & Paultre, P. (2020) FRAGILITY SURFACES FOR EFFICIENT SEISMIC ASSESSMENT OF GRAVITY DAMS VIA SURROGATE MODELING.
- Sen, Ufuk. "Risk Assessment of Concrete Gravity Dams Under Earthquake Loads." (2018).
- Si, X. S., Wang, W., Hu, C. H., Chen, M. Y., & Zhou, D. H. (2013). A Wiener-process-based degradation model with a recursive filter algorithm for remaining useful life estimation. *Mechanical Systems and Signal Processing*, 35(1-2), 219-237.
- Singpurwalla, N. D. (1995). Survival in dynamic environments. *Statistical science*, 86-103.
- Sun, J., Zuo, H., Wang, W., & Pecht, M. G. (2012). Application of a state space modeling technique to system prognostics based on a health index for condition-based maintenance. *Mechanical Systems and Signal Processing*, 28, 585-596.

- Tekie, P. B., & Ellingwood, B. R. (2003). Seismic fragility assessment of concrete gravity dams. *Earthquake engineering & structural dynamics*, 32(14), 2221-2240.
- Vaidya, P., & Rausand, M. (2011). Remaining useful life, technical health, and life extension. *Proceedings of the Institution of Mechanical Engineers, Part O: Journal of Risk and Reliability*, 225(2), 219-231.
- Vamvatsikos, D., & Dolšek, M. (2011). Equivalent constant rates for performance-based seismic assessment of ageing structures. *Structural Safety*, 33(1), 8-18.
- Van Noortwijk, J. M. (2009). A survey of the application of gamma processes in maintenance. *Reliability Engineering & System Safety*, 94(1), 2-21.
- Van Noortwijk, J. M., & Klatter, H. E. (1999). Optimal inspection decisions for the block mats of the Eastern-Scheldt barrier. *Reliability Engineering & System Safety*, 65(3), 203-211.
- Van Noortwijk, J. M., & Pandey, M. D. (2004, July). A stochastic deterioration process for time-dependent reliability analysis. In *Proceedings of the Eleventh IFIP WG (Vol. 7, pp. 259-265)*.
- Van Noortwijk, J. M., van der Weide, J. A. M., Kallen, M. J., and Pandey, M. D. (2007). "Gamma processes and peaks-over-threshold distributions for time-dependent reliability." *J. Reliab. Eng. Syst. Saf.*, 92(12), 1651–1658.
- Vatn, J. (2012, June). A state-based model for opportunity-based maintenance. In *11th International Probabilistic Safety Assessment and Management Conference and the Annual European Safety and Reliability Conference 2012 Volume (Vol. 1, pp. 1-4)*.
- Vermeer, P. A., & De Borst, R. (1984). Non-associated plasticity for soils, concrete and rock. *HERON*, 29 (3), 1984.
- Wahlstrom, E. E., & EE, W. (1975). The safety of dams and reservoirs
- Wang, W., Carr, M., Xu, W., & Kobbacy, K. (2011). A model for residual life prediction based on Brownian motion with an adaptive drift. *Microelectronics Reliability*, 51(2), 285-293.
- Washa, G. W., Saemann, J. C., & Cramer, S. M. (1989). Fifty-year properties of concrete made in 1937. *Materials Journal*, 86(4), 367-371.
- Welte, T. M., Vatn, J., & Heggset, J. (2006, June). Markov state model for optimization of maintenance and renewal of hydro power components. In *2006 International Conference on Probabilistic Methods Applied to Power Systems (pp. 1-7)*. IEEE.
- Westberg Wilde, M., & Johansson, F. (2016). Probabilistic model code for concrete dams.: Report 2016: 292.
- Westberg, M. (2010). Reliability-based assessment of concrete dam stability (Doctoral dissertation, Division of Structural Engineering, Lund University).
- Westergaard, H. M. (1933). Analytical tools for judging results of structural tests of concrete pavements. *Public Roads*, 14(10), 185-188.

- Whitmore, G. A. (1995). Estimating degradation by a Wiener diffusion process subject to measurement error. *Lifetime data analysis*, 1(3), 307-319.
- Yao, W., Jiang, S., Fei, W., & Cai, T. (2017). Correlation between the compressive, tensile strength of old concrete under marine environment and prediction of long-term strength. *Advances in Materials Science and Engineering*, 2017.
- Yeh, C. H., & Baier, D. R. (1992). Pore pressure in finite element analysis of concrete dams. In *Annu. Conf. Proc* (pp. 195-200).
- Zeidan, B. A. (2014, June). Finite Element Modeling For Acoustic Reservoir-Dam-Foundation Coupled System. In *International Symposium on Dams in a Global Environmental Challenges, ICOLD2014, Bali, Indonesia* (pp. 1-6).
- Zenz, G. (2008). Long Term Behaviour of Dams-Earthquake Loading Design. In *International Conference on Long Time Effects and Seepage Behaviour of Dams* (pp. 1-13).
- Zienkiewicz, O. C., & OC, Z. (1981). Computational models for the transient dynamic analysis of concrete dams.

Appendix A: Values of the limit state functions obtained from the finite element modeling and simulation analysis

Table A-1: Values of the limit state function g_3 by considering age equal to 1 year (MPa)

Comb.		1	2	3	4	5	6	7	8	9	10	11	12
0.1g	σ_{ta}	3.16	3.08	3.05	3.19	3.14	3.06	3.08	3.12	3.04	3.19	3.09	3.08
	σ_{max}	1.17	1.14	1.13	1.15	1.12	1.12	1.17	1.14	1.14	1.15	1.15	1.15
0.2g	σ_{ta}	3.12	3.14	3.08	3.08	3.04	3.09	3.08	3.19	3.05	3.19	3.06	3.16
	σ_{max}	1.14	1.12	1.14	1.17	1.14	1.15	1.15	1.15	1.13	1.15	1.12	1.17
0.3g	σ_{ta}	3.05	3.12	3.08	3.19	3.08	3.19	3.08	3.16	3.04	3.09	3.06	3.14
	σ_{max}	1.13	1.14	1.14	1.15	1.17	1.15	1.15	1.17	1.14	1.15	1.12	1.12
0.4g	σ_{ta}	3.05	3.19	3.09	3.08	3.04	3.14	3.19	3.16	3.08	3.08	3.12	3.06
	σ_{max}	1.13	1.15	1.15	1.17	1.14	1.13	1.15	1.46	1.14	1.15	1.14	1.12
0.5g	σ_{ta}	3.19	3.16	3.08	3.06	3.08	3.09	3.04	3.08	3.14	3.16	3.19	3.05
	σ_{max}	1.15	1.14	1.92	1.12	1.17	1.15	1.14	1.14	1.20	1.27	1.33	1.13
0.6g	σ_{ta}	3.14	3.06	3.08	3.04	3.12	3.08	3.05	3.19	3.08	3.09	3.16	3.19
	σ_{max}	1.20	1.16	1.15	1.39	1.14	1.17	1.13	1.58	1.25	1.62	1.17	2.32
0.7g	σ_{ta}	3.08	3.06	3.19	3.04	3.12	3.16	3.14	3.05	3.08	3.09	3.08	3.19
	σ_{max}	1.66	1.41	1.15	1.36	1.14	1.54	1.74	1.72	1.31	1.26	1.17	2.69
0.8g	σ_{ta}	3.08	3.04	3.08	3.16	3.05	3.14	3.12	3.09	3.08	3.06	3.19	3.19
	σ_{max}	2.36	1.58	3.03	1.83	1.15	1.58	1.39	1.56	1.15	1.86	1.45	2.17
0.9g	σ_{ta}	3.19	3.14	3.08	3.12	3.16	3.04	3.08	3.08	3.05	3.19	3.09	3.06
	σ_{max}	1.73	1.14	1.78	3.12	1.35	1.46	2.42	2.02	1.67	2.32	2.32	1.84
1.0g	σ_{ta}	3.16	3.06	3.04	3.14	3.09	3.19	3.08	3.08	3.12	3.05	3.19	3.08
	σ_{max}	1.96	1.61	1.96	1.97	1.43	2.19	2.40	2.77	1.39	2.69	3.20	1.56
1.1g	σ_{ta}	3.16	3.14	3.19	3.08	3.09	3.08	3.12	3.08	3.05	3.04	3.06	3.19
	σ_{max}	2.80	1.51	1.94	2.30	3.13	2.26	2.35	2.96	2.03	1.70	2.56	1.55
1.2g	σ_{ta}	3.12	3.14	3.04	3.08	3.19	3.05	3.06	3.19	3.08	3.09	3.08	3.16
	σ_{max}	3.15	2.40	2.43	2.47	1.69	2.02	2.72	2.60	2.87	1.75	1.84	3.17

Table B-2: Values of the limit state function g_3 by considering age equal to 25 year (MPa)

Comb.		1	2	3	4	5	6	7	8	9	10	11	12
0.1g	σ_{ta}	3.49	3.49	3.50	3.33	3.43	3.50	3.42	3.43	3.49	3.47	3.28	3.43
	σ_{max}	1.15	1.17	1.17	1.14	1.12	1.15	1.16	1.12	1.15	1.15	1.12	1.16
0.2g	σ_{ta}	3.50	3.33	3.42	3.50	3.47	3.49	3.49	3.28	3.43	3.43	3.43	3.49
	σ_{max}	1.17	1.14	1.16	1.15	1.15	1.15	1.17	1.12	1.12	1.16	1.12	1.15
0.3g	σ_{ta}	3.49	3.47	3.28	3.50	3.49	3.33	3.43	3.42	3.49	3.43	3.50	3.43
	σ_{max}	1.15	1.15	1.12	1.17	1.15	1.14	1.12	1.16	1.17	1.12	1.15	1.16
0.4g	σ_{ta}	3.42	3.33	3.43	3.50	3.47	3.43	3.49	3.28	3.49	3.43	3.49	3.50
	σ_{max}	1.16	1.14	1.16	1.18	1.15	1.12	1.17	1.12	1.43	1.12	1.15	1.15

0.5g	σ_{ta}	3.49	3.42	3.47	3.49	3.43	3.49	3.43	3.50	3.28	3.43	3.33	3.50
	σ_{max}	1.17	1.16	1.30	1.80	1.12	1.37	1.16	1.15	1.12	1.12	1.14	1.17
0.6g	σ_{ta}	3.49	3.43	3.50	3.49	3.47	3.28	3.43	3.43	3.42	3.33	3.49	3.50
	σ_{max}	1.33	1.22	1.17	1.15	1.21	1.50	1.51	1.12	1.16	1.14	1.44	2.11
0.7g	σ_{ta}	3.33	3.43	3.49	3.49	3.49	3.28	3.50	3.50	3.42	3.47	3.43	3.43
	σ_{max}	1.14	1.16	2.60	1.15	1.94	1.12	1.34	2.07	1.48	1.41	1.55	1.26
0.8g	σ_{ta}	3.33	3.50	3.49	3.43	3.50	3.47	3.28	3.49	3.43	3.42	3.43	3.49
	σ_{max}	1.19	1.46	2.00	1.74	2.87	1.60	1.12	2.20	1.19	1.58	1.67	1.36
0.9g	σ_{ta}	3.43	3.50	3.43	3.47	3.49	3.33	3.43	3.42	3.49	3.50	3.28	3.49
	σ_{max}	1.68	2.15	2.26	1.33	1.32	1.46	2.51	1.81	3.40	1.24	1.63	1.86
1.0g	σ_{ta}	3.42	3.43	3.28	3.43	3.50	3.33	3.49	3.43	3.50	3.49	3.47	3.49
	σ_{max}	2.87	3.34	1.84	2.42	1.96	1.29	1.90	2.12	2.39	1.47	1.67	1.56
1.1g	σ_{ta}	3.50	3.33	3.49	3.42	3.43	3.28	3.50	3.43	3.49	3.43	3.49	3.47
	σ_{max}	1.70	3.06	2.32	1.68	3.44	1.37	2.42	2.55	2.40	2.06	1.87	2.08
1.2g	σ_{ta}	3.43	3.28	3.50	3.49	3.49	3.50	3.47	3.49	3.43	3.43	3.42	3.33
	σ_{max}	1.67	2.20	3.29	2.27	2.04	1.86	3.49	2.52	2.63	2.53	3.09	1.78

**Table C-3: Values of the limit state function g_3 by considering age equal to 36 year
(MPa)**

Comb.		1	2	3	4	5	6	7	8	9	10	11	12
0.1g	σ_{ta}	3.44	3.40	3.44	3.43	3.45	3.40	3.32	3.42	3.16	3.44	3.24	3.33
	σ_{max}	1.17	1.12	1.14	1.18	1.15	1.14	1.14	1.18	1.13	1.14	1.15	1.15
0.2g	σ_{ta}	3.45	3.40	3.43	3.33	3.32	3.42	3.16	3.44	3.24	3.44	3.44	3.40
	σ_{max}	1.15	1.12	1.18	1.15	1.14	1.18	1.13	1.14	1.15	1.17	1.14	1.14
0.3g	σ_{ta}	3.40	3.44	3.42	3.45	3.43	3.24	3.32	3.44	3.33	3.44	3.40	3.16
	σ_{max}	1.14	1.14	1.18	1.15	1.18	1.15	1.14	1.14	1.15	1.17	1.12	1.13
0.4g	σ_{ta}	3.44	3.44	3.16	3.40	3.44	3.40	3.32	3.24	3.45	3.42	3.43	3.33
	σ_{max}	1.14	1.14	1.13	1.12	1.22	1.14	1.30	1.15	1.15	1.24	1.18	1.15
0.5g	σ_{ta}	3.44	3.33	3.32	3.45	3.24	3.16	3.42	3.40	3.43	3.40	3.44	3.44
	σ_{max}	1.14	1.15	1.44	1.15	1.60	1.13	1.18	1.12	1.18	1.14	1.14	1.43
0.6g	σ_{ta}	3.44	3.44	3.40	3.42	3.32	3.43	3.44	3.45	3.16	3.33	3.40	3.24
	σ_{max}	1.14	1.60	1.12	1.34	1.30	1.30	1.22	2.32	1.15	1.15	1.14	1.89
0.7g	σ_{ta}	3.43	3.16	3.45	3.44	3.42	3.40	3.24	3.40	3.44	3.44	3.32	3.33
	σ_{max}	1.52	1.13	1.40	1.22	2.11	2.12	1.15	2.50	1.44	1.50	1.51	1.15
0.8g	σ_{ta}	3.42	3.32	3.33	3.44	3.44	3.44	3.24	3.16	3.43	3.45	3.40	3.40
	σ_{max}	1.18	2.51	1.27	1.73	2.37	1.30	1.64	1.64	1.70	1.66	2.23	1.15
0.9g	σ_{ta}	3.44	3.33	3.44	3.24	3.43	3.16	3.42	3.44	3.32	3.40	3.45	3.40
	σ_{max}	1.82	1.66	2.53	1.44	2.11	1.77	1.57	1.37	1.15	2.38	1.97	3.25
1.0g	σ_{ta}	3.44	3.40	3.42	3.44	3.45	3.32	3.44	3.16	3.40	3.43	3.24	3.33
	σ_{max}	2.01	1.73	3.08	1.29	3.46	2.01	1.52	1.53	2.79	2.34	2.05	1.84
1.1g	σ_{ta}	3.40	3.16	3.42	3.43	3.44	3.32	3.44	3.44	3.40	3.45	3.33	3.24
	σ_{max}	2.20	1.69	2.67	2.59	1.58	3.17	2.24	2.97	1.82	3.46	1.55	2.20
1.2g	σ_{ta}	3.45	3.40	3.44	3.24	3.33	3.43	3.32	3.44	3.44	3.16	3.42	3.40
	σ_{max}	2.47	2.06	3.32	2.62	2.45	2.57	1.82	3.44	2.45	1.63	1.83	3.41

**Table D-4: Values of the limit state function g_3 by considering age equal to 50 year
(MPa)**

Comb.		1	2	3	4	5	6	7	8	9	10	11	12
0.1g	σ_{ta}	3.35	3.26	3.40	3.39	3.30	3.17	3.31	3.38	3.36	3.35	3.30	3.38
	σ_{max}	1.17	1.13	1.25	1.17	1.15	1.12	1.14	1.17	1.15	1.15	1.14	1.18
0.2g	σ_{ta}	3.39	3.38	3.31	3.38	3.35	3.17	3.26	3.36	3.35	3.40	3.30	3.30
	σ_{max}	1.17	1.18	1.14	1.17	1.14	1.12	1.13	1.15	1.17	1.23	1.15	1.14
0.3g	σ_{ta}	3.38	3.38	3.39	3.35	3.30	3.30	3.17	3.40	3.31	3.36	3.35	3.26
	σ_{max}	1.17	1.22	1.17	1.14	1.14	1.15	1.12	1.24	1.14	1.15	1.17	1.13
0.4g	σ_{ta}	3.35	3.38	3.36	3.30	3.30	3.35	3.40	3.38	3.26	3.31	3.39	3.17
	σ_{max}	1.14	1.17	1.15	1.22	1.15	1.17	1.25	1.17	1.13	1.14	1.46	1.12
0.5g	σ_{ta}	3.35	3.26	3.35	3.31	3.36	3.30	3.30	3.40	3.17	3.38	3.38	3.39
	σ_{max}	1.17	1.45	1.14	1.14	1.15	1.14	1.15	1.24	1.20	1.81	1.58	1.17
0.6g	σ_{ta}	3.38	3.17	3.35	3.30	3.36	3.31	3.35	3.30	3.39	3.40	3.26	3.38
	σ_{max}	1.23	1.73	1.17	1.34	1.21	1.14	1.20	1.94	1.17	1.25	1.45	1.92
0.7g	σ_{ta}	3.38	3.35	3.26	3.30	3.17	3.40	3.36	3.31	3.30	3.35	3.39	3.38
	σ_{max}	1.57	1.17	1.77	1.16	2.02	1.62	1.66	2.45	1.17	1.14	1.17	1.67
0.8g	σ_{ta}	3.38	3.30	3.38	3.40	3.36	3.26	3.17	3.35	3.35	3.39	3.30	3.31
	σ_{max}	2.20	1.62	1.37	3.02	1.37	2.01	1.12	1.57	1.33	1.51	2.72	1.81
0.9g	σ_{ta}	3.38	3.31	3.39	3.17	3.30	3.35	3.30	3.35	3.36	3.40	3.26	3.38
	σ_{max}	3.28	1.31	1.39	1.78	2.69	1.38	2.27	1.67	1.97	2.08	1.23	2.36
1.0g	σ_{ta}	3.17	3.35	3.40	3.30	3.38	3.30	3.26	3.38	3.39	3.31	3.35	3.36
	σ_{max}	1.68	1.31	1.61	1.46	3.38	2.02	1.59	2.38	3.40	2.84	2.73	2.02
1.1g	σ_{ta}	3.38	3.35	3.39	3.17	3.40	3.38	3.36	3.31	3.35	3.26	3.30	3.30
	σ_{max}	2.90	1.45	1.97	2.19	3.41	2.73	1.78	2.25	3.01	1.53	1.55	3.25
1.2g	σ_{ta}	3.38	3.35	3.30	3.30	3.40	3.36	3.17	3.38	3.31	3.35	3.26	3.39
	σ_{max}	3.38	2.38	2.50	2.95	2.38	1.70	1.85	1.91	2.74	3.35	3.27	1.89

**Table E-5: Values of the limit state function g_3 by considering age equal to 75 year
(MPa)**

Comb.		1	2	3	4	5	6	7	8	9	10	11	12
0.1g	σ_{ta}	2.79	2.89	2.57	2.94	2.38	2.83	2.50	2.62	2.67	2.74	2.71	3.05
	σ_{max}	1.16	1.16	1.25	1.30	1.23	1.35	1.15	1.31	1.16	1.20	1.21	1.27
0.2g	σ_{ta}	2.89	2.94	2.83	2.74	2.67	2.57	3.05	2.38	2.50	2.79	2.71	2.62
	σ_{max}	1.16	1.31	1.35	1.23	1.16	1.25	1.26	1.12	1.15	1.16	1.20	1.31
0.3g	σ_{ta}	2.50	2.89	2.62	2.94	2.57	2.83	2.67	3.05	2.74	2.38	2.71	2.79
	σ_{max}	1.15	1.16	1.33	1.28	1.25	1.35	1.16	1.27	1.22	1.12	1.23	1.16
0.4g	σ_{ta}	2.62	2.83	2.94	2.79	2.74	2.89	2.57	2.50	2.67	3.05	2.71	2.38
	σ_{max}	1.31	1.35	1.28	1.39	1.23	1.17	1.26	1.15	1.22	1.24	1.28	1.12
0.5g	σ_{ta}	2.71	3.05	2.50	2.67	2.83	2.94	2.89	2.62	2.79	2.57	2.38	2.74
	σ_{max}	1.21	1.26	1.34	1.16	1.34	1.30	1.16	1.42	1.16	1.79	1.52	1.23
0.6g	σ_{ta}	2.83	3.05	2.89	2.71	2.38	2.79	2.50	2.57	2.67	2.62	2.74	2.94
	σ_{max}	1.77	1.58	1.61	1.32	1.12	1.16	1.44	1.32	1.16	1.80	2.17	1.27

0.7g	σ_{ta}	2.62	2.79	2.83	3.05	2.74	2.50	2.71	2.94	2.67	2.57	2.38	2.89
	σ_{max}	1.55	1.27	2.07	1.68	2.10	1.29	1.30	2.71	2.09	1.59	1.51	1.16
0.8g	σ_{ta}	2.94	2.83	2.71	2.79	2.74	3.05	2.62	2.89	2.38	2.67	2.50	2.57
	σ_{max}	1.52	2.10	1.48	1.76	1.59	2.34	2.52	1.96	1.49	1.16	2.51	2.23
0.9g	σ_{ta}	2.38	2.71	2.62	2.83	2.50	2.79	2.89	2.74	2.94	2.57	2.67	3.05
	σ_{max}	2.39	1.97	1.87	2.11	2.14	1.63	2.35	1.62	2.39	1.39	2.20	3.06
1.0g	σ_{ta}	2.89	2.71	2.50	2.83	2.57	2.62	2.38	2.74	2.79	2.94	2.67	3.05
	σ_{max}	2.89	2.20	1.71	2.60	1.69	2.08	2.13	2.75	2.64	2.77	1.35	2.39
1.1g	σ_{ta}	2.67	3.05	2.74	2.38	2.71	2.62	2.94	2.57	2.79	2.50	2.89	2.83
	σ_{max}	1.48	2.20	2.36	2.33	2.41	2.26	2.94	2.47	2.00	2.51	2.89	2.85
1.2g	σ_{ta}	2.94	2.79	2.38	2.67	2.74	3.05	2.71	2.62	2.50	2.89	2.57	2.83
	σ_{max}	2.72	2.80	2.37	1.62	2.74	3.06	2.20	2.38	2.25	2.89	2.58	2.84

Table F-6: Values of the limit state function g_3 by considering age equal to 100 year (MPa)

Comb.		1	2	3	4	5	6	7	8	9	10	11	12
0.1g	σ_{ta}	2.65	2.84	2.72	2.77	2.87	2.81	2.50	2.88	2.87	2.34	2.57	2.83
	σ_{max}	1.55	1.37	1.47	1.51	1.49	1.34	1.28	1.45	1.43	1.14	1.24	1.22
0.2g	σ_{ta}	2.81	2.83	2.88	2.84	2.57	2.87	2.87	2.72	2.50	2.34	2.65	2.77
	σ_{max}	1.37	1.22	1.45	1.37	1.24	1.50	1.43	1.49	1.26	1.14	1.54	1.52
0.3g	σ_{ta}	2.87	2.81	2.72	2.57	2.65	2.88	2.77	2.87	2.50	2.34	2.83	2.84
	σ_{max}	1.50	1.35	1.50	1.24	1.56	1.44	1.50	1.43	1.27	1.15	1.23	1.39
0.4g	σ_{ta}	2.57	2.84	2.34	2.83	2.65	2.77	2.87	2.88	2.81	2.50	2.87	2.72
	σ_{max}	1.24	1.39	1.15	1.72	1.55	1.50	1.42	1.50	1.35	1.26	1.50	1.46
0.5g	σ_{ta}	2.65	2.72	2.57	2.83	2.81	2.87	2.77	2.50	2.87	2.84	2.88	2.34
	σ_{max}	1.55	1.73	1.24	1.22	1.38	1.40	1.60	1.86	1.51	1.74	1.44	1.46
0.6g	σ_{ta}	2.57	2.34	2.77	2.72	2.50	2.81	2.83	2.88	2.84	2.87	2.65	2.87
	σ_{max}	1.24	1.15	1.51	1.69	1.84	2.74	1.92	1.50	1.88	1.45	1.57	1.77
0.7g	σ_{ta}	2.34	2.65	2.81	2.88	2.72	2.83	2.57	2.87	2.84	2.50	2.77	2.87
	σ_{max}	1.89	1.84	1.59	2.42	1.71	1.22	2.27	1.52	1.40	2.44	2.24	1.78
0.8g	σ_{ta}	2.87	2.50	2.81	2.88	2.83	2.87	2.84	2.57	2.87	2.84	2.87	2.65
	σ_{max}	2.87	1.26	1.80	2.89	1.73	2.17	1.55	2.22	1.63	2.46	2.87	1.91
0.9g	σ_{ta}	2.81	2.72	2.87	2.34	2.84	2.87	2.77	2.57	2.65	2.50	2.88	2.83
	σ_{max}	2.21	1.67	2.87	1.55	2.85	1.71	2.77	2.02	2.38	2.51	2.23	1.81
1.0g	σ_{ta}	2.72	2.81	2.88	2.50	2.65	2.87	2.77	2.34	2.83	2.87	2.84	2.57
	σ_{max}	2.10	2.81	2.88	1.81	2.64	2.06	2.78	2.35	2.31	2.74	2.40	2.23
1.1g	σ_{ta}	2.57	2.83	2.84	2.87	2.65	2.81	2.34	2.50	2.88	2.72	2.77	2.87
	σ_{max}	2.59	1.77	2.63	2.87	2.65	2.09	2.33	2.42	2.17	2.72	2.76	2.88
1.2g	σ_{ta}	2.77	2.57	2.34	2.50	2.87	2.83	2.87	2.72	2.88	2.84	2.81	2.65
	σ_{max}	2.78	2.55	1.90	2.51	2.35	2.59	2.88	2.72	2.20	2.85	2.82	2.65

**Table A-7: Values of the limit state function g_4 by considering age equal to 1 year
(MPa)**

Comb.		1	2	3	4	5	6	7	8	9	10	11	12
0.1g	σ_{ta}	3.08	2.97	3.17	3.19	3.01	3.09	3.17	3.14	3.16	3.15	3.02	3.16
	σ_{max}	1.95	1.99	2.05	2.03	1.91	1.92	2.07	1.99	1.83	1.88	1.92	1.95
0.2g	σ_{ta}	3.14	3.01	2.98	3.17	3.16	3.02	3.16	3.19	3.18	3.15	3.09	3.08
	σ_{max}	1.96	1.93	1.99	2.09	1.80	1.92	1.85	1.97	2.07	1.89	1.95	1.89
0.3g	σ_{ta}	3.18	3.14	2.98	3.15	3.17	3.19	3.16	3.08	3.16	3.02	3.09	3.02
	σ_{max}	2.00	1.99	1.98	1.88	2.03	2.00	1.92	1.92	1.77	1.93	1.99	1.88
0.4g	σ_{ta}	3.18	3.15	3.02	3.17	3.16	3.02	3.19	3.08	2.98	3.16	3.14	3.09
	σ_{max}	2.03	1.89	1.97	2.07	1.80	1.92	2.05	1.95	2.01	1.94	1.97	1.92
0.5g	σ_{ta}	3.15	3.14	3.16	3.09	3.17	3.02	3.16	2.98	3.02	3.08	3.19	3.18
	σ_{max}	1.85	1.98	2.39	1.97	2.08	1.99	1.78	1.92	2.06	1.92	2.02	2.04
0.6g	σ_{ta}	3.02	3.09	3.16	3.16	3.14	3.17	3.18	3.19	2.98	3.02	3.08	3.15
	σ_{max}	1.86	1.99	1.92	1.79	1.99	2.07	2.04	2.48	1.95	1.99	1.92	2.79
0.7g	σ_{ta}	2.98	3.09	3.15	3.16	3.14	3.08	3.02	3.18	3.16	3.02	3.17	3.19
	σ_{max}	2.00	1.99	2.08	1.87	1.97	2.13	2.08	2.83	1.93	1.98	2.69	3.26
0.8g	σ_{ta}	3.17	3.16	2.98	3.08	3.18	3.02	3.14	3.02	3.16	3.09	3.15	3.19
	σ_{max}	2.45	2.33	3.04	2.09	2.42	2.19	2.24	1.89	2.86	3.13	1.84	2.32
0.9g	σ_{ta}	3.19	3.02	2.98	3.14	3.08	3.16	3.16	3.17	3.18	3.15	3.02	3.09
	σ_{max}	2.01	3.05	2.46	3.22	2.81	2.30	2.54	2.78	2.19	2.45	3.09	2.45
1.0g	σ_{ta}	3.08	3.09	3.16	3.02	3.02	3.15	2.98	3.17	3.14	3.18	3.19	3.16
	σ_{max}	2.38	2.74	2.89	2.74	3.06	2.51	2.59	3.23	2.89	2.83	3.26	2.05
1.1g	σ_{ta}	3.08	3.02	3.19	2.98	3.02	3.17	3.14	3.16	3.18	3.16	3.09	3.15
	σ_{max}	3.11	2.09	3.07	3.01	3.08	2.65	2.72	3.07	2.92	2.06	3.16	3.18
1.2g	σ_{ta}	3.14	3.02	3.16	3.17	3.15	3.18	3.09	3.19	2.98	3.02	3.16	3.08
	σ_{max}	3.21	3.05	3.07	2.85	3.18	3.21	3.16	3.22	3.05	3.06	2.45	3.15

**Table A-8: Values of the limit state function g_4 by considering age equal to 25 year
(MPa)**

Comb.		1	2	3	4	5	6	7	8	9	10	11	12
0.1g	σ_{ta}	3.49	3.30	3.41	3.49	3.43	3.35	3.51	3.49	3.43	3.51	3.47	3.46
	σ_{max}	2.00	1.91	2.17	2.00	1.95	1.80	1.92	1.81	1.80	1.92	1.92	1.75
0.2g	σ_{ta}	3.41	3.49	3.51	3.35	3.51	3.43	3.30	3.47	3.49	3.46	3.43	3.49
	σ_{max}	2.14	2.05	1.91	1.80	1.94	1.78	1.91	1.92	1.83	1.82	2.04	1.95
0.3g	σ_{ta}	3.43	3.51	3.47	3.41	3.47	3.49	3.43	3.51	3.30	3.49	3.35	3.46
	σ_{max}	1.77	1.92	1.91	2.13	1.94	1.99	2.05	1.90	1.87	1.19	1.78	1.75
0.4g	σ_{ta}	3.51	3.49	3.46	3.41	3.51	3.43	3.30	3.47	3.43	3.49	3.49	3.35
	σ_{max}	1.96	1.97	1.83	2.19	1.92	2.02	1.92	1.95	1.82	1.85	1.94	1.80
0.5g	σ_{ta}	3.30	3.51	3.51	3.43	3.49	3.49	3.46	3.35	3.47	3.43	3.49	3.41
	σ_{max}	1.90	1.90	2.13	2.20	1.85	1.94	1.79	1.83	1.89	2.03	1.98	2.14
0.6g	σ_{ta}	3.30	3.46	3.41	3.43	3.51	3.47	3.49	3.43	3.51	3.49	3.49	3.35
	σ_{max}	1.88	1.78	2.15	1.83	2.00	2.43	1.86	2.28	1.89	1.98	1.95	2.64

0.7g	σ_{ta}	3.49	3.46	3.43	3.49	3.30	3.47	3.35	3.41	3.51	3.51	3.49	3.43
	σ_{max}	2.27	1.79	3.16	2.26	2.17	1.87	1.98	3.26	1.93	2.13	1.85	2.02
0.8g	σ_{ta}	3.49	3.35	3.43	3.46	3.41	3.51	3.47	3.30	3.49	3.51	3.43	3.49
	σ_{max}	2.71	1.83	3.20	2.11	3.46	2.43	2.94	2.50	1.86	2.27	2.22	2.17
0.9g	σ_{ta}	3.43	3.41	3.49	3.51	3.49	3.49	3.46	3.51	3.30	3.35	3.47	3.43
	σ_{max}	2.45	2.33	2.79	1.97	2.90	2.31	3.45	2.57	3.34	3.29	2.05	2.26
1.0g	σ_{ta}	3.51	3.49	3.47	3.43	3.35	3.49	3.30	3.46	3.41	3.49	3.51	3.43
	σ_{max}	3.13	3.53	2.67	3.48	2.72	3.51	2.39	2.50	2.59	3.22	2.67	1.76
1.1g	σ_{ta}	3.41	3.49	3.30	3.51	3.46	3.47	3.35	3.49	3.49	3.43	3.43	3.51
	σ_{max}	2.17	3.54	2.95	3.53	3.50	3.49	2.73	3.54	2.96	2.99	2.70	2.64
1.2g	σ_{ta}	3.46	3.47	3.35	3.49	3.43	3.41	3.51	3.30	3.49	3.43	3.51	3.49
	σ_{max}	3.47	3.21	3.40	2.82	2.91	2.33	3.55	3.23	3.03	3.31	3.56	3.51

**Table B-9: Values of the limit state function g_4 by considering age equal to 36 year
(MPa)**

Comb.		1	2	3	4	5	6	7	8	9	10	11	12
0.1g	σ_{ta}	3.45	3.39	3.17	3.33	3.35	3.44	3.46	3.26	3.45	3.38	3.41	3.45
	σ_{max}	2.10	2.02	2.03	1.94	2.10	2.24	1.97	1.81	2.07	1.90	2.00	2.20
0.2g	σ_{ta}	3.35	3.39	3.33	3.45	3.46	3.26	3.45	3.38	3.41	3.45	3.17	3.44
	σ_{max}	2.05	2.10	1.93	2.20	1.96	1.83	2.07	1.90	2.01	2.12	1.97	2.30
0.3g	σ_{ta}	3.43	3.38	3.26	3.35	3.33	3.41	3.46	3.17	3.45	3.45	3.39	3.45
	σ_{max}	2.22	1.91	1.83	2.15	1.99	2.02	2.00	1.98	2.23	2.12	2.09	2.07
0.4g	σ_{ta}	3.17	3.38	3.45	3.39	3.45	3.44	3.46	3.41	3.35	3.26	3.33	3.45
	σ_{max}	2.07	1.85	2.07	2.04	2.10	2.27	2.05	2.01	2.07	1.82	1.97	2.22
0.5g	σ_{ta}	3.17	3.43	3.46	3.35	3.41	3.45	3.26	3.39	3.33	3.44	3.38	3.45
	σ_{max}	1.99	2.23	1.97	2.13	2.32	2.04	1.83	2.08	1.99	2.19	1.91	2.33
0.6g	σ_{ta}	3.17	3.38	3.39	3.26	3.46	3.33	3.45	3.35	3.45	3.45	3.44	3.41
	σ_{max}	2.32	2.45	2.08	1.83	2.02	1.91	2.05	2.97	2.02	2.25	2.31	1.98
0.7g	σ_{ta}	3.33	3.45	3.35	3.17	3.26	3.44	3.41	3.39	3.45	3.38	3.46	3.45
	σ_{max}	2.08	2.51	2.13	1.97	2.90	2.55	1.99	3.27	2.10	1.91	2.03	2.84
0.8g	σ_{ta}	3.26	3.46	3.45	3.17	3.45	3.38	3.41	3.45	3.33	3.35	3.39	3.44
	σ_{max}	2.86	3.50	2.93	2.11	3.47	1.91	2.32	2.07	2.01	2.14	2.74	2.27
0.9g	σ_{ta}	3.17	3.45	3.38	3.41	3.33	3.45	3.26	3.45	3.46	3.39	3.35	3.44
	σ_{max}	2.27	2.67	2.76	3.02	2.28	2.84	2.12	2.09	3.48	3.41	2.30	3.82
1.0g	σ_{ta}	3.17	3.44	3.26	3.38	3.35	3.56	3.45	3.45	3.39	3.33	3.41	3.45
	σ_{max}	2.67	2.83	3.28	3.40	3.39	2.48	2.08	3.47	3.41	2.55	2.90	2.98
1.1g	σ_{ta}	3.44	3.45	3.26	3.33	3.38	3.46	3.45	3.17	3.39	3.35	3.45	3.41
	σ_{max}	3.46	3.48	2.68	2.56	1.90	3.50	3.02	3.20	2.78	3.39	3.47	2.63
1.2g	σ_{ta}	3.35	3.44	3.17	3.41	3.45	3.33	3.46	3.45	3.38	3.45	3.26	3.39
	σ_{max}	3.33	3.40	3.20	3.01	3.48	3.00	3.47	3.49	2.95	3.47	2.01	3.42

**Table A-10: Values of the limit state function g_4 by considering age equal to 50 year
(MPa)**

Comb.		1	2	3	4	5	6	7	8	9	10	11	12
0.1g	σ_{ta}	3.28	3.43	3.33	3.34	3.43	3.35	3.26	3.43	3.40	3.41	3.39	3.39
	σ_{max}	2.19	2.17	2.11	2.02	2.13	1.98	1.97	1.95	2.19	2.01	2.14	2.21
0.2g	σ_{ta}	3.34	3.39	3.26	3.43	3.41	3.35	3.43	3.40	3.28	3.33	3.43	3.39
	σ_{max}	2.03	2.12	2.02	1.96	2.09	2.00	2.14	2.23	2.25	2.10	2.02	2.06
0.3g	σ_{ta}	3.43	3.39	3.34	3.41	3.39	3.43	3.35	3.33	3.26	3.40	3.28	3.43
	σ_{max}	1.96	2.27	2.02	2.06	2.14	2.13	2.01	2.08	2.02	2.23	2.19	2.13
0.4g	σ_{ta}	3.41	3.43	3.40	3.43	3.39	3.28	3.33	3.39	3.43	3.26	3.34	3.35
	σ_{max}	2.07	1.96	2.23	2.14	2.10	2.19	2.12	2.21	2.10	1.97	2.02	2.01
0.5g	σ_{ta}	3.28	3.43	3.41	3.26	3.40	3.39	3.43	3.33	3.35	3.43	3.39	3.34
	σ_{max}	2.25	2.69	2.06	2.01	2.22	2.09	2.12	2.07	2.02	1.97	2.22	2.03
0.6g	σ_{ta}	3.43	3.35	3.28	3.43	3.40	3.26	3.41	3.39	3.34	3.33	3.43	3.39
	σ_{max}	2.07	2.79	2.18	2.10	2.16	2.29	2.16	2.15	2.03	2.09	2.15	2.72
0.7g	σ_{ta}	3.39	3.28	3.43	3.43	3.35	3.33	3.40	3.26	3.39	3.41	3.34	3.43
	σ_{max}	2.21	2.19	2.84	2.08	3.37	2.37	2.19	2.38	2.64	2.81	2.03	1.98
0.8g	σ_{ta}	3.39	3.39	3.43	3.33	3.40	3.43	3.35	3.41	3.28	3.34	3.43	3.26
	σ_{max}	2.22	2.85	1.98	3.35	2.42	3.26	3.05	2.15	2.19	2.96	2.87	2.07
0.9g	σ_{ta}	3.39	3.26	3.34	3.35	3.39	3.41	3.43	3.28	3.40	3.33	3.43	3.43
	σ_{max}	3.24	1.99	3.36	2.37	3.43	2.68	2.24	3.31	2.45	3.05	2.13	3.44
1.0g	σ_{ta}	3.35	3.41	3.33	3.43	3.39	3.39	3.43	3.43	3.34	3.26	3.28	3.40
	σ_{max}	3.37	3.43	2.10	2.41	3.42	3.41	3.20	2.33	3.38	3.28	2.68	2.78
1.1g	σ_{ta}	3.43	3.41	3.34	3.35	3.33	3.39	3.40	3.26	3.28	3.28	3.43	3.39
	σ_{max}	3.46	3.43	3.14	2.92	3.37	3.08	3.41	3.27	2.95	2.55	2.08	3.42
1.2g	σ_{ta}	3.39	3.41	3.43	3.39	3.33	3.40	3.35	3.43	3.26	3.28	3.43	3.34
	σ_{max}	3.42	3.43	3.35	3.05	3.34	2.21	3.37	3.44	3.11	3.31	3.46	2.77

**Table A-11: Values of the limit state function g_4 by considering age equal to 75 year
(MPa)**

Comb.		1	2	3	4	5	6	7	8	9	10	11	12
0.1g	σ_{ta}	3.25	2.99	3.07	3.31	3.31	3.32	3.12	3.31	3.19	3.21	2.86	3.31
	σ_{max}	2.13	2.56	2.52	2.38	2.25	2.45	2.25	2.39	2.31	2.35	2.21	2.40
0.2g	σ_{ta}	2.99	3.31	3.32	3.21	3.19	3.07	3.31	3.31	3.12	3.25	2.86	3.31
	σ_{max}	2.57	2.44	2.47	2.32	2.36	2.49	2.37	2.22	2.25	2.16	2.22	2.42
0.3g	σ_{ta}	3.12	2.99	3.31	3.31	3.07	3.32	3.19	3.31	3.21	3.31	2.86	3.25
	σ_{max}	2.27	2.55	2.45	2.46	2.53	2.46	2.34	2.41	2.29	2.26	2.28	2.14
0.4g	σ_{ta}	3.31	3.32	3.31	3.25	3.21	2.99	3.07	3.12	3.19	3.31	2.86	3.31
	σ_{max}	2.39	2.48	2.47	2.14	2.33	2.51	2.49	2.19	2.35	2.37	2.30	2.28
0.5g	σ_{ta}	2.86	3.31	3.12	3.19	3.32	3.31	2.99	3.31	3.25	3.07	3.31	3.21
	σ_{max}	2.22	2.41	2.33	2.34	2.40	2.45	2.56	2.42	2.14	2.52	2.34	2.30
0.6g	σ_{ta}	3.32	3.31	2.99	2.86	3.31	3.25	3.12	3.07	3.19	3.31	3.21	3.31
	σ_{max}	2.45	2.39	3.00	2.28	2.28	2.14	2.24	2.50	2.36	2.94	2.54	2.89

0.7g	σ_{ta}	3.39	3.25	3.32	3.31	3.21	3.12	2.86	3.31	3.19	3.07	3.31	2.99
	σ_{max}	2.40	2.14	2.67	2.51	3.22	2.27	2.87	3.03	3.20	2.98	2.29	2.56
0.8g	σ_{ta}	3.31	3.31	2.86	3.25	3.21	3.31	3.31	2.99	3.31	3.19	3.12	3.21
	σ_{max}	2.45	3.19	2.88	2.47	2.28	3.32	3.33	2.39	2.88	2.34	3.12	2.95
0.9g	σ_{ta}	3.31	2.86	3.31	3.32	3.12	3.25	2.99	3.21	3.31	3.07	3.19	3.31
	σ_{max}	3.35	2.28	2.37	3.22	2.89	2.14	3.02	3.22	3.33	2.53	3.20	3.32
1.0g	σ_{ta}	2.99	2.86	3.12	3.32	3.07	3.31	3.31	3.21	3.25	3.31	3.19	3.31
	σ_{max}	3.02	2.38	3.13	3.34	2.53	2.60	3.25	3.24	3.26	3.32	2.61	3.32
1.1g	σ_{ta}	3.19	3.31	3.21	3.31	2.86	3.31	3.31	3.07	3.25	3.12	2.99	3.32
	σ_{max}	2.87	2.63	3.22	3.33	2.61	3.31	3.34	3.08	2.34	3.14	3.02	3.33
1.2g	σ_{ta}	3.31	3.25	3.31	3.19	3.21	3.31	2.86	3.31	3.12	2.99	3.07	3.32
	σ_{max}	3.32	3.26	3.33	3.13	3.22	3.02	2.25	3.31	2.82	3.01	3.10	3.34

Table A-12: Values of the limit state function g_4 by considering age equal to 100 year (MPa)

Comb.		1	2	3	4	5	6	7	8	9	10	11	12
0.1g	σ_{ta}	3.10	3.00	3.01	2.91	3.04	3.01	3.07	2.94	2.97	2.99	3.00	3.08
	σ_{max}	3.13	2.61	2.65	2.81	2.91	2.60	2.66	2.22	2.73	2.77	2.49	3.04
0.2g	σ_{ta}	3.01	3.08	2.94	3.00	3.00	3.04	2.97	3.01	3.07	2.99	3.10	2.91
	σ_{max}	2.54	3.06	2.15	2.61	2.52	2.92	2.73	2.67	2.70	2.79	3.13	2.84
0.3g	σ_{ta}	3.04	3.01	3.01	3.00	3.10	2.94	2.91	2.97	3.07	2.99	3.08	3.00
	σ_{max}	2.89	2.59	2.64	2.50	3.13	2.21	2.82	2.73	2.66	2.73	3.01	2.63
0.4g	σ_{ta}	3.00	3.00	2.99	3.08	3.10	2.91	2.97	2.94	3.01	3.07	3.04	3.01
	σ_{max}	2.54	2.56	2.79	3.04	3.13	2.77	2.74	2.21	2.61	2.69	2.83	2.65
0.5g	σ_{ta}	3.10	3.01	3.00	3.08	3.01	2.97	2.91	3.07	3.04	3.00	2.94	2.99
	σ_{max}	3.13	2.60	2.51	3.06	2.60	2.75	2.76	2.70	2.94	2.70	2.18	2.80
0.6g	σ_{ta}	3.00	2.99	2.91	3.01	3.07	3.01	3.08	2.94	3.00	2.97	3.10	3.04
	σ_{max}	2.50	2.73	2.80	2.59	3.02	2.99	3.11	2.23	2.94	2.70	3.13	2.94
0.7g	σ_{ta}	2.99	3.10	3.00	2.94	3.01	3.08	3.00	3.04	3.00	3.07	2.91	2.97
	σ_{max}	3.01	3.13	2.11	2.95	2.66	3.06	3.02	2.94	2.64	3.09	2.80	2.75
0.8g	σ_{ta}	3.04	3.07	3.01	2.94	3.08	2.97	3.00	3.00	2.99	2.91	3.01	3.10
	σ_{max}	3.07	2.69	2.54	2.97	3.04	3.00	2.64	2.75	2.80	2.92	3.03	3.13
0.9g	σ_{ta}	3.01	3.01	3.04	2.99	3.00	2.97	2.91	3.00	3.10	3.07	2.94	3.08
	σ_{max}	3.02	2.60	3.07	2.81	3.02	2.66	2.94	2.59	3.13	3.08	2.37	3.10
1.0g	σ_{ta}	3.01	3.01	2.94	3.07	3.10	3.04	2.91	2.99	3.08	2.97	3.00	3.00
	σ_{max}	2.73	3.01	2.96	2.68	3.13	2.94	2.94	3.00	3.11	2.99	2.70	2.99
1.1g	σ_{ta}	3.00	3.08	3.00	3.04	3.10	3.01	2.99	3.07	2.94	3.01	2.91	2.97
	σ_{max}	3.01	3.04	3.02	3.07	3.13	2.56	3.02	3.09	2.39	3.03	2.92	3.00
1.2g	σ_{ta}	2.91	3.00	2.99	3.07	2.97	3.08	3.04	3.01	2.94	3.00	3.01	3.10
	σ_{max}	2.94	3.01	3.02	3.09	2.99	3.10	3.07	3.04	2.24	3.02	3.02	3.13

Table A-13: Values of $\delta_x^{crest} - \delta_x^{Toe}$ by considering age equal to 1 year (cm)

Comb.	1	2	3	4	5	6	7	8	9	10	11	12
-------	---	---	---	---	---	---	---	---	---	----	----	----

0.1g	0.406	0.429	0.392	0.414	0.413	0.427	0.407	0.389	0.406	0.405	0.408	0.395
0.2g	0.389	0.413	0.429	0.407	0.406	0.408	0.395	0.414	0.392	0.405	0.427	0.409
0.3g	0.392	0.389	0.429	0.405	0.407	0.495	0.395	0.409	0.406	0.408	0.427	0.413
0.4g	0.616	0.405	0.408	0.407	0.406	0.463	0.476	0.452	0.515	0.395	0.389	0.517
0.5g	0.623	0.770	0.552	0.546	0.407	0.502	0.465	0.471	0.605	0.593	0.414	0.542
0.6g	0.567	1.045	0.742	0.673	0.560	0.447	0.649	0.727	0.565	0.408	0.575	0.669
0.7g	0.811	0.687	0.709	1.148	0.703	0.610	0.413	0.799	0.772	0.524	0.891	0.811
0.8g	0.407	0.668	0.987	0.741	0.743	1.343	0.604	0.963	0.984	0.989	0.764	0.966
0.9g	0.879	1.138	1.604	1.007	0.916	0.647	0.395	0.809	0.973	1.062	1.106	0.881
1.0g	1.157	0.747	0.837	1.679	1.285	0.911	1.150	1.209	0.930	0.436	1.152	1.012
1.1g	1.295	0.761	0.824	1.029	1.310	1.279	0.977	0.461	1.695	1.007	1.402	1.383
1.2g	1.342	1.038	1.077	1.410	1.508	0.910	1.553	1.977	1.374	1.268	1.199	0.527

Table A-14: Values of $\delta_x^{crest} - \delta_x^{Toe}$ by considering age equal to 25 year (cm)

Comb.	1	2	3	4	5	6	7	8	9	10	11	12
0.1g	0.423	0.446	0.451	0.443	0.423	0.431	0.430	0.435	0.422	0.418	0.413	0.410
0.2g	0.451	0.443	0.430	0.431	0.418	0.422	0.446	0.413	0.435	0.410	0.423	0.423
0.3g	0.422	0.418	0.499	0.451	0.413	0.443	0.423	0.430	0.446	0.435	0.431	0.410
0.4g	0.480	0.443	0.410	0.546	0.418	0.532	0.446	0.664	0.450	0.435	0.423	0.440
0.5g	0.968	0.430	0.597	0.563	0.592	0.423	0.626	0.443	0.472	0.530	0.557	0.596
0.6g	0.645	0.998	0.718	0.706	0.529	0.717	0.435	0.795	0.530	0.456	0.692	0.680
0.7g	0.939	0.646	0.784	0.759	0.446	0.517	1.277	0.949	0.691	0.613	0.773	0.889
0.8g	0.895	0.953	0.974	0.902	1.009	0.703	1.011	0.446	0.666	1.418	0.848	0.600
0.9g	1.569	1.022	0.435	0.837	0.972	0.677	1.051	0.813	1.088	1.175	1.059	0.854
1.0g	0.453	1.139	1.656	1.293	0.881	1.330	1.217	0.916	1.136	1.079	0.731	0.877
1.1g	0.971	0.516	1.032	1.198	1.224	1.386	1.228	1.392	1.082	1.917	0.804	1.294
1.2g	1.480	1.986	0.532	1.464	0.873	1.061	1.373	1.125	1.334	1.262	1.536	1.351

Table A-15: Values of $\delta_x^{crest} - \delta_x^{Toe}$ by considering age equal to 36 year (cm)

Comb.	1	2	3	4	5	6	7	8	9	10	11	12
0.1g	0.468	0.462	0.459	0.457	0.452	0.476	0.471	0.447	0.463	0.442	0.446	0.455
0.2g	0.446	0.462	0.457	0.455	0.471	0.447	0.463	0.442	0.446	0.468	0.459	0.476
0.3g	0.637	0.442	0.447	0.452	0.457	0.446	0.471	0.459	0.455	0.468	0.462	0.463
0.4g	0.459	0.489	0.564	0.462	0.468	0.476	0.471	0.451	0.452	0.538	0.815	0.483
0.5g	0.596	0.602	0.471	0.500	0.632	1.030	0.447	0.462	0.567	0.606	0.684	0.711
0.6g	0.876	0.802	0.494	0.653	0.665	1.222	0.616	0.773	0.723	0.538	0.757	0.446
0.7g	1.425	0.863	0.698	0.579	0.944	0.476	0.605	0.903	0.842	0.783	0.773	0.980
0.8g	1.099	0.929	0.968	0.962	1.142	0.625	1.527	0.888	0.804	1.001	0.462	0.686
0.9g	1.108	0.908	0.442	1.067	1.028	1.847	0.687	0.754	1.261	1.305	1.039	1.127
1.0g	1.226	0.833	1.355	1.373	1.305	1.105	0.836	1.234	0.500	1.138	1.906	1.009
1.1g	2.324	1.357	1.169	1.240	0.950	0.531	1.123	1.644	0.907	1.423	1.546	1.366
1.2g	1.202	1.000	1.830	1.346	2.306	1.464	1.469	0.554	1.303	1.704	0.962	1.530

Table A-16: Values of $\delta_x^{crest} - \delta_x^{Toe}$ by considering age equal to 50 year (cm)

Comb.	1	2	3	4	5	6	7	8	9	10	11	12
0.1g	0.539	0.538	0.498	0.514	0.498	0.513	0.511	0.493	0.526	0.530	0.511	0.524
0.2g	0.514	0.524	0.511	0.493	0.530	0.513	0.538	0.526	0.539	0.498	0.498	0.511
0.3g	0.493	0.524	0.514	0.530	0.511	0.498	0.513	0.498	0.511	0.526	0.539	0.575
0.4g	1.035	0.531	0.526	0.608	0.511	0.539	0.523	0.605	0.538	0.638	0.514	0.513
0.5g	0.815	0.781	0.722	0.511	0.626	0.640	1.160	0.498	0.587	0.493	0.616	0.792
0.6g	0.797	0.949	0.539	0.676	0.824	0.956	1.550	0.511	0.555	0.801	0.689	0.726
0.7g	0.997	0.539	0.812	0.848	1.118	1.706	0.839	0.511	0.957	1.111	0.647	0.789
0.8g	0.997	1.955	0.711	1.274	1.157	0.927	1.269	1.086	0.559	1.115	0.498	1.004
0.9g	0.568	0.856	1.425	1.222	1.414	1.274	1.027	1.427	1.125	2.192	0.587	1.091
1.0g	1.398	1.583	0.916	0.777	1.674	2.443	1.434	1.117	0.618	1.231	1.314	1.373
1.1g	1.323	1.741	1.514	1.484	0.599	1.419	1.568	2.860	1.444	0.769	0.954	1.769
1.2g	0.706	3.103	1.481	1.356	1.617	1.145	1.675	1.825	1.514	1.418	2.002	0.873

Table A-17: Values of $\delta_x^{crest} - \delta_x^{Toe}$ by considering age equal to 75 year (cm)

Comb.	1	2	3	4	5	6	7	8	9	10	11	12
0.1g	0.498	0.623	0.583	0.551	0.505	0.542	0.546	0.555	0.582	0.549	0.539	0.534
0.2g	0.623	0.551	0.542	0.549	0.582	0.583	0.534	0.505	0.546	0.498	0.539	0.555
0.3g	0.546	1.220	0.555	0.551	0.932	0.542	0.582	0.534	0.549	0.505	0.539	0.498
0.4g	0.854	0.542	0.551	0.498	0.549	1.389	0.583	0.695	1.262	0.770	0.540	0.505
0.5g	0.539	1.517	0.707	0.582	0.749	0.551	1.285	0.917	0.868	0.583	1.080	0.630
0.6g	1.126	0.534	2.519	0.973	0.505	0.631	1.232	2.000	0.817	0.870	0.549	1.294
0.7g	1.100	0.761	1.339	2.181	1.036	0.957	1.659	0.598	2.293	0.583	1.274	0.623
0.8g	0.853	0.716	1.921	1.470	1.094	2.272	1.214	1.523	2.398	0.582	0.709	1.535
0.9g	0.688	1.542	1.278	2.621	1.925	1.020	3.531	2.084	0.767	0.583	1.737	1.432
1.0g	2.266	1.734	2.338	0.924	1.065	1.434	1.875	0.927	2.266	1.866	0.582	3.178
1.1g	0.631	1.547	3.572	2.075	1.925	2.611	1.789	0.846	1.278	2.185	1.241	3.093
1.2g	3.852	2.072	1.081	0.703	2.616	1.943	1.366	2.864	1.735	2.263	4.001	1.143

Table A-18: Values of $\delta_x^{crest} - \delta_x^{Toe}$ by considering age equal to 100 year (cm)

Comb.	1	2	3	4	5	6	7	8	9	10	11	12
0.1g	0.929	0.843	0.823	0.939	0.862	0.800	0.859	0.779	0.852	0.826	0.803	0.879
0.2g	0.799	0.879	0.779	0.843	0.803	0.862	0.852	0.816	0.859	0.826	0.933	0.939
0.3g	0.862	0.800	0.816	0.803	1.219	0.779	0.939	1.200	0.859	0.883	0.879	0.843
0.4g	0.803	0.843	0.820	1.775	0.933	0.945	0.868	0.944	0.799	1.294	1.721	0.876
0.5g	0.936	1.607	0.803	0.879	1.129	0.852	2.157	2.159	0.862	1.218	1.083	0.820
0.6g	0.803	0.823	1.035	1.109	0.859	2.849	1.495	1.362	1.972	1.262	0.929	2.652
0.7g	2.258	0.929	1.299	0.906	1.638	0.879	1.784	1.167	0.947	3.072	3.076	1.638
0.8g	1.211	1.113	1.506	2.033	1.826	0.852	0.843	3.631	1.376	3.127	3.661	2.056

0.9g	4.140	1.344	1.377	1.567	3.883	0.852	2.306	2.127	0.929	3.092	2.117	1.710
1.0g	0.895	4.671	1.381	1.695	1.912	1.471	2.600	3.324	4.511	0.861	2.252	2.435
1.1g	3.631	1.641	2.068	2.916	1.825	1.923	2.717	2.714	0.836	4.967	1.081	4.965
1.2g	5.479	1.035	1.092	5.437	1.981	2.811	4.219	2.333	1.722	3.111	2.921	1.980

Curriculum Vitae

Name: Jungmyung Kim

**Post-secondary
Education and
Degrees:** Kyungpook National University
Daegu, South Korea
1995-2003 B.Sc.

The Yonsei University
Seoul, South Korea
2003-2005 M.S. in civil engineering

The University of Western Ontario
London, Ontario, Canada
2016-2021 Ph.D.

**Related Work
Experience** Senior Manager
The Korea Water Resources Corporation(K-water)
2005-2020

Professional Engineer (85319PE)
Oregon state, United States
2011-2020